NASA CONTRACTOR REPORT 181965

FRACTOGRAPHY OF COMPOSITE DELAMINATION

W. D. Bascom
University of Utah
Salt Lake City, Utah

July 1990
Grant NAG1-705

National Aeronautics and
Space Administration

Langley Research Center
Hampton, Virginia 23665-5225

TABLE OF CONTENTS

INTRODUCTION

Delamination is a major failure mode of carbon fiber organic-matrix composites. It can occur under a variety of loading conditions; tensile and compression loading of angle ply laminates (1,2), Mode I and Mode II loading of notched specimens (3), thermal stresses and environmental stresses (4). Specifically relevant to this report, is the fact that delamination is one of the primary failure modes in low level impact loading. This problem is especially serious in that low level impacts produce relatively little damage on the laminate surface but the internal damage can be sufficiently sever as to reduce the residual compression strength by as much as 50%. Considerable work has been done on impact damage much of which has been reviewed in a recent anthology (5).

Efforts to develop predictive models of the delamination of carbon fiber composites are hampered by a lack of information about the micromechanics of impact damage and delamination growth. Crack formation and propagation in these materials cannot be observed in sufficient detail to determine micro-damage using currently available NDE methods such as acoustic backscattering or X-ray imaging. Consequently, destructive methods are required.

In the work reported here, delamination of composites in Mode I, Mode II and after low energy impact loads were investigated using metallographic techniques of potting the failed specimens, sectioning and examining the cut sections for damage modes. This technique has been used to investigate impact damage (6) and more recently microdamage due to compressive failure (7).

MODE I DELAMINATION

EXPERIMENTAL

Width tapered double cantilever beam (WTDCB) specimens were cut from a plate of Hercules IM6/2502 carbon fiber/epoxy matrix composite. The plate was fabricated by hand lay-up of 24 plys of unidirectional tape and autoclave cured at 177°C (350°F) for 2 hrs.

The tapered specimens were cut from the cured panels with the fibers oriented along the length of the specimen. The dimensions are given in Fig. I. Aluminum loading tabs were bonded as shown in the figure and the precrack was initiated by notching with a razor blade. Details of this test have been published (8,9).

The specimens were fractured to about the mid-point of the tapered section and the fracture load used to calculate interlaminar fracture energy. While still in the test machine, a steel rod was placed between the tabs as shown in Fig. 2 so that the specimen could be removed without closing the fracture surfaces. The wedged specimen was then placed in a mold and potted in an epoxy resin. The potting resin was a diepoxide (DER 332, Shell Chemical Co.) cured with a polyamine (Jeffamine D-230, Texaco) and an accelerator (399, Texaco). Prior to curing, the assembly was evacuated to remove trapped air and to force the potting resin into the crack tip and any adjoining microcracks or voids. The cure conditions were 54°C (130°F) for 3hrs.

The potted specimen was sliced into eight longitudinal sections as shown in Fig. 3. Sections were cut using a 0.30mm (0.012in) thick, low speed diamond wafering saw. The sliced sections were 0.64mm (0.025in) in thickness. An additional slice was taken from the middle of the specimen and cut to a thickness of 0.38mm (0.015in). The sections were polished with 320 and 600 grit paper followed by a 1.0 micron alumina water slurry on a wet polishing wheel. The polished sections were examined using a light microscope in both transmitted and reflected illumination.

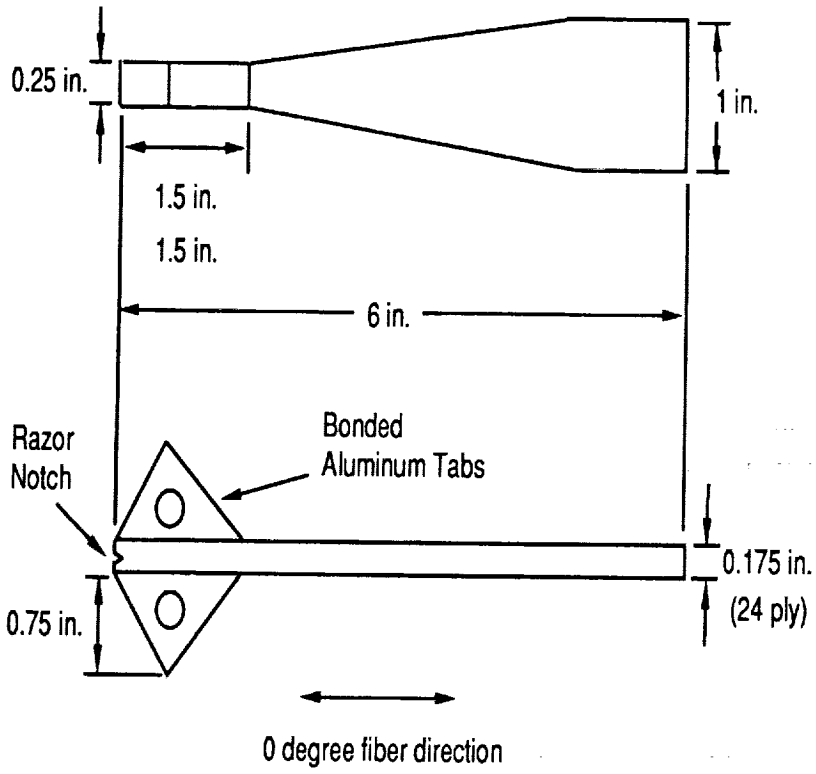

Figure 1 - Dimensions of the WTDCB test specimen

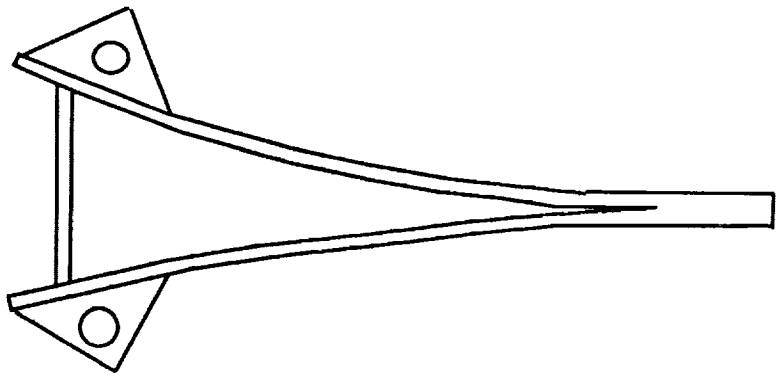

Figure 2 - Schematic of the partially fractured WTDCB specimen wedged open with a steel rod.

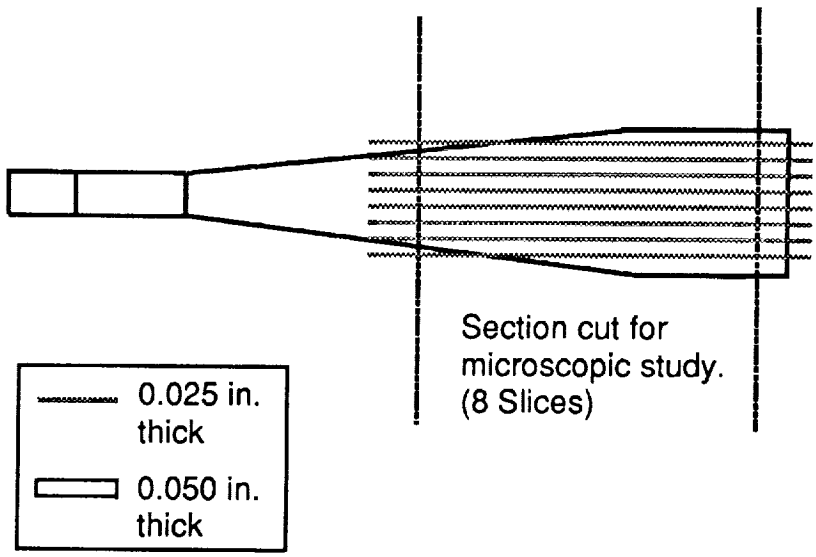

Figure 3 - Schematic of specimen sectioning procedure

RESULTS

The most prominent feature observed in the microscopy study of the polished sections was fiber bridging between the fractured surfaces. The bridging fibers and fiber bundles are clearly evident in Fig. 4. The cross-over fibers were most highly concentrated near the crack tip. In fact, the density of fibers at the crack tip was sufficient to prevent light transmission through the specimen so that the actual position of the crack front could only be seen using reflected light (Fig 5).

Two other observations were made that are pertinent to the delamination process. Satellite cracks were observed both above and below the main crack. One such crack can be seen in Fig 5. In some WTDCB specimens the advancing crack shifted from the main crack to one of these adjacent satellite cracks. This resulted in a thick ligament spanning the separated arms. The fracture load increased significantly when this occurred and then decreased as the front moved away from the ligament.

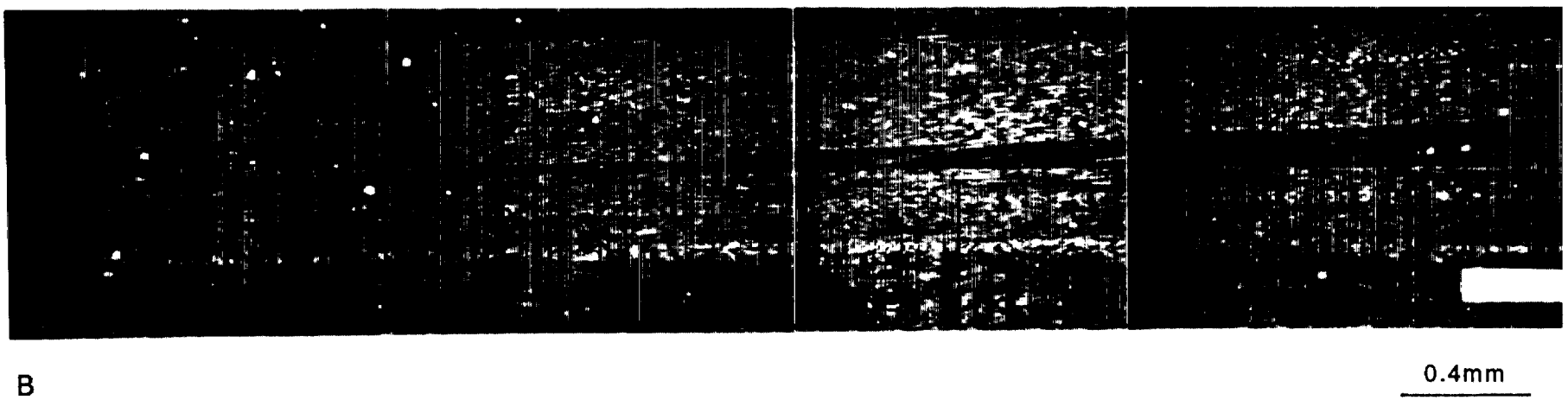

Figure 4 - Transmission (A) and reflection photomicrographs of a 0.64mm thick section showning fiber bridging

Figure 5: Reflection photomicrograph showing "satellite" micro-crack near main crack

The other observation was that for the thinner (0.38mm) specimens micro-cracks became visible near the main crack front as shown in Fig 6. Some of these features included the satellite cracks already mentioned. Other, usually shorter cracks were randomly distributed around the main crack. In Fig 6 they appear to be advance crack front damage. However, sectioning of laminates that had not been fractured revealed a similar population of these microcracks.

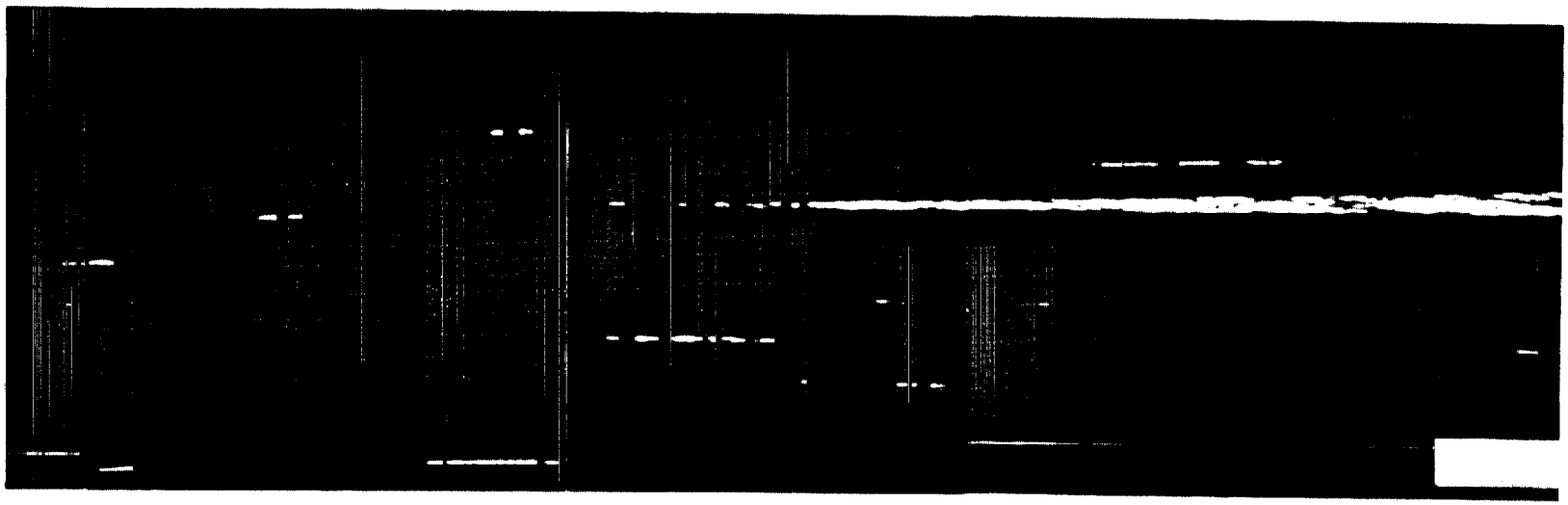

Figure 6 - Transmission photomicrograph of a 0.38mm thick section showing micro-cracks ahead and around the main crack.

Measurements were made of the distance from the loading pins to the crack tip (as determined by both reflected and transmitted illumination) for each of the eight sections. The results are given in Table I. It would appear that the crack front is essentially linear across the width of the specimen which would imply that the stress condition is essentially plane strain with no detectable plane stress condition at the specimen edges. Locally, the stress state in the matrix and on the individual fibers is much more complex.

Table I: Distance From Crack Front to Loading Pin Centers

Section No.	Distance (mm)	
	Transmission	Reflection
1	112.0	113.5
2	112.5	113.5
3	113.0	113.5
4	112.5	113.5
5	111.0	113.5
6	111.0	112.5
7	110.0	111.0
8	109.0	111.0

Transverse sections of potted IM6/2502 laminates were cut about 0.3mm behind the crack front. A series of photographs taken at five equally spaced positions along a transverse section are shown in Fig. 7. Bridging fibers appear as dark objects in the crack opening since the section was viewed using transmitted illumination .

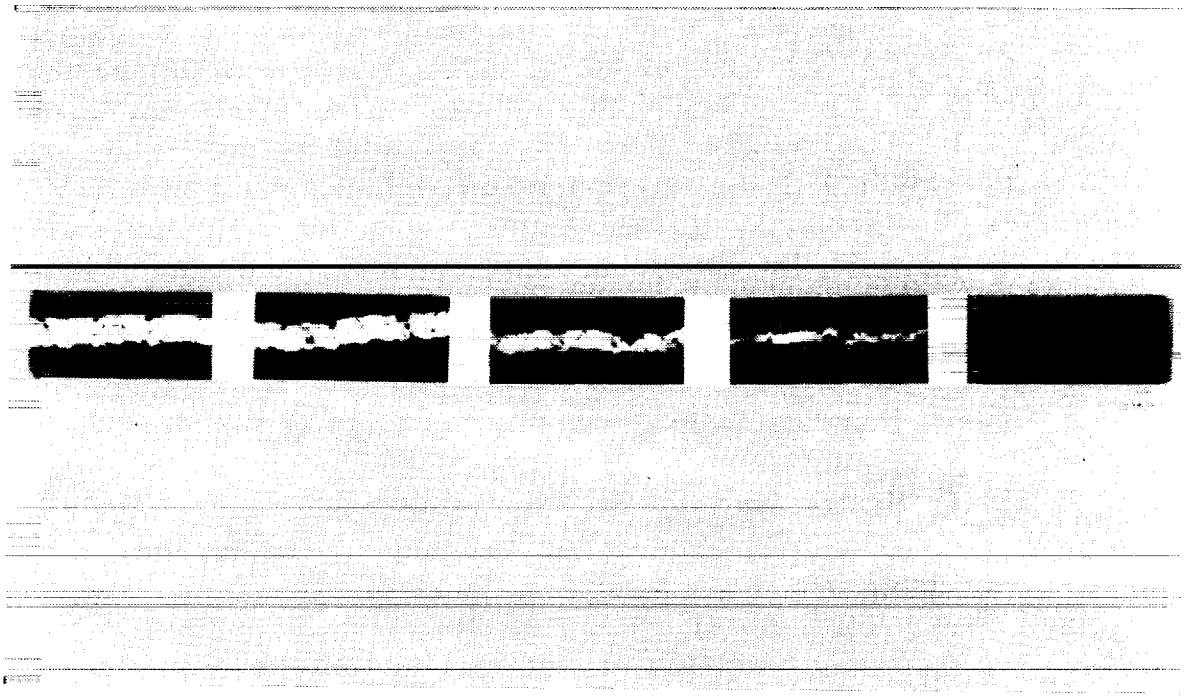

Figure 7 - Transmission photomicrographs along a transverse section through the delaminated specimen about 3mm behind the crack front.

The first (LHS) and the last (RHS) photographs in Fig. 7 were taken near the specimen edges. It is clear that going from left to right the crack opening decreases significantly to the extent that at the right hand edge, the crack is essentially closed. Actually, there was a ligament of fibers extending across the crack opening at the right hand side of the specimen. The resistance of this ligament to the advancement of the crack front could have redirected the plane of the delamination. Inspection of the specimen indicated that this did not occur. None the less, the effect of these ligaments of bridging fiber bundles must effect the delamination fracture energy and any calculation of the crack opening displacement.

DISCUSSION

The principal observations of this study were the massive fiber bundle crossover at the crack tip of the delaminated specimens and the ligaments of fiber bundles that persist behind the main crack front. The density of crossovers decreased away from the

crack front where the fibers had pulled out and/or fractured. Clearly, there are two energy consuming processes involved; the pull-out (or more exactly the peel-out) of fibers from both sides of the delamination and the breaking of these fibers. For the material studied here, must of the bridging involved fiber bundles and very few individual filaments.

Fiber bridging may be more prevalent and possibly unique in the delamination of unidirectional laminates compared to angle ply laminates. Although, the unidirectional laminates are fabricated from prepreg plys, there is considerable nesting and intermingling of the filaments during the compaction steps of the vacuum bag/autoclave processing. In viewing the cut sections it is not possible to identify the individual plies. In angle ply laminates, there is little opportunity for fiber nesting and the plies with different orientation can be easily identified in sectioned and polished specimens (8). This distinction between unidirectional and angle-ply laminates is significant in that crack propagation through a resin rich layer probably requires less energy than through a "maze" of bridging fibers and fiber bundles. Actually, the situation is more complex as discussed in the next section on Mode II delamination.

One of the objectives of this investigation was to examine for evidence of micro-cracking or other damage in advance of the main crack front. No precrack damage was found. The micro-cracks observed ahead of the crack front shown in Fig. 6 were found at a comparable density well away from the delamination in undamaged regions of the composite. Presumably these microcracks are voids or resin rich areas. It is also possible that some of these microcracks are artifacts resulting from the sectioning and polishing. If the microcracks are in fact laminate defects, then this sectioning technique can be used to determine laminate quality.

Other fiber-matrix combinations were fractured and sectioned to determine if the density of cross-over fibers varies with matrix fracture energy and fiber strength. The 2502 epoxy matrix has a relatively high fracture energy (270 J/m^2) and the IM6 is a relatively strong fiber (4.9 GPa). None the less, tests with an AS4/3501-6 laminate for which the matrix fracture energy is 130J/m2 and the fiber strength is 3.6 GPa also exhibited considerable fiber bridging.

The zone of bridging fibers and fiber bundles evident in Figs. 4 and A1 suggest the line zone of crack tip damage assumed in the Dugdale model of crack tip plasticity (10). Accordingly, the length of the plastic zone R is given by,

$$R = \frac{\Pi}{8}\left(\frac{K_{Ic}}{\sigma_y}\right)^2 \qquad \text{Eq. 1}$$

Where K_{Ic} is the stress intensity factor and σ_y the tensile yield strength of the material. The stress intensity factor is given in terms of the strain energy release rate, G_{Ic}, by,

$$K_{Ic}^2 = \frac{EG_{Ic}}{1-\nu^2} \qquad \text{Eq. 2}$$

where E is the tensile modulus and ν Poisson's ratio. Taking some typical values for carbon fiber, epoxy matrix composites, i.e.,

$E = 1.25 \times 10^{11}$ Pa
$G_c = 721$ Pa·m
$\sigma_y = 40 \times 10^6$ Pa[a]

gives a value for R of about 25mm. which is more than three times the length of the crack shown in Fig.4. This distance seems excessively long but may reflect the influence of bridging fibers and ligaments well behind the crack front.

MODE II DELAMINATION

EXPERIMENTAL

The test fixture shown in Figure 8 was constructed to load end-notched carbon fiber laminates in order to induce pure Mode II cracking and then pot the cracked specimen in a clear epoxy for

[a] The tensile strength of the 2502 epoxy is used here for σ_y which probably under estimates the yield strength.

sectioning and microscopy. As shown in Figure 9 the specimen is clamped at one end and deflected downward at the other end by turning a bolt with a short wooden dowel contacting the specimen. Crack growth at the edge of the specimen was observed using a telescope and when the crack reached about half the length of the specimen a mold was built around the free end of the laminate (including the dowel), filled with the potting resin and heat cured.

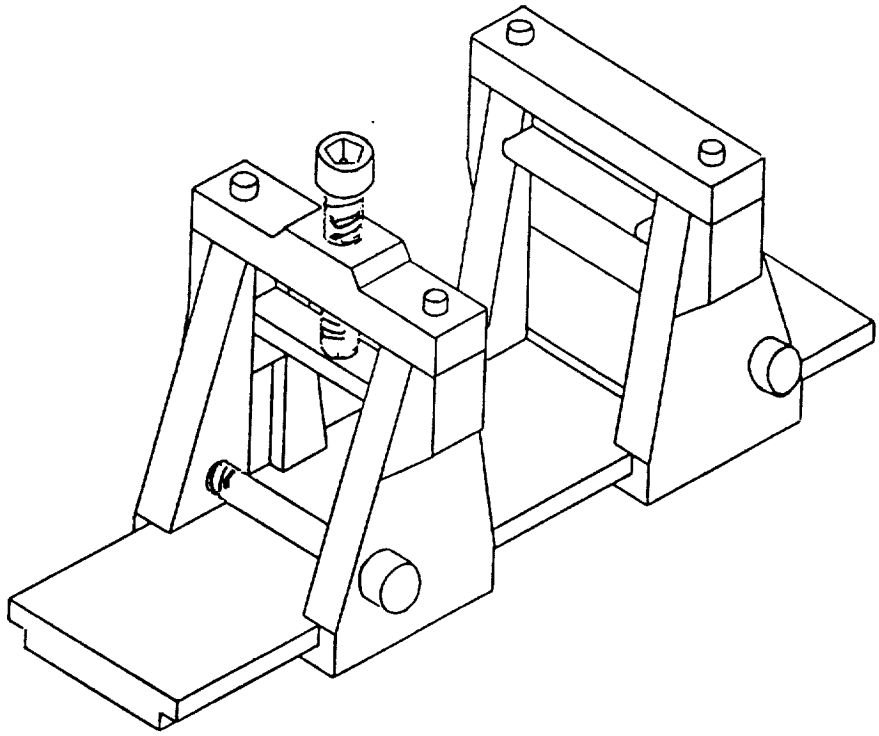

Figure 8 - Flexture load frame for Mode II delamination

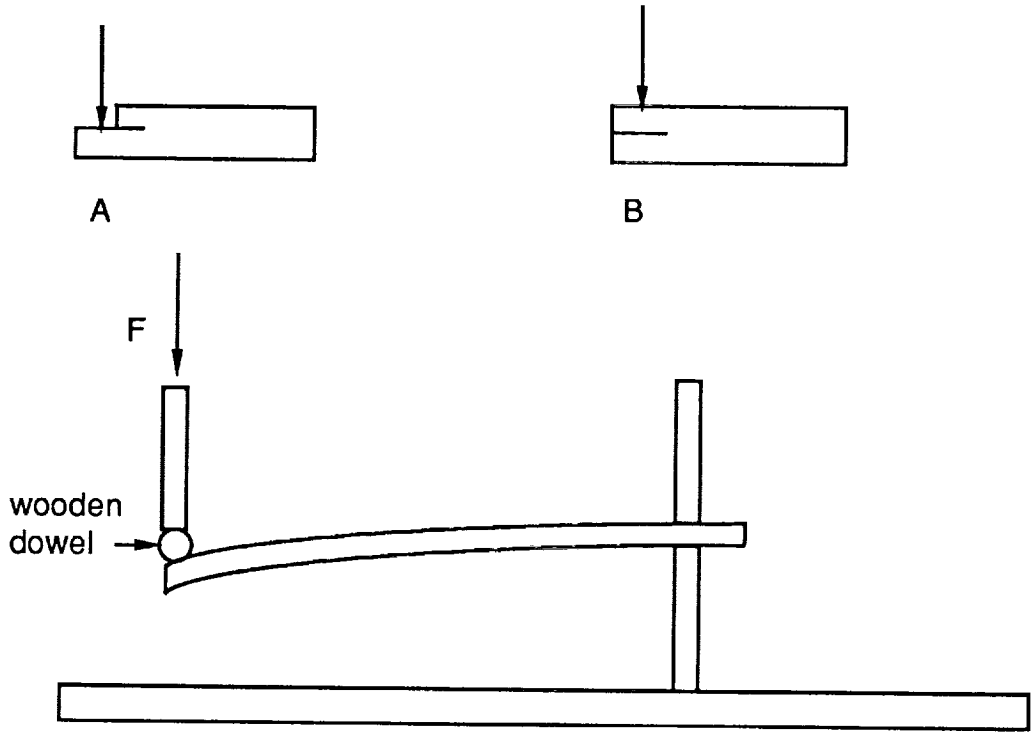

Figure 9 - Schematic of Mode II loading and the end notch configurations.

The test laminate was a unidirectional 16ply, AS4/3501-6 composite 1in. wide and 4in. in length. Excessive bending of the specimen near the clamped end resulted in failure before a delamination could be produced. This problem was solved by supporting the specimen with two laminates 0.5in. wide and 2.25in. and 3.25in. long respectively. Using this configuration, a mid-plane crack could be initiated without any breakage at the clamped end.

Two loading configurations are shown in Figure 9. In one case (Figure 9A) the laminate was precracked using a knife blade, the upper section cut away and the dowel positioned against the protruding lower section. In order to minimize Mode I loading, a wire was wrapped around the specimen. Judging from visual observations the Mode I opening displacements are minimal at the crack front that had propagated one-half the length of the specimen.

The same test procedure was used to investigate Mode II delamination of a cross-ply $(0/90)_{8S}$ laminate. In these experiments the laminate did not have to be end cut but was precracked using a razor blade (Fig 9B). The specimen was loaded to about 0.5 in. deflection at which point a crack propagated about 3/4 of the specimen length. The specimen was then potted, cut into sections

about 2mm thick and the sections polished.

RESULTS

Unidirectional Laminates: The loading configurations shown in Figure 9B should produce a pure Mode II delamination. However, we were unable to induced a crack in this fashion. The fractography results reported here are for cracks produced using the "split end" configuration, Fig. 9B.

The general appearance of the cut sections is shown in Figure 10. Two major cracks developed in the specimen; the major crack along the central plane and a pure Mode II crack in the upper half of the specimen. The crack in the upper half of the specimen is designated as a "pure" Mode II crack based on the fact that there was relatively little displacement of the crack faces. In principle, a Mode II crack should not be visible since it involves only shear displacements. None the less, the cracks generated in this study are the result of primarily Mode II loads.

For the most part, these cracks progressed through the matrix with relatively little fiber bridging. Occasionally, there was evidence of fibers spanning the crack (Figure 11). The Mode II crack was not continuous. As shown in Figure 12, the crack is distinct on the left and right hand sides of the photomicrograph but disappears in the center.

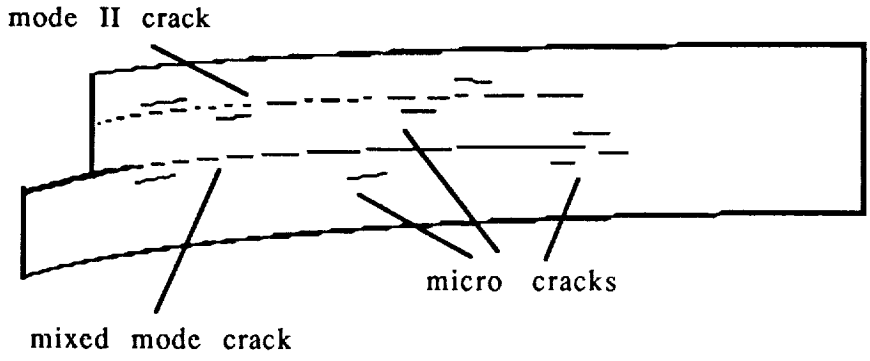

Figure 10 - Schematic of cracking in a Mode II specimen

As shown schematically in Figure 10, there were microcracks

near the major crack and especially ahead of the crack front. It was sometimes difficult to distinguish microcracks from laminate imperfections but there is the distinct possibility that "satellite" microcracks develop ahead of the main crack front but then close-up once the crack front has passed. The formation of these satellite cracks probably constitute part of the energy of Mode II crack propagation, at least for the test configuration used here.

The stressed laminate revealed extensive fiber breakage throughout the specimen. In Figure 13, photomicrographs are shown of a section cut through an unstressed laminate and a section through the stressed laminate. In the latter, many of the fibers appear to have broken into short segments.

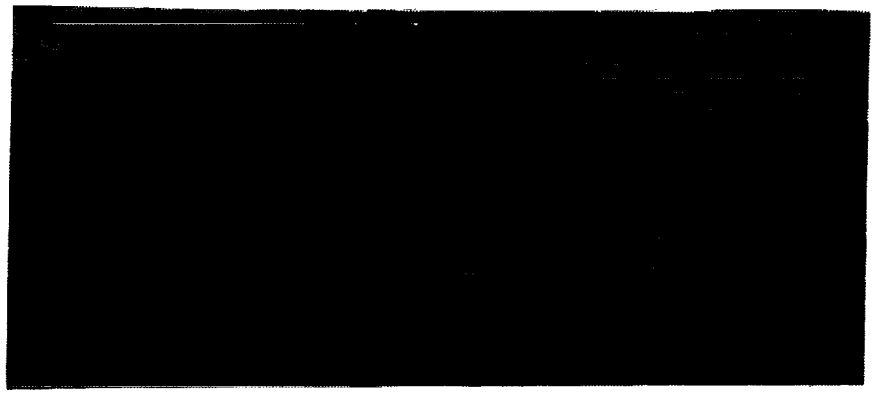

Figure 11 - Mode II crack showing bridging filament.

Figure 12 - Mode II opening was barely perceptible in some regions.

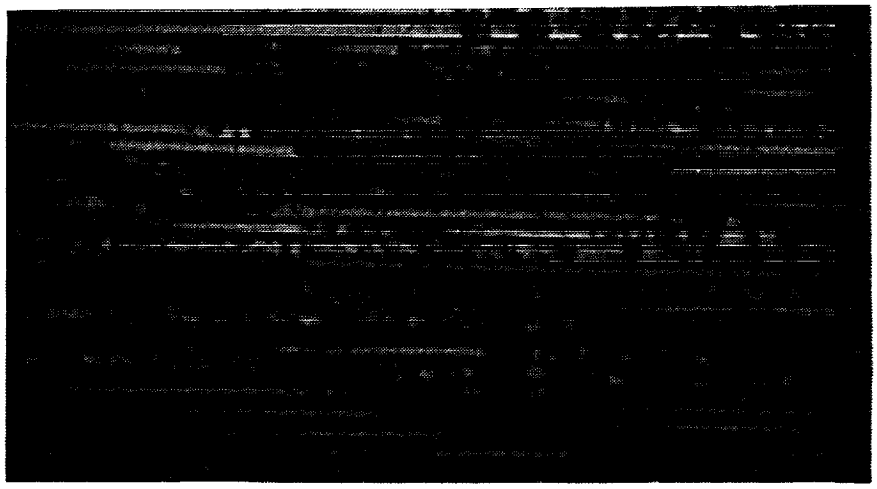

A 0.04mm

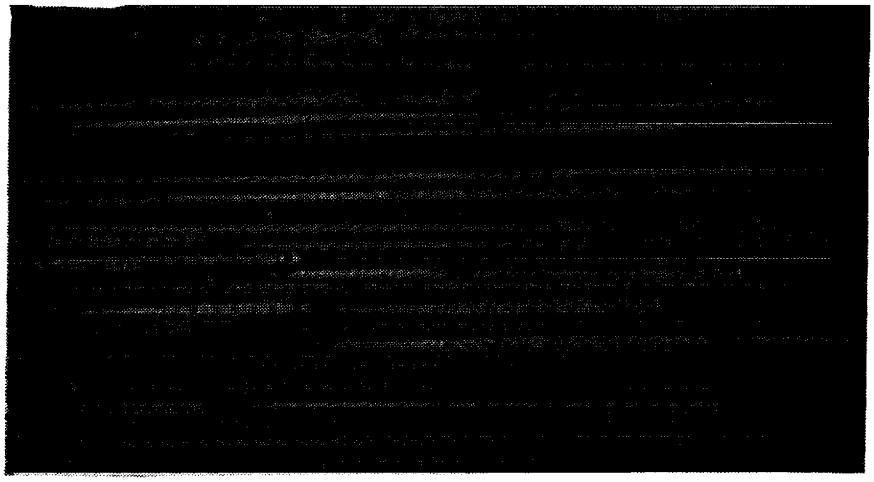

B 0.04mm

Figure 13 - Fiber fracture in tested specimen (A) not observed in untested laminate.

Cross-ply Laminates: Crack propagation occurred at a bending stress of 9.6×10^6 psi. and was always through a 0° ply. In one specimen it was observed that the major crack shifted to the next 0° ply. There was no evidence of any transverse cracking through the adjacent 90° ply. In general, the crack propagated near the edge of the 0° ply, close to the resin rich area between plys but always at least a few fiber diameters into the ply. In addition there was no evidence of fiber bridging.

DISCUSSION

It is difficult to draw general conclusions about Mode II propagation from these studies because of the rather specific loading conditions necessitated by the need to be able to pot the cracked specimens. The high loads required to initiate propagation of the unidirectional specimen resulted in fiber breakage which is not generally typical of Mode II testing. In addition, loading was not pure Mode II but mixed mode albeit predominantly Mode II. Indeed, as stated earlier, a pure Mode II crack should not be visible since there is no crack opening. The only crack that was purely Mode II was in the unidirectional specimen and, in fact, was difficult to discern (Fig 12)

Contrary to expectations, the Mode II crack did not propagate through the resin rich regions between plys in the cross-ply laminates. Instead, propagation was solely within the 0° plys near the boundary with the resin layer. This phenomena was encountered in a study of impact damage (6) as shown in Fig. 14. The explanation offered in reference 6 is that there are residual thermal stresses near the ply-resin boundary that make propagation within this boundary more energetically favorable than propagation in the resin layer.

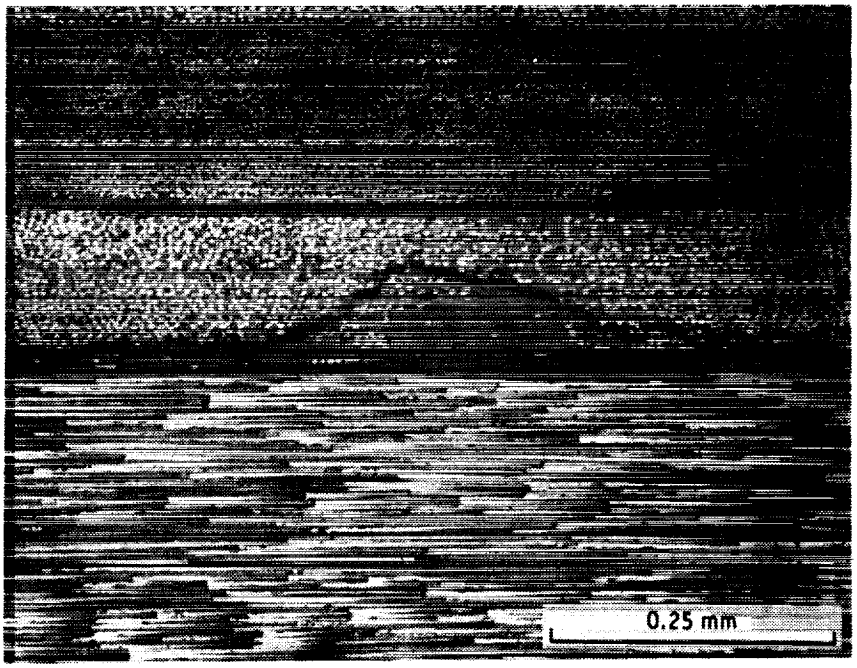

Figure 14 - Delamination produced by impact showing preferential propagation along the fiber/matrix boundary (reference 6).

No fiber cross-over was observed in any of the Mode II laminates. This fact suggests a lower crack resistance under Mode II loading than under Mode I loading. The Mode I study indicated fiber pull-out and fiber fracture as important energy dissipative effects which are evidently absent in Mode II cracking. Russel and Street (11) have presented evidence that crack propagation in Mode II occurs at a lower energy than in Mode I

IMPACT TESTS

INTRODUCTION

This part of the study was predicated on reports in the literature (12) that repetitive impact of a laminate specimen with increasing impact energy revealed changes in the type of impact damage, e.g., delamination vs fiber breakage. If correct, this technique would be a useful tool for determining the impact energy at which different damage modes occur for different laminate materials.

As shown in the following sections, the claims made in reference 12 are unfounded[b]. Instead, the changes in the response of the laminate to repetitive impact with increasing impact energy are the result of changes in the extent of damage rather than the type of damage. None the less, the results reported here revealed some subtle effects in the impact resistance of thermoset matrix laminates vs thermoplastic laminates, the effects of ply orientation, static vs dynamic loading, differences in laminate thickness and simple fatigue (repetitive impact at constant impact loading) vs repetitive impact with increasing impact energy (RIIE)

EXPERIMENTAL

Materials: Four different composite materials were studied, AS4/3501-6, IM6/3501-6, AS4/PEEK and AS4/polycarbonate. The manufacture, thickness and stacking sequence of the various

[b] We have learned of a manuscript being reviewed for publication that makes the same claims as in reference 12. The reviewer could not, of course, provide any further information.

specimens are summarized in Table 11. The AS4/3501-6 and IM6/3501-6 laminates were cured in an autoclave at the University of Utah, Mechanical & Industrial Engineering Dept. according to the manufacturer's recommended cure schedule. Each impact plate specimen was cut from a large panel (15cm x 15cm) to 5cm x 8cm dimension using a diamond cutting saw. For a 5cm x 8cm coupon, 1.5 cm at each end were clamped to the support so that the unsupported dimension was 5cm x 5cm. In order to measure the effect of sample dimensions on impact response, specimens with unsupported dimension of 10cm x 10cm were also tested. To investigate the effect of laminate thickness, 32 ply and 16 ply specimens were tested. Ultrasonic C-scan acoustic imaging available at Hercules Aerospace, Magna, Utah was used to check the quality of each panel before they were impacted and to determine the location of the damage after they were impacted.

Table II

Dimension and stacking sequence of composites

	Dimensions			Stacking Sequence
	# of Plies	Thickness (cm)	Size (cm)	
AS4/3501-6 *	32	0.435	10x10	(90/0) 16s
			5x5	(90/0) 16s and (±45) 16s
	16	0.23	5x5	(90/0) 8s
IM6/3501-6 *	32	0.435	5x5	(90/0) 16s and (±45) 16s
	16	0.24	5x5	(90/0) 8s
AS4/PEEK **	32	0.416	10x10	(90/0) 16s
			5x5	(90/0) 16s and (±45) 16s
AS4/Polycarbonate ***	32	0.512	5x5	(90/0) 16s and (±45) 16s

* Prepreg supplied by Hercules Aerospace (UT), panel fabricated at U of U
** Panels supplied by Fiberite
*** Panels supplied by NASA Langley Research Center

Impact Apparatus: The instrumented impact tester used in this study is similar to that described by Zoller (13). The free-fall drop weight is within a cylindrical drop tower as shown in Fig. 15 . When the drop weight bounces up, it is caught by a ratchet mechanism. This impactor consists of four main parts; load transducer, oscilloscope, IBM PC and printer. A piezoelectric crystal accelerometer (PCB Piezotronics 305A02) is mounted inside the drop weight. During the impact the output of the transducer is fed to a transient signal recorder. A Data Precision D6000 digital oscilloscope records the acceleration versus time during the impact event. The output is filtered using Fourier transformation to remove data above 7000 Hz. Then the data is back transformed to acceleration versus time. Fourier transforming the data reported here showed that a reproducible resonance between 7000 and 8000 was independent of sample size indicating it is a resonance frequency characteristic of the equipment and not of the test sample. However, due to a natural vibrational frequency of some of the composite specimens between 6000~7000 Hz, the cut-off filtering frequency could not be less than 7000 Hz.

Acceleration, a(t), is calculated from the digitized voltage-time information j(t) and the sensitivity of the accelerometer, s, in mv/g,

$$a(t)=1-(j(t)/s)$$

then velocity v(t) and displacement u(t) are obtained from,

$$v(t) = v_o + \int a(t)\, dt$$
$$u(t) = u_o + \int v(t)\, dt$$

Also the absorbed energy U(t) and the force exerted on the sample are obtained from,

$$U(t) = mgh_o - (1/2)\, m\, \{v_o^2 - v(t)^2\}$$
$$F(t) = m\, \{g - a(t)\}$$

The accuracy of the initial velocity measurement is important in calculating the absorbed energy and displacement(14). Impact velocity v_o was measured by two photoswitches. Finally the following data and plots are printed; percent of transferred energy,

ORIGINAL PAGE
BLACK AND WHITE PHOTOGRAPH

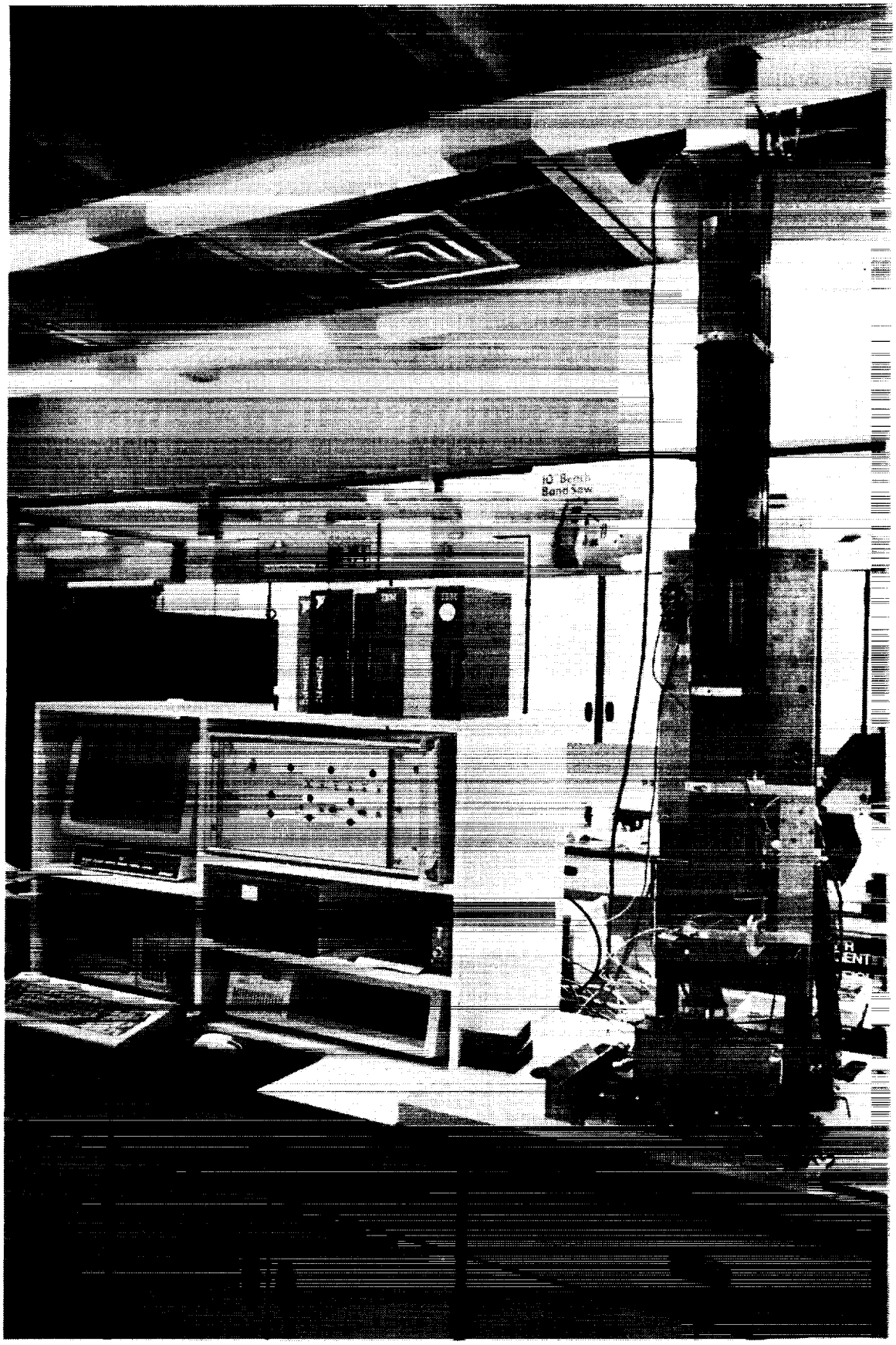

Figure 15 - Drop-weight impact test equipment.

impact energy, maximum force, maximum deflection, time of zero velocity, and impact time. Force *vs* displacement, energy *vs* time and amplitude of vibration verse frequency can also be plotted.

C-scan: Ultrasonic transmission C-scan was used to determine the overall panel quality and the location of damage. Ultrasonic equipment was available at Hercules Aerospace, Magna, Utah. Alcohol or an alcohol-water mixture acted as a coupling fluid between a piezoelectric transducer and the specimen.

Specimen sectioning and Damage Mapping: The impacted specimens were potted in an epoxy mixed with an amine curative and an amine accelerator to preserve the damage and were cured at room temperature over night. The epoxy mixture contained diglycidylether bisphenol A epoxy (Shell 828), polyamine (Jeffamine 230) and accelerator (Texaco 399) in the ratio of 10 : 5 : 1. Slices were cut from the sample at 0.075 inch (0.19 cm) intervals from the center of the damaged region (Fig.16). One face of each slice was polished sequentially with #320 and #400 grit papers followed by wet polishing with 1 μm and 0.3 μm Al_2O_3 paste on a velvet cloth. The polished surface was examined using reflected light microscopy for the type and extent of damage in each ply. Each of the damaged regions were plotted in three dimensions using a computer program (Appendix 2).

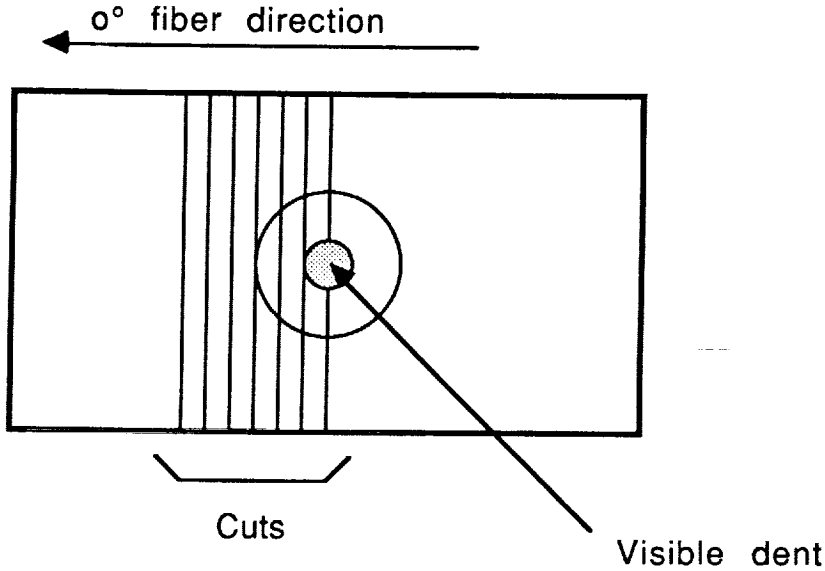

Figure 16 - Schematic of sectioning through the impact damage area.

Test Method: The repetitive drop weight test with increasing energy (RIIE) was performed by a repeated drop weight impact on the same spot of the same specimen with constant incrementally increasing impact energy. A similar procedure was used by Stellbrink (15,16). The specimen was clamped by two toggle clamps on steel support as shown in Fig. 17. The impact energy was increased by increasing the impactor height from 10cm to 72cm. The increment in height was 1cm, the weight of the impactor was 1085g and the impactor tip was hemispherical (radius 0.5 cm).

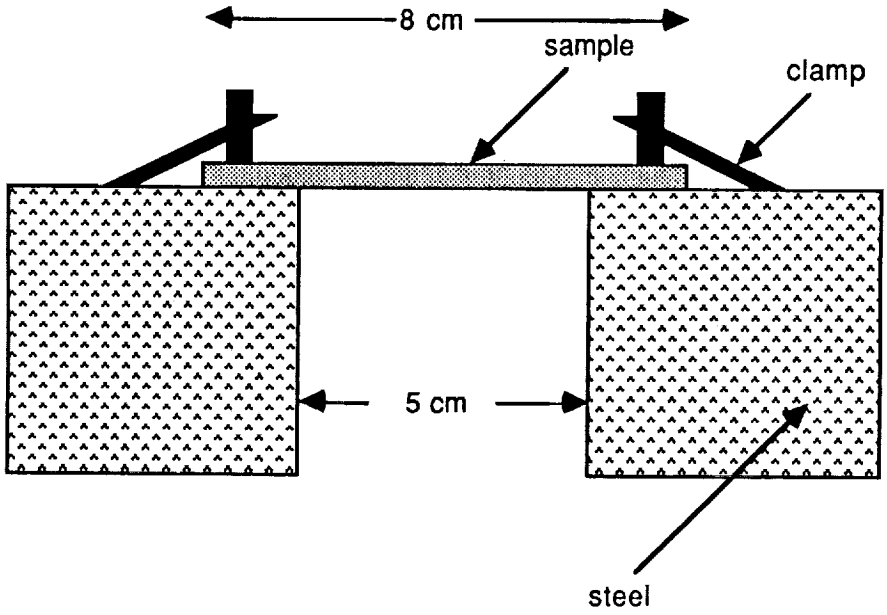

Figure 17 - Clamping arrangement of impact specimens

Fatigue impact tests were performed by repeatedly dropping an impact mass(1085g) at a fixed height(35cm).

Static tests were performed using a hydraulic powered test machine (MTS 800). The test conditions such as the specimen geometry, dimensions of the sample, clamping conditions and impact tip were the same as for the impact tests. The force was applied on each sample up to and beyond the elastic limit. These samples were then C-scanned, the damage area cut and sectioned. The sections were examined microscopically from which damage maps were constructed.

The post-impact residual tensile modulus was determined using the MTS test machine. The strain rate was 0.005mm/sec. Extensional stiffness was calculated from the slope of the load *vs* displacement plot.

RESULTS

AS4/3501-6 (0/90) laminate: The stiffness was calculated by two different methods. One was from the maximum force divided by the maximum deflection and the other was from the impact time, i.e., the stiffness k from the mass-spring model is given by $k=(m\pi^2)/t^2$ where m is the total mass (impactor + sample) and t the impact time. Stiffness *vs* accumulated impact energy (ΣI.E.) is shown in Fig.18 and percent of transferred energy *vs* cumulative impact energy (ΣI.E.) is shown in Fig.19. Three distinct stages of more or less constant stiffness were found, ~5200 N/mm, ~2100 N/mm and ~630 N/mm. The stiffness calculated by the two different methods gave essentially the same value.

In Fig.19, the percent of transferred energy of the first and second stages were 35%. The third stage showed an energy absorption of ~60%. There was a significant peak in the percent of transferred energy between stage one and two. This phenomena was observed for other laminate materials and geometries.

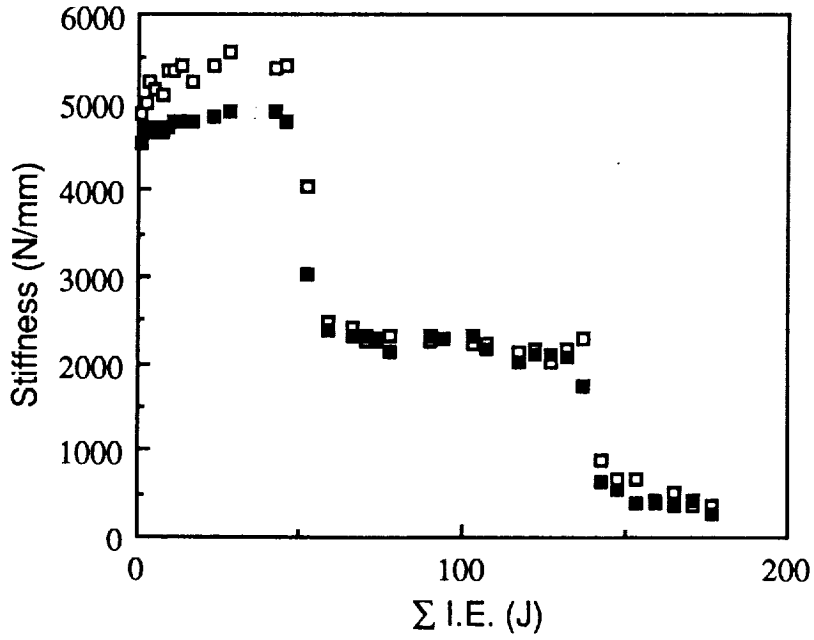

Figure 18 - Stiffness vs cumulative impact energy for AS4/3501-6, $(0/90)_{16s}$

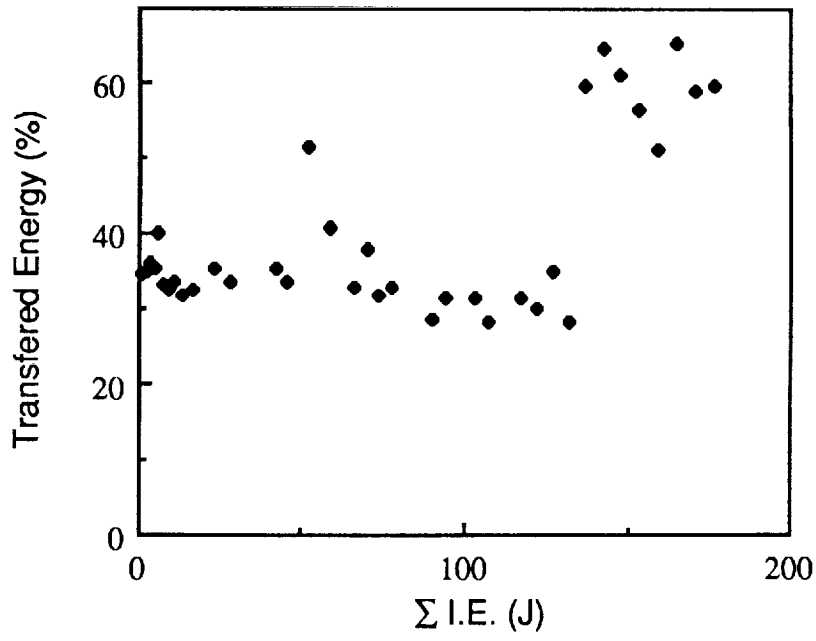

Figure 19 - Percent transfered energy vs cumulative impact energy for AS4/3501-6 $(0/90)_{16s}$

plotted in Fig.20. Curves a,b and c are respectively stages 1,2 and 3. The slope of each curve represents stiffness, and the area of each curve represents absorbed impact energy.

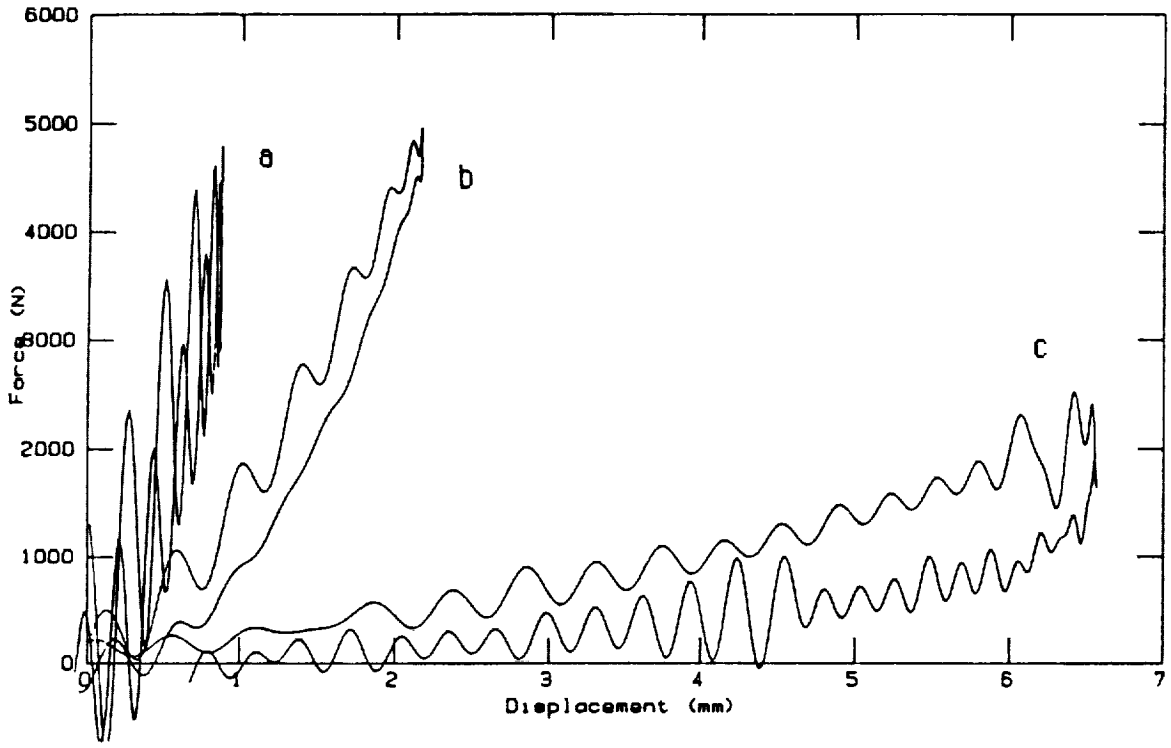

Figure 20 - Force vs displacement for AS4/3501-6,$(0/90)_{16s}$

These data clearly show the decrease in stiffness and increase in absorbed energy for the three stages. There was a large variation in the force during stage 1 (Fig.20a) which is probably the result of elastic vibrational noise.

C-scans were taken of impacted specimens selected from each of the stages. The specimens were then sectioned and damage maps generated. Figure 21 are C-scans of stages 1, 2 and 3. The damage maps of each stage are presented in Fig.22-24.

a

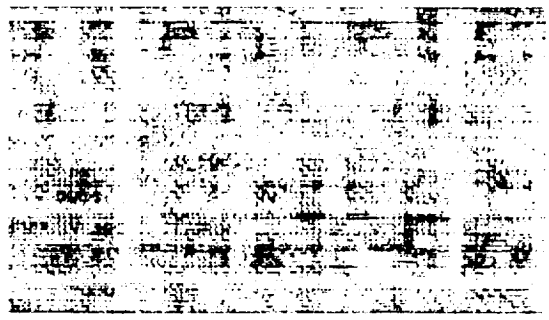

b

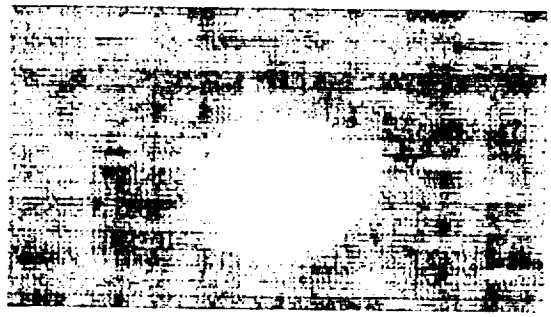

c

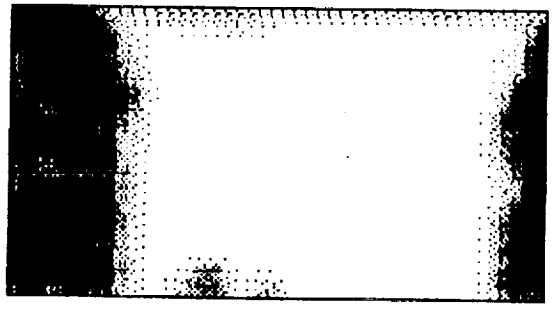

Figure 21 - C-scans of impact damage in AS4/3501-6, $(0/90)_{16s}$ after Σ I. E. at10J (a), 80J (b) and 170J (c).

In the first stage obtained after 7 impacts, the damage was concentrated on the front surface (Fig. 22) and the amount of the damage was very small. Only a few transverse cracks were found. The damage at this stage from the C-scan was hardly detectable (Fig. 21a).

In the second stage, the damage was through the thickness of the sample (Fig.23) and the C-scan clearly showed a damaged area (Fig. 21b). Most damage was transverse cracking and delamination in the 90° plies as shown in Fig. 25a.

In the third stage, the damage had propagated to the edges of the sample (Fig. 21c) and fiber breakage was observed (Fig. 25b).

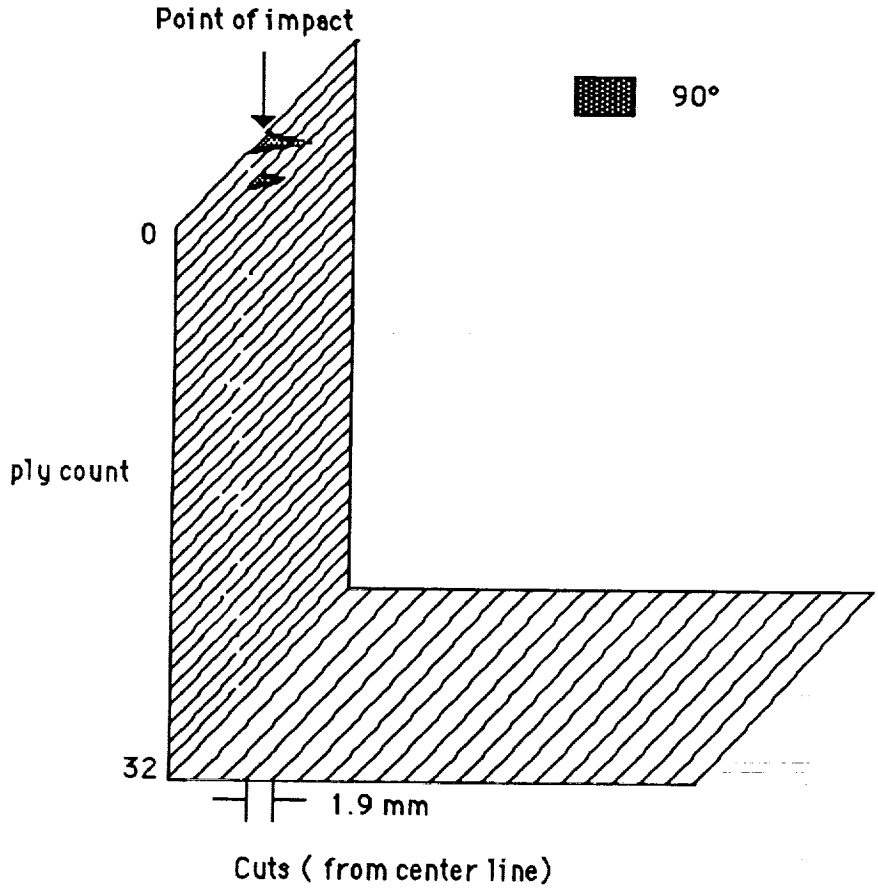

Figure 22 - Damage map of AS4/3501-6, $(0/90)_{16s}$ after Σ I.E. = 10J.

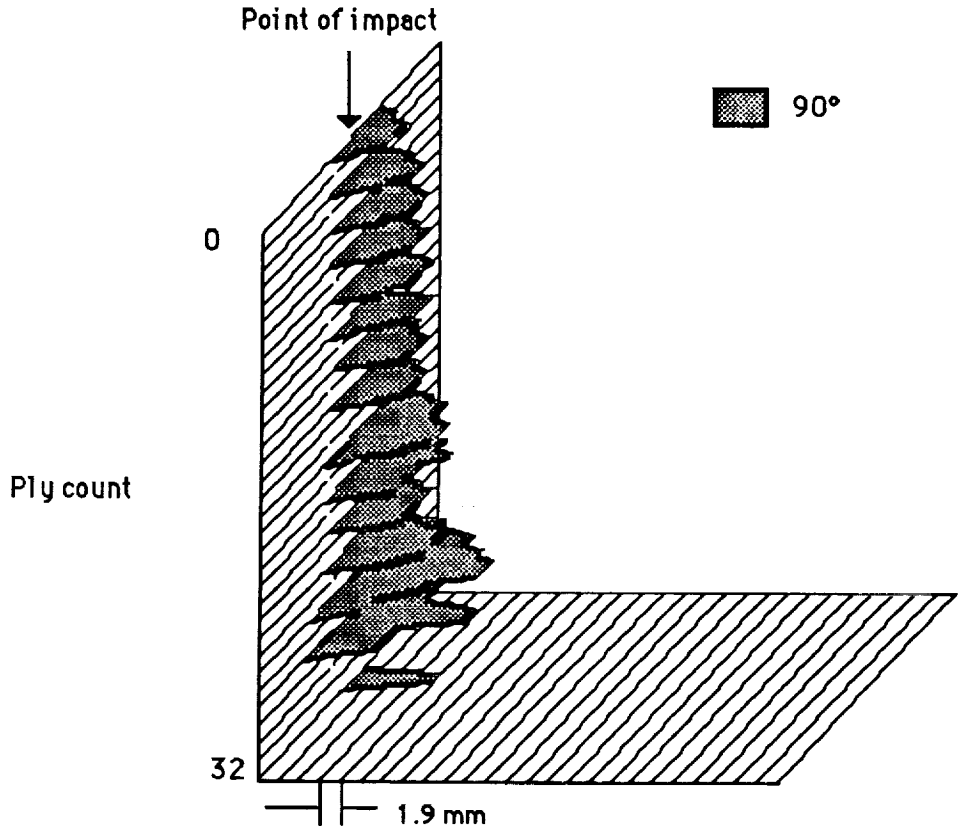

Figure 23 - Damage map of AS4/3501-6, $(0/90)_{16s}$ after Σ I.E. = 80J.

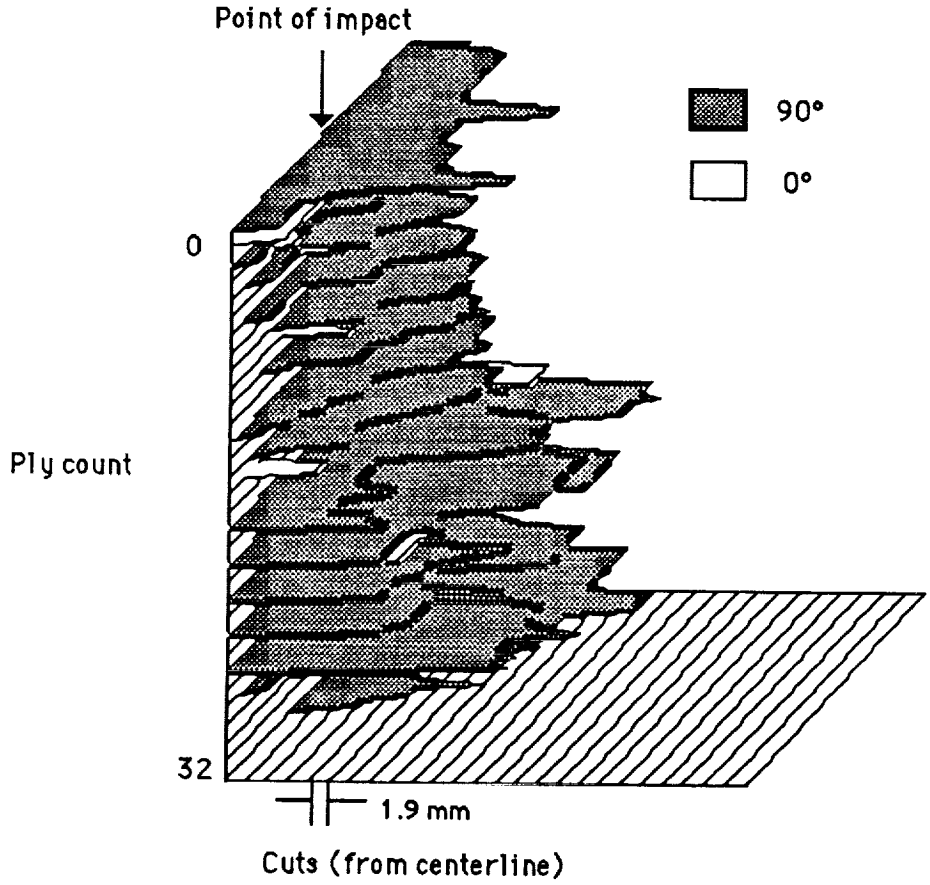

Figure 24 - Damage map of AS4/3501-6, $(0/90)_{16s}$ after Σ I.E. = 170J.

A

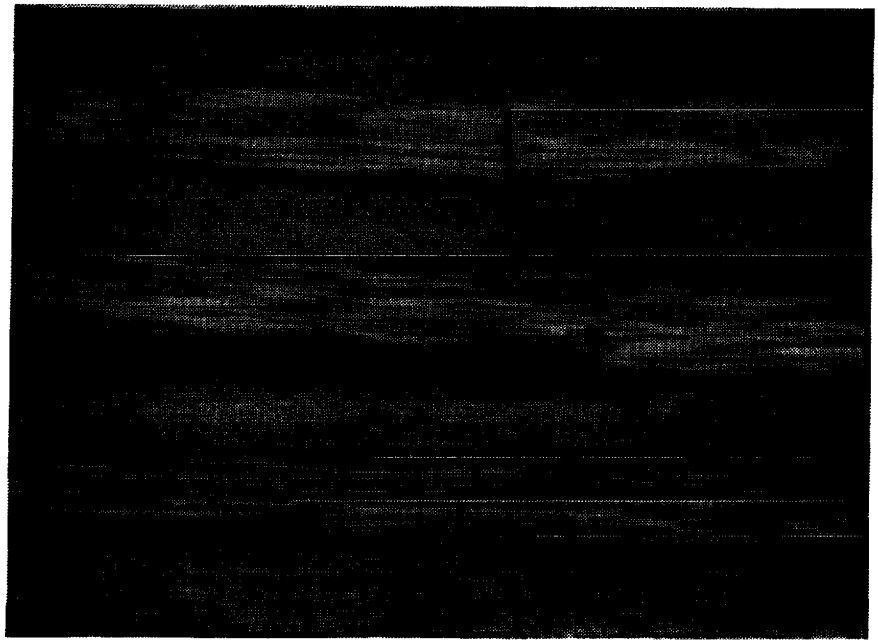

B

Figure 25 - Photomicrographs (80X) of impact damage after Σ I. E. = 30J (A) and 150J (B)

AS4/3501-6 (± 45°) Laminates: Very similar results were obtained for laminates with (± 45°) fiber orientation. The stiffness vs cumulative impact energy and the percent transfered energy vs cumulative impact energy are shown in Figs. 26 and 27.

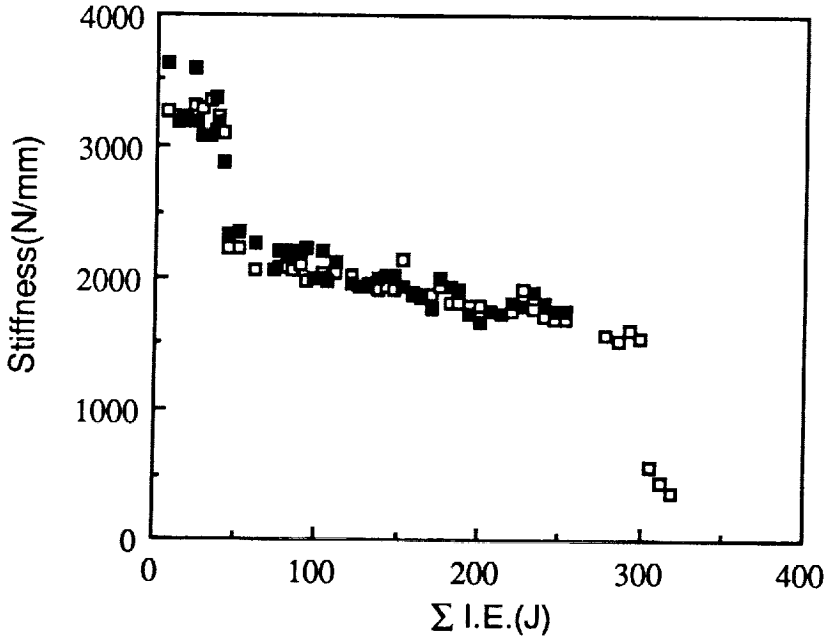

Figure 26- Stiffness vs cumulative impact energy for AS4/3501-6, $(\pm 45)_{16s}$

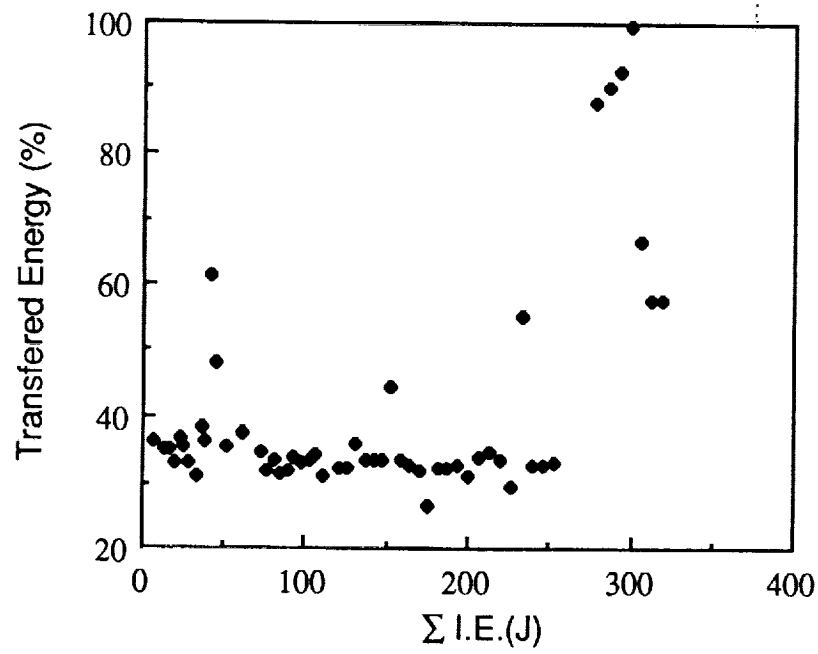

Figure 27 - Percent transfered energy vs cumulative impact energy for AS4/3501-6 $(\pm 45)_{16s}$

The second stage in the stiffness plot extended to higher cumulative impact energies and the third stage was not as clearly defined compared to the (0/90) laminate. The second stage corresponded to through the thickness damage as shown by the damage map in Fig 28. This damage extended to the edges of the laminate after a Σ I. E. of 300 J (Fig. 29)

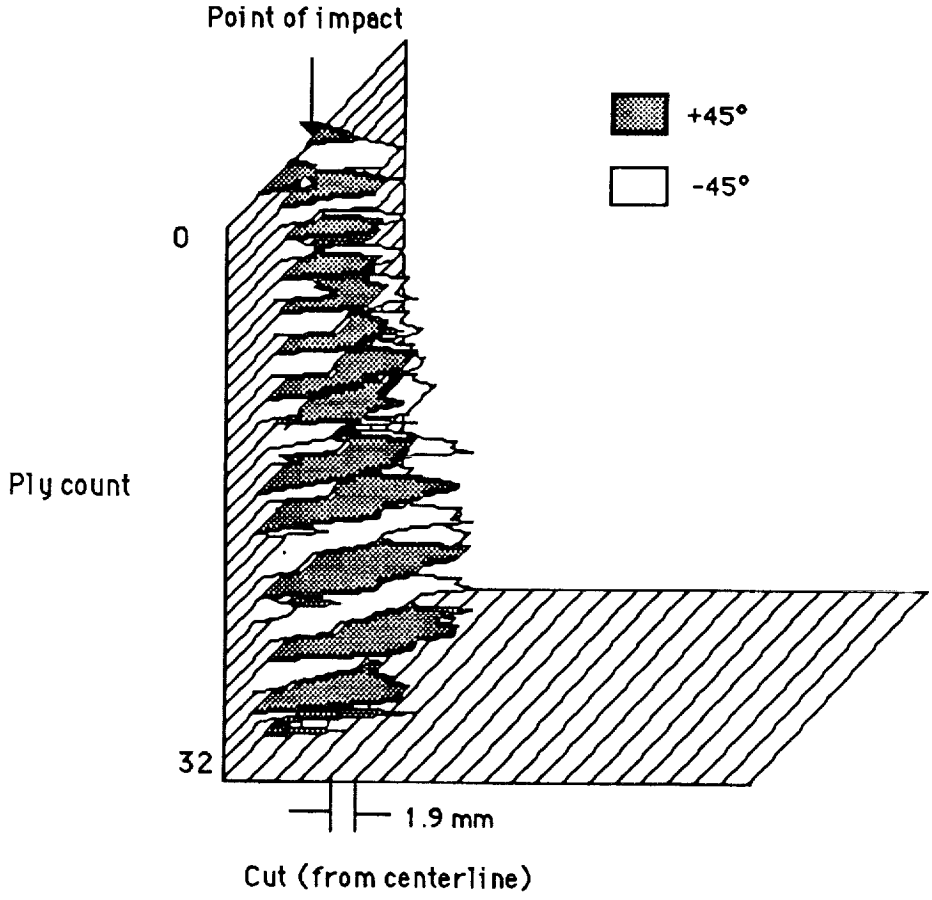

Figure 28 - Damage map of AS4/3501-6, $(\pm 45)_{16s}$ after Σ I.E. = 80J.

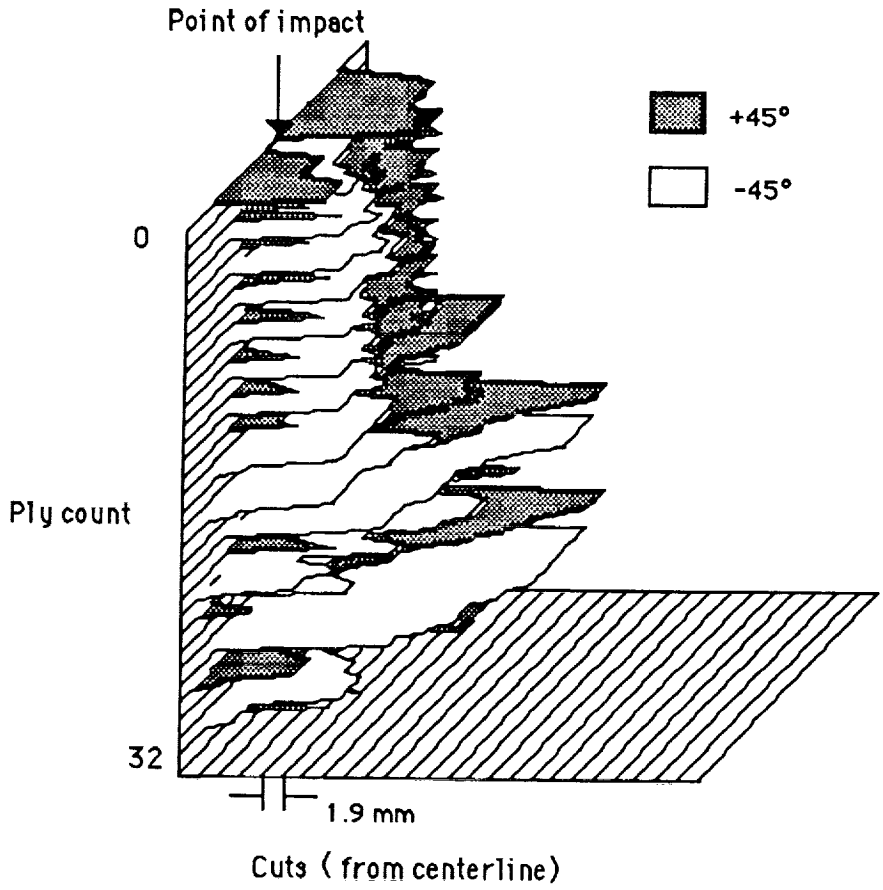

Figure 29 - Damage map of AS4/3501-6, $(\pm 45)_{16s}$ after Σ I.E. = 310J.

IM6/3501-6 (0/90) and IM6/3501-6 (±45) Laminates: The stiffness and percent transfered energy vs cumulative impact energy for IM6/3501-6, (0/90) and (±45) are presented in Figs 30 and 31. Three distinct stages were observed in the stiffness plot for the (0/90) laminate (Fig 30) and as with the AS4 materials the second and third stage corresponded to through the thickness damage and extension of the damage to the edges of the specimen. The corresponding damage maps are shown in Figs 32 and 33.

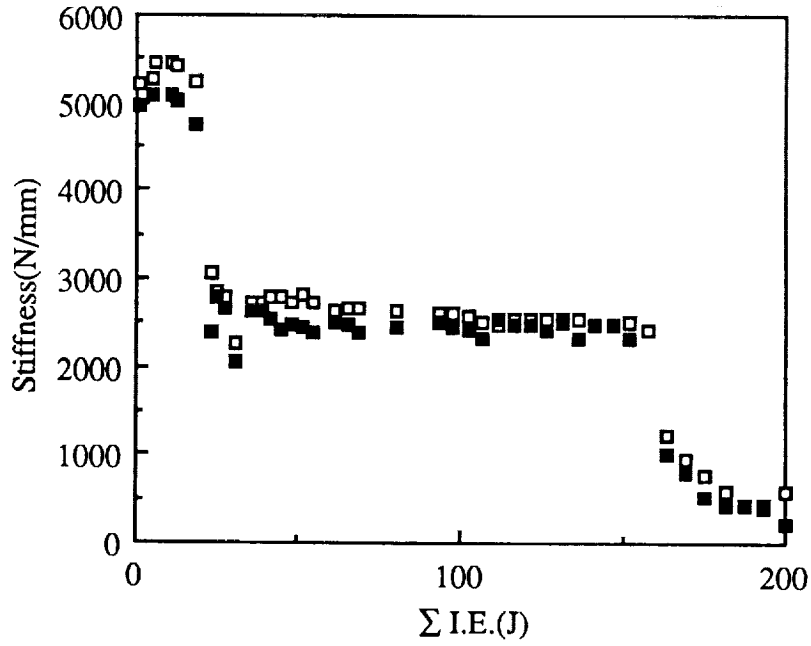

Figure 30A - Stiffness vs cumulative impact energy for IM6/3501-6, $(0/90)_{16s}$

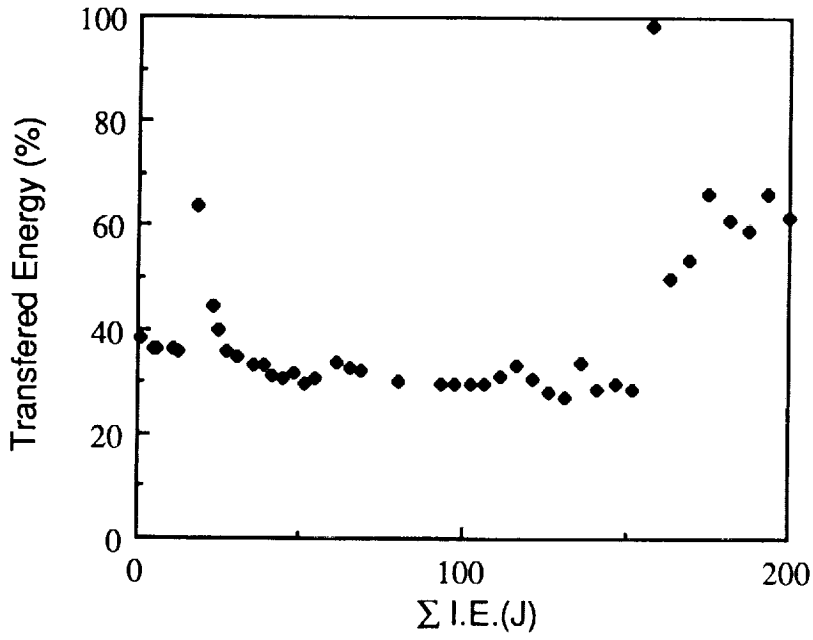

Figure 30B - Percent transfered energy vs cumulative impact energy for IM6/3501-6 $(0/90)_{16s}$

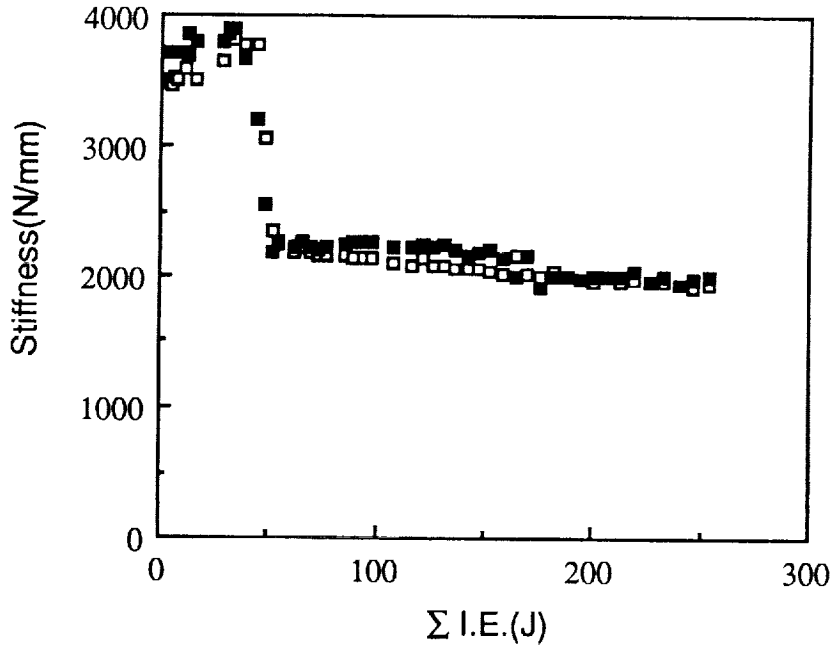

Figure 31A - Stiffness vs cumulative impact energy for IM6/3501-6, $(\pm 45)_{16s}$

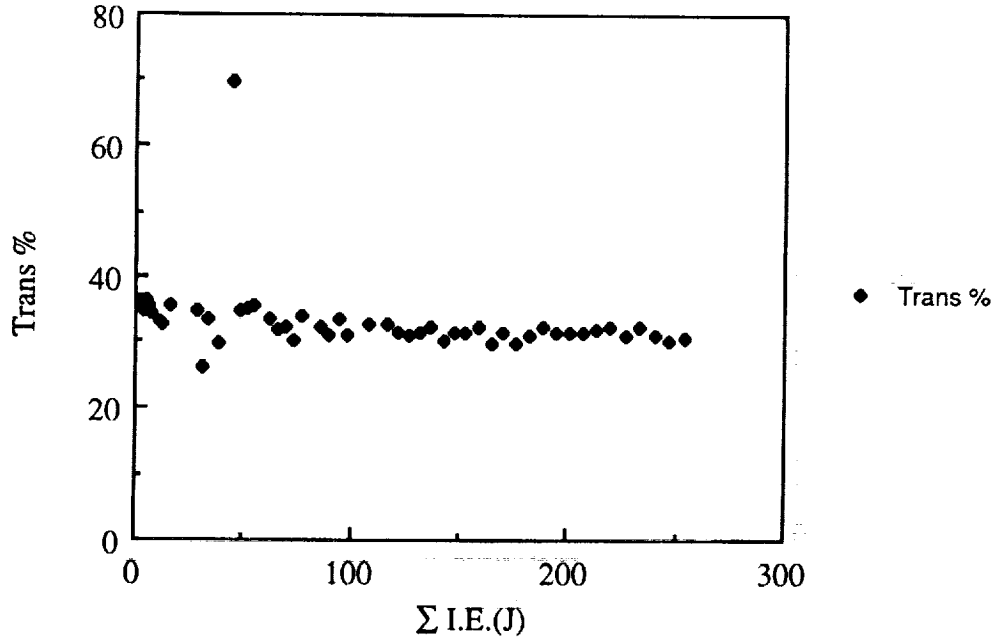

Figure 31B - Percent transfered energy vs cumulative impact energy for IM6/3501-6 $(\pm 45)_{16s}$

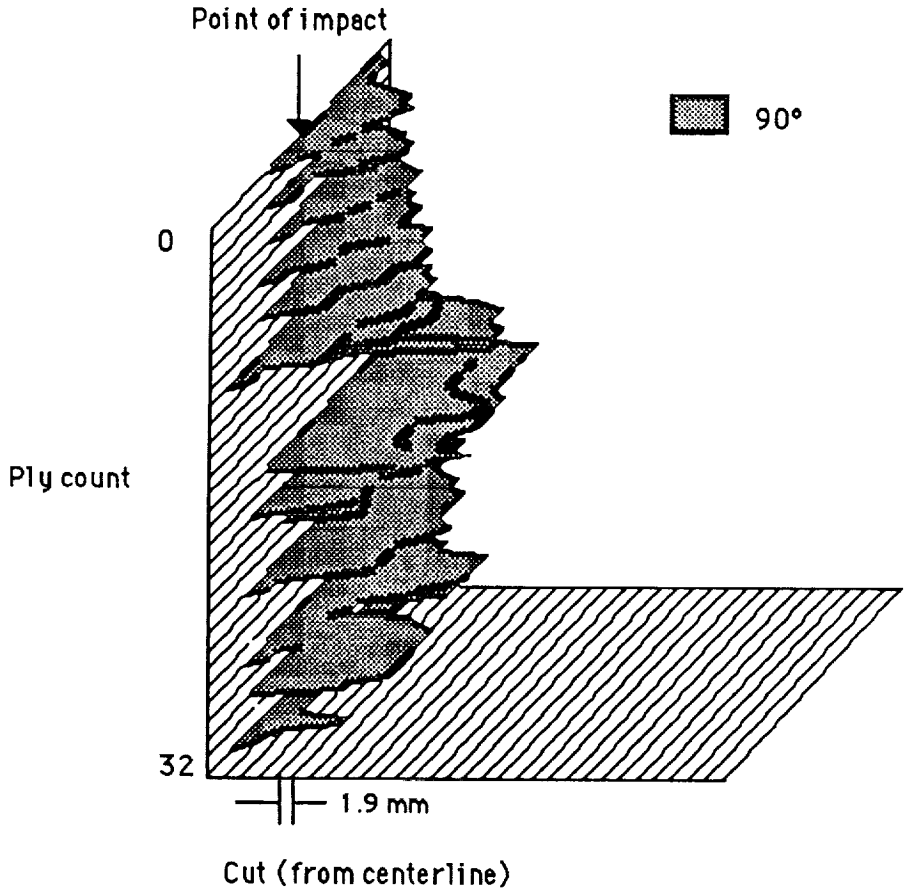

Figure 32 - Damage map of IM6/3501-6, $(0/90)_{16s}$ after Σ I.E. = 110J.

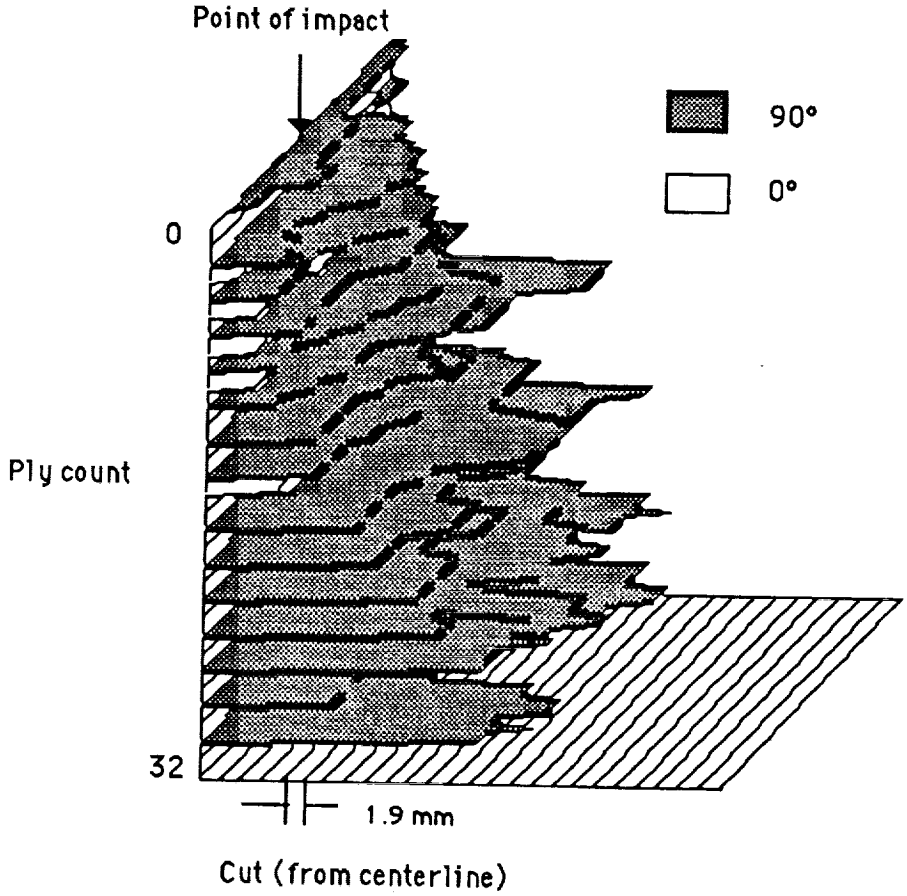

Figure 33 - Damage map of IM6/3501-6, $(0/90)_{16s}$ after Σ I.E. = 190J.

In the case of the (±45) laminate the cumulative impact energy was not taken to a high enough level to develop a third stiffness plateau (Fig. 31A).

AS4/PEEK (90/0) Laminate: Figure 34A and 34B present the stiffness and percent of transferred energy *vs* Σ I.E. for AS4/PEEK (0/90) laminates respectively. Unlike the results with the 3501-6 matrix laminates there were no distinct stages of relatively constant stiffness except for an initial plateau. Up to 80J of Σ I.E., the stiffness was about 4300N/mm and the percent of transferred energy between 30-40% (Fig.34B). Subsequently, the stiffness started to decrease gradually with high energy absorption (~70%) and the percent of transferred energy was very scattered compared with the 3501-6 materials The stiffness calculated from maximum force divided by maximum deflection was more scattered than that calculated from impact time (Fig.34A). The last impact showed almost zero stiffness and about 100% of energy absorption. The load *vs* displacement curves are plotted in Fig.35.

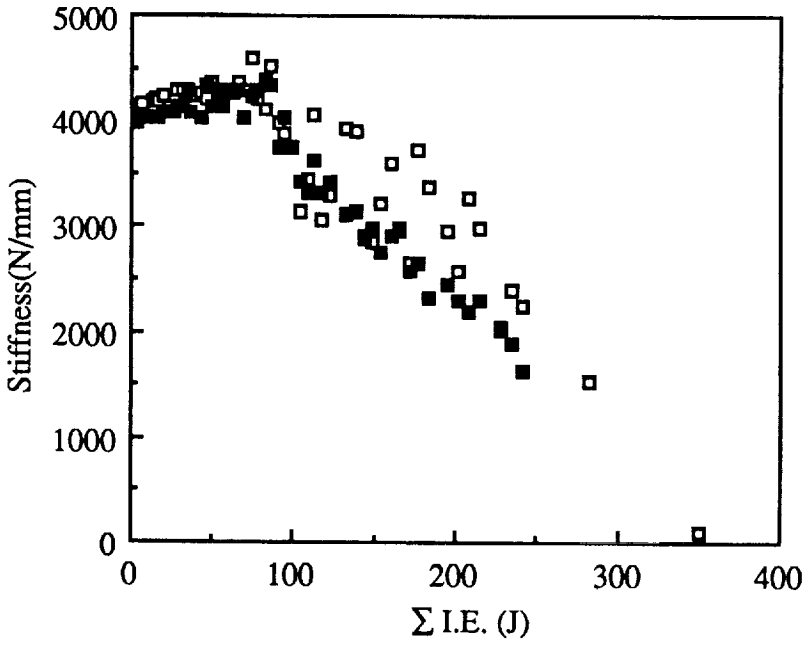

Figure 34A - Stiffness vs cumulative impact energy for AS4/PEEK, $(0/90)_{16s}$

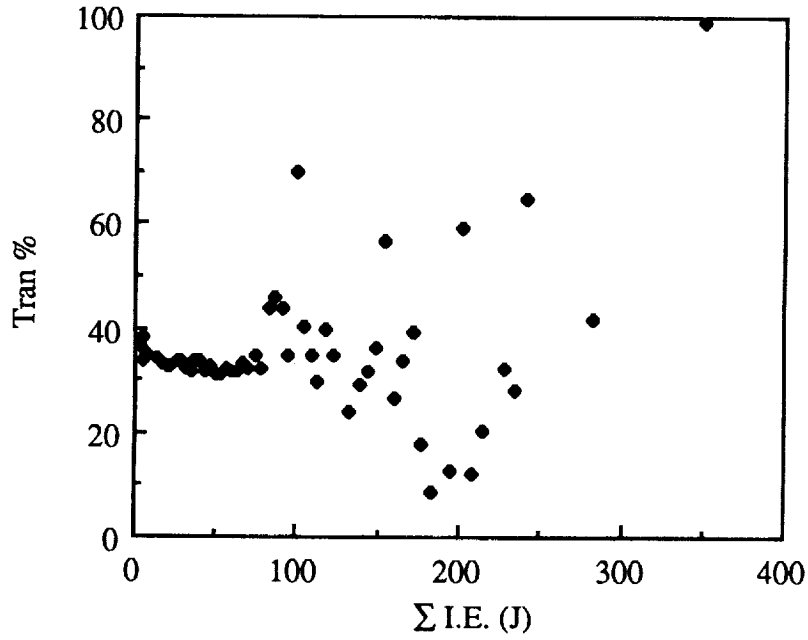

Figure 34B - Percent transfered energy vs cumulative impact energy for AS4/PEEK, $(0/90)_{16s}$

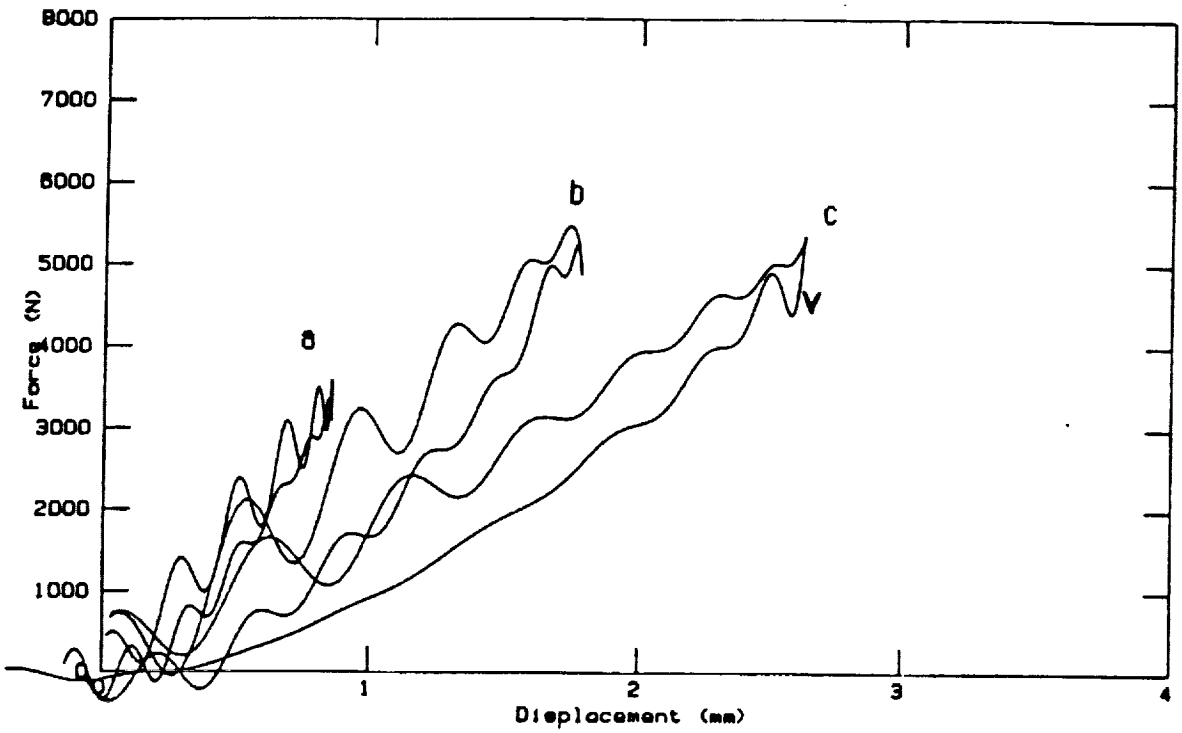

Figure 35 - Force vs displacement plots for AS4/PEEK,$(0/90)_{16s}$ at Σ I.E. of 50J (a), 150J (b) and 230J (c).

The results of the C-scans are given in Fig. 36 and the damage maps in Figs. 37, 38 and 39. In the initial stage (Σ I.E.= 35 J), the damage was small but clearly evident from the C-scan. (This C-scan was done at a higher impact energy than for the corresponding AS4/3501-6 laminate.) The map shows that damage was confined to the front and back plies. and was primarily transverse cracking. Damage at a Σ I.E. of 115 (J) was more localized compared to the 3501-6 systems. The major damage was in the mid plane of the laminate (Fig.38) and usually consisted of transverse-cracking and delamination (Fig.40) as well as some fiber breakage (Fig.41).

a

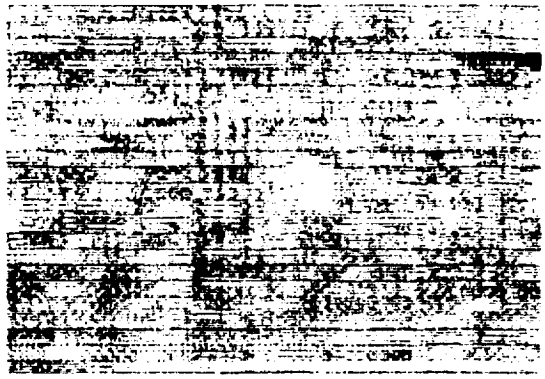

b

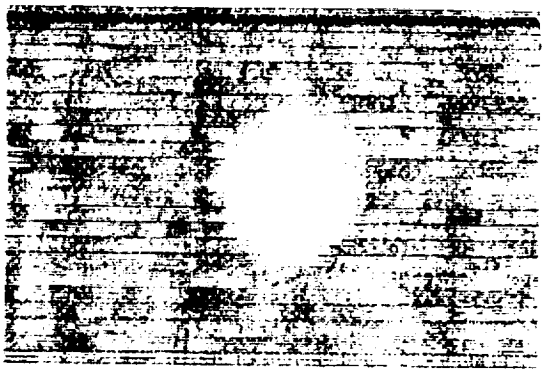

c

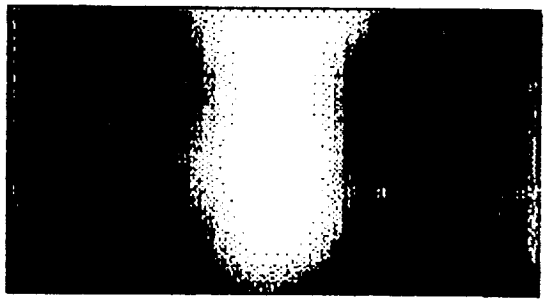

Figure 36 - C-scans of impact damage in AS4/PEEK,$(0/90)_{16s}$ at Σ I.E. 35J(a), 115J (b) and 280J (c)

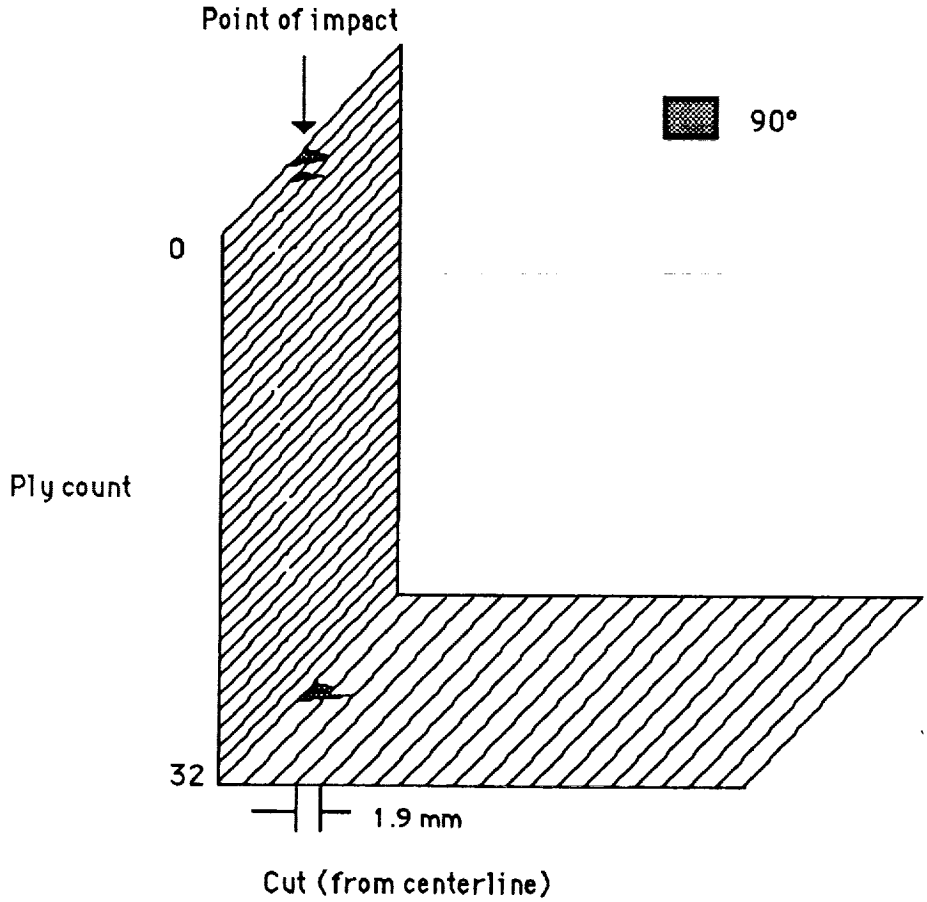

Figure 37 - Damage map of AS4/PEEK, $(0/90)_{16s}$ after Σ I.E. = 35J.

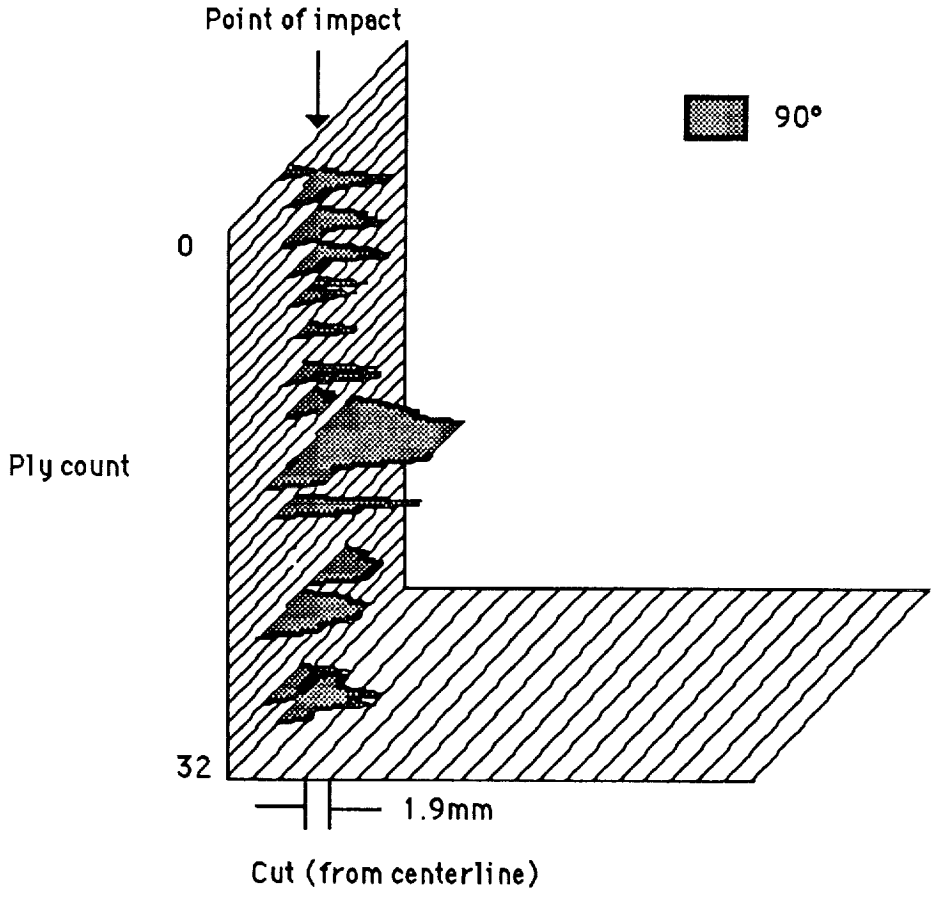

Figure 38 - Damage map of AS4/PEEK, $(0/90)_{16s}$ after Σ I.E. = 115J.

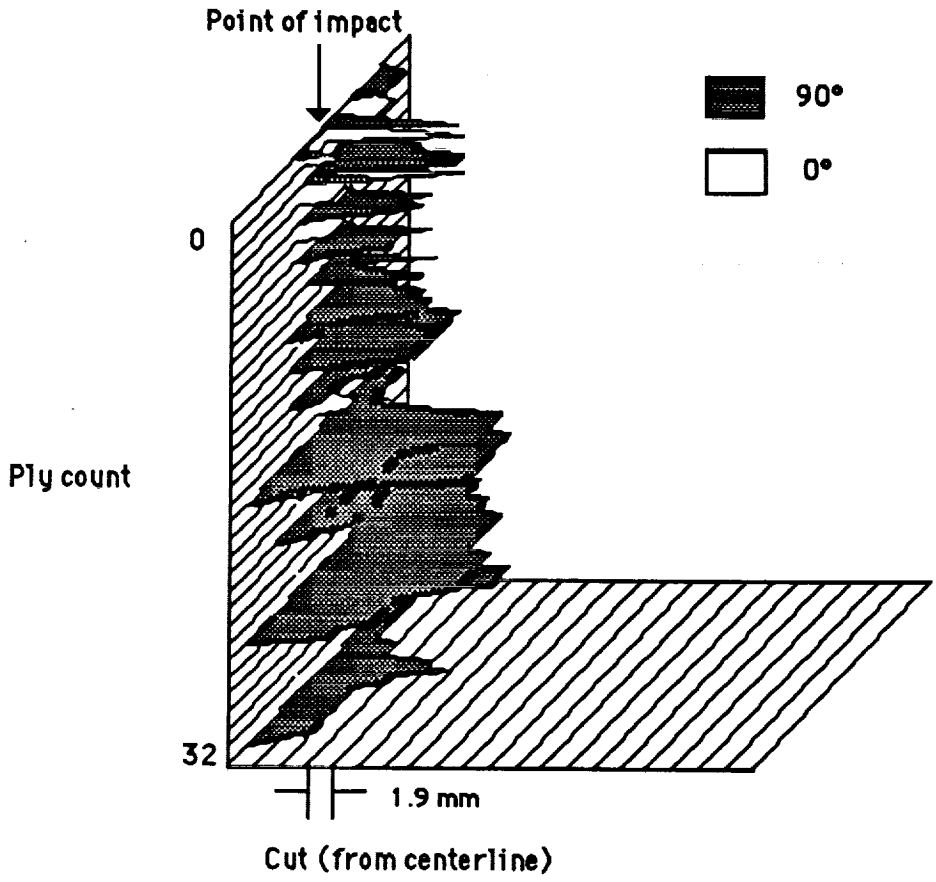

Figure 39 - Damage map of AS4/PEEK,$(0/90)_{16s}$ at ΣI.E.= 280 J

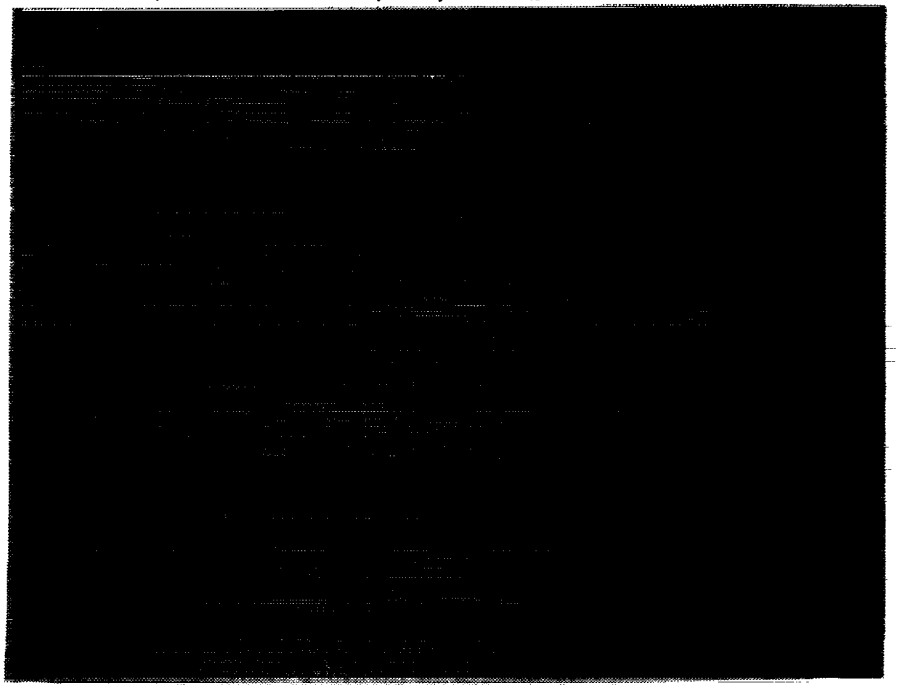

Figure 40 - Damage of AS4/PEEK, $(0,90)_{16s}$ at Σ I. E. = 115J (80X)

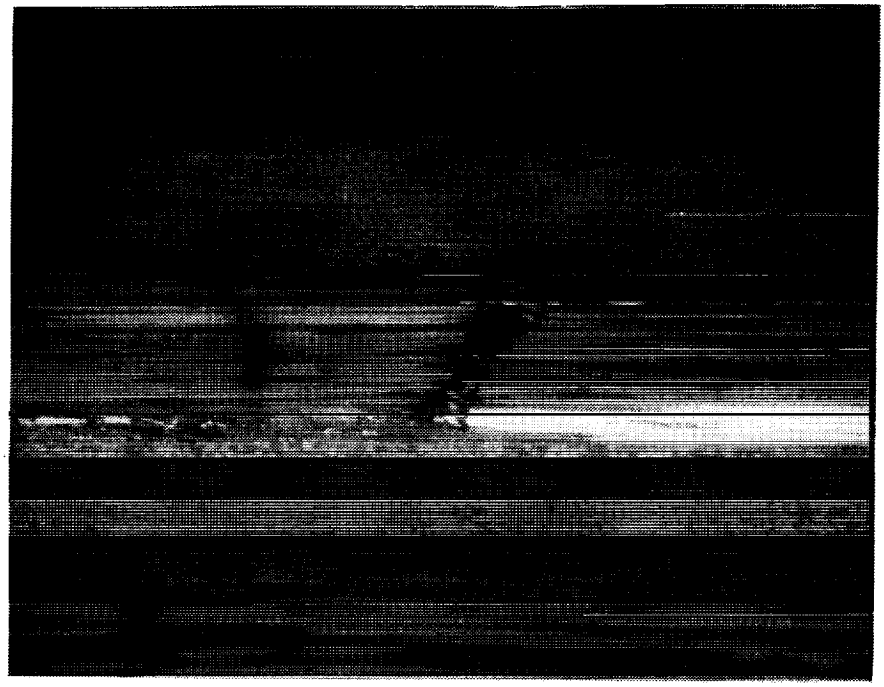

Figure 41 - Damage of AS4/PEEK, $(0,90)_{16s}$ at Σ I. E. = 115J (80X)

Damage at Σ I.E. of 280 (J) extended to the edge of the sample but was confined to the midsection (Fig.36c) whereas in the 3501-6 matrix laminate the damage spread more or less uniformly. Extensive fiber breakage was observed (Fig.42).

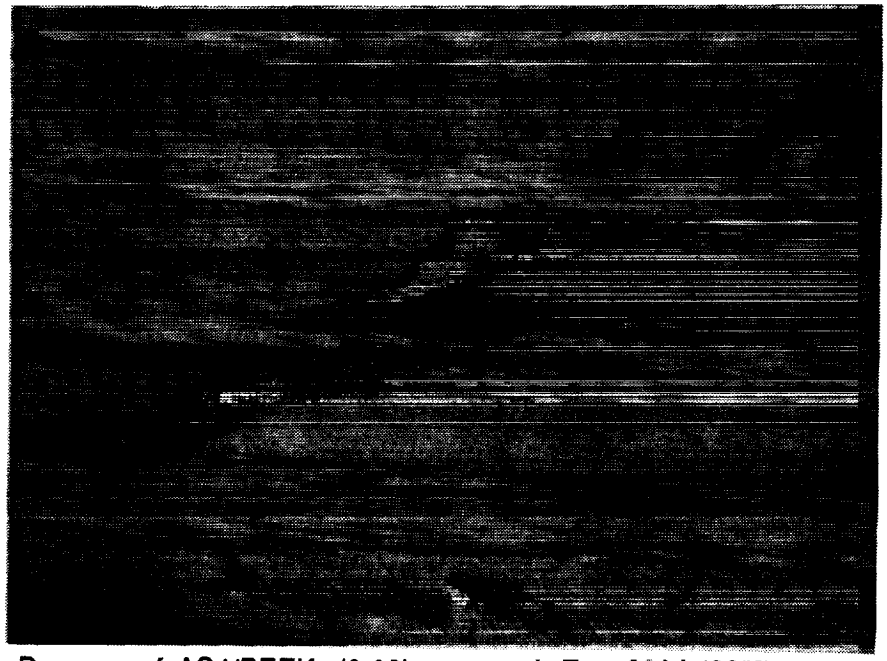

Figure 42 - Damage of AS4/PEEK, $(0,90)_{16s}$ at Σ I. E. = 280J (80X)

AS4/PEEK (±45) Laminate: Stiffnesses and percent transferred energy *vs* Σ I.E. are presented in Fig 43. In the initial plateau, the stiffness was about 3000 N/mm which was less than for the (90/0) orientation but extended over a wider range of Σ I.E. Then the stiffness started to decrease at a higher energy absorption but the rate of decrease was lower.

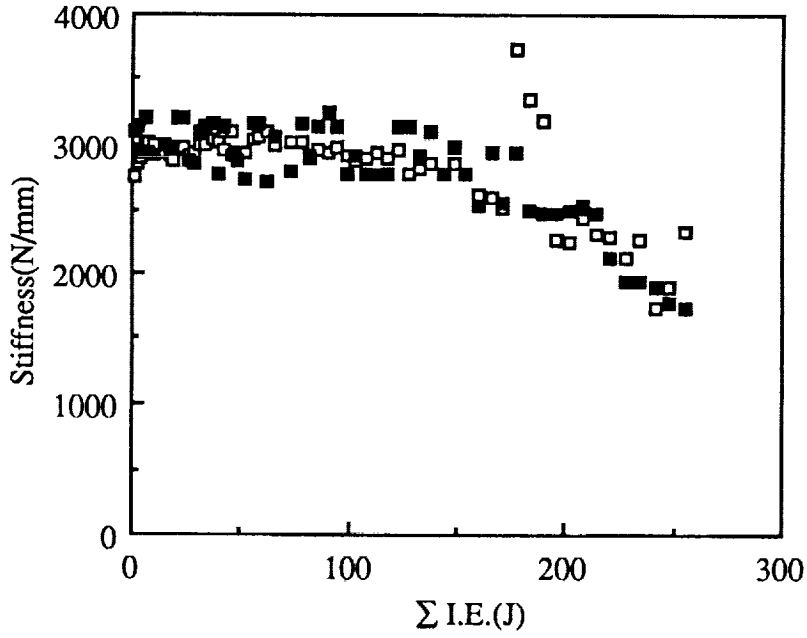

Figure 43A - Stiffness vs cumulative impact energy for AS4/PEEK, $(\pm 45)_{16s}$

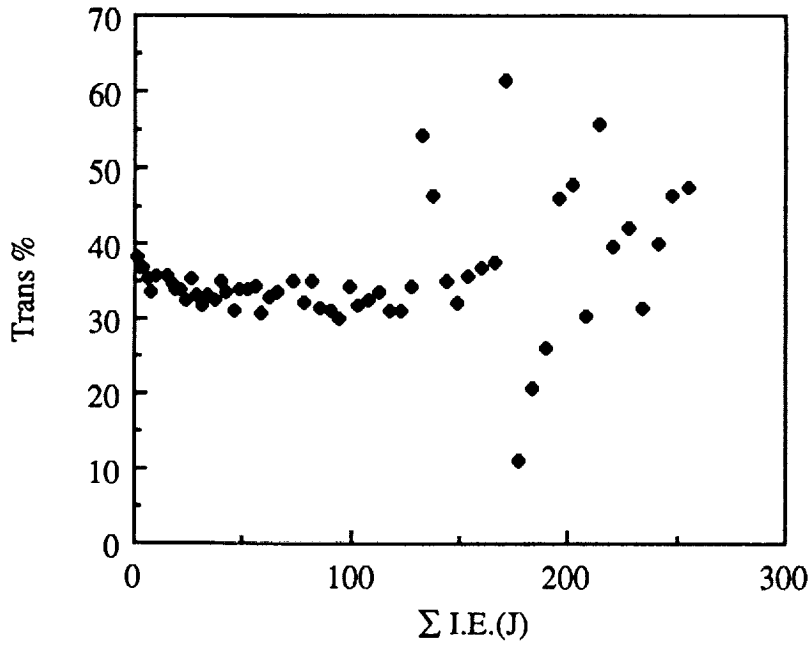

Figure 43B - Percent transfered energy vs cumulative impact energy for AS4/PEEK, $(\pm 45)_{16s}$

A C-scan at ΣI.E of 250 J is shown in Fig. 44 and a corresponding damage map in Fig. 45. The damage was confined to the center of the laminate and through the thickness. The tests were not conducted beyond 250J.

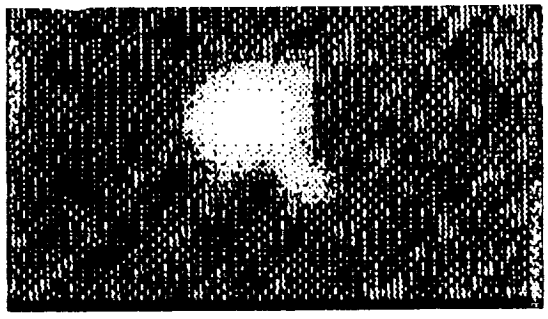

Figure 44 - C-scan of impact damage of AS4/PEEK, (±45) at Σ I. E. = 250J

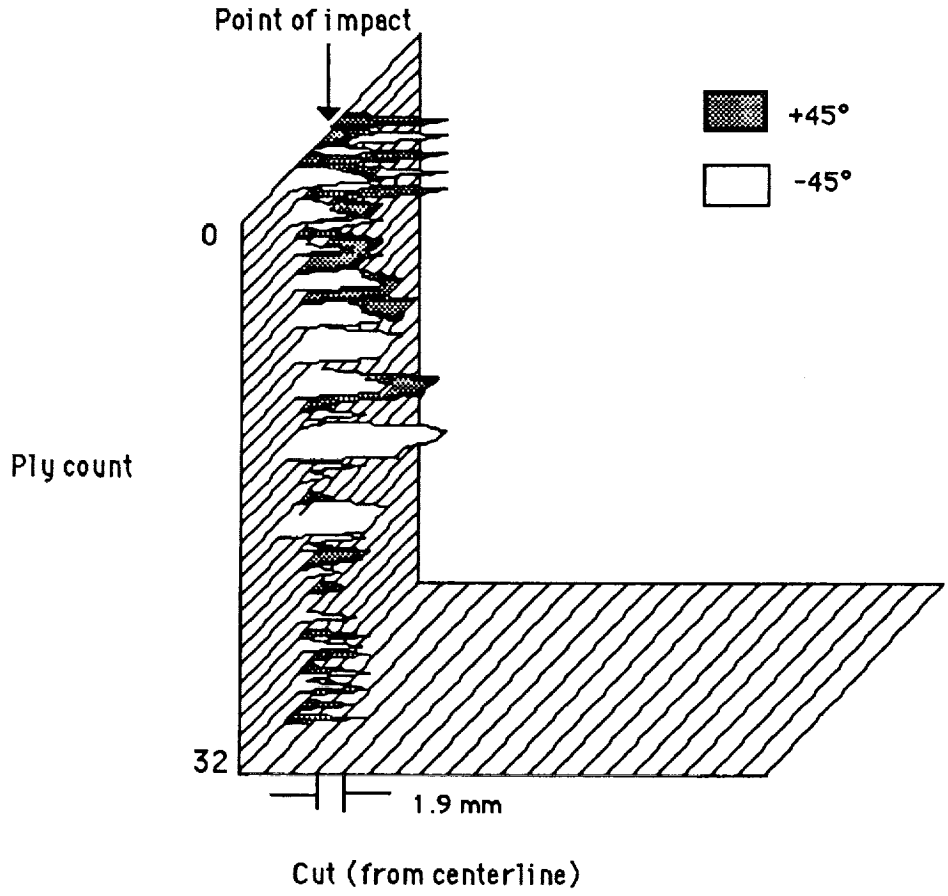

Figure 45 - Damage map of AS4/PEEK, (±45) at Σ I.E. = 240J

AS4/polycarbonate (90/0) Laminate: Figure 46 presents the stiffness and percent transferred energy *vs* ΣI.E.. Initially the stiffness gradually increased from 4000 N/mm to 5300 N/mm and then started to slowly decrease at about 150 J (Fig.57).

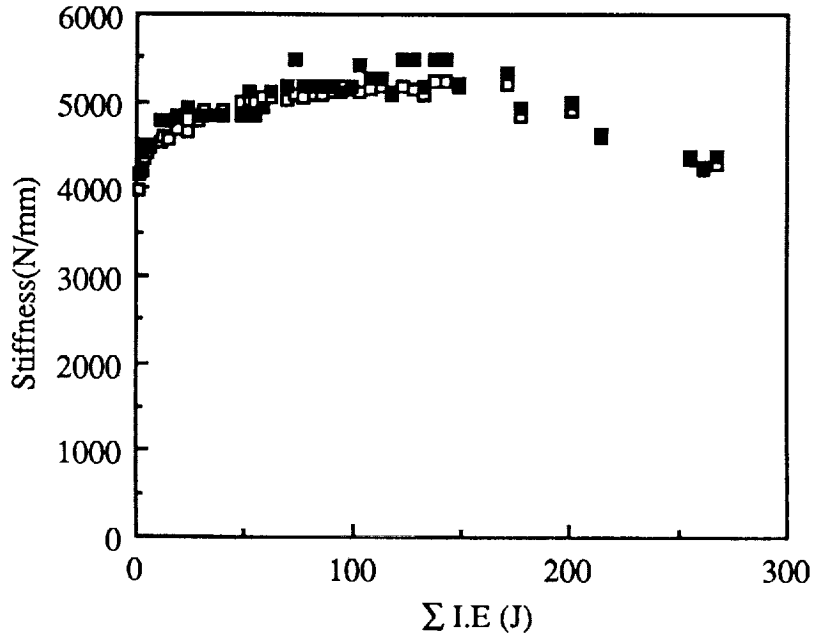

Figure 46A - Stiffness vs cumulative impact energy for AS4/polycarbonate, $(0/90)_{16s}$

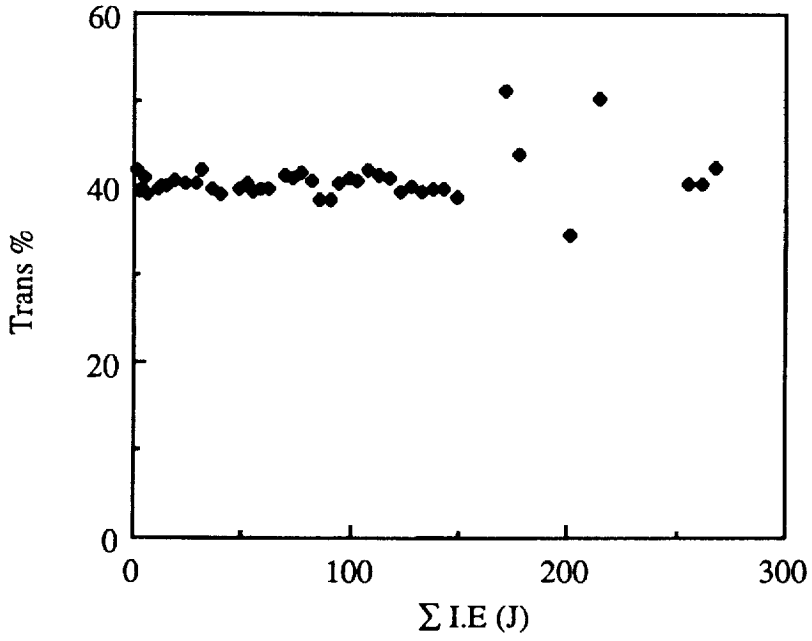

Figure 46B - Percent transfered energy vs cumulative impact energy for AS4/polycarbonate, $(0/90)_{16s}$

The C-scan and the damage map at Σ I.E. of 270 J are shown in Figs.47 and 48 respectively. The damage was highly localized and restricted to the front and the back plys. Some fiber breakage was observed. This material appears to be more damage resistant than the other composite materials in these tests.

Figure 47 - C-scan of impact damage of AS4/polycarbonate, $(0/90)_{16s}$ at Σ I. E. = 270J

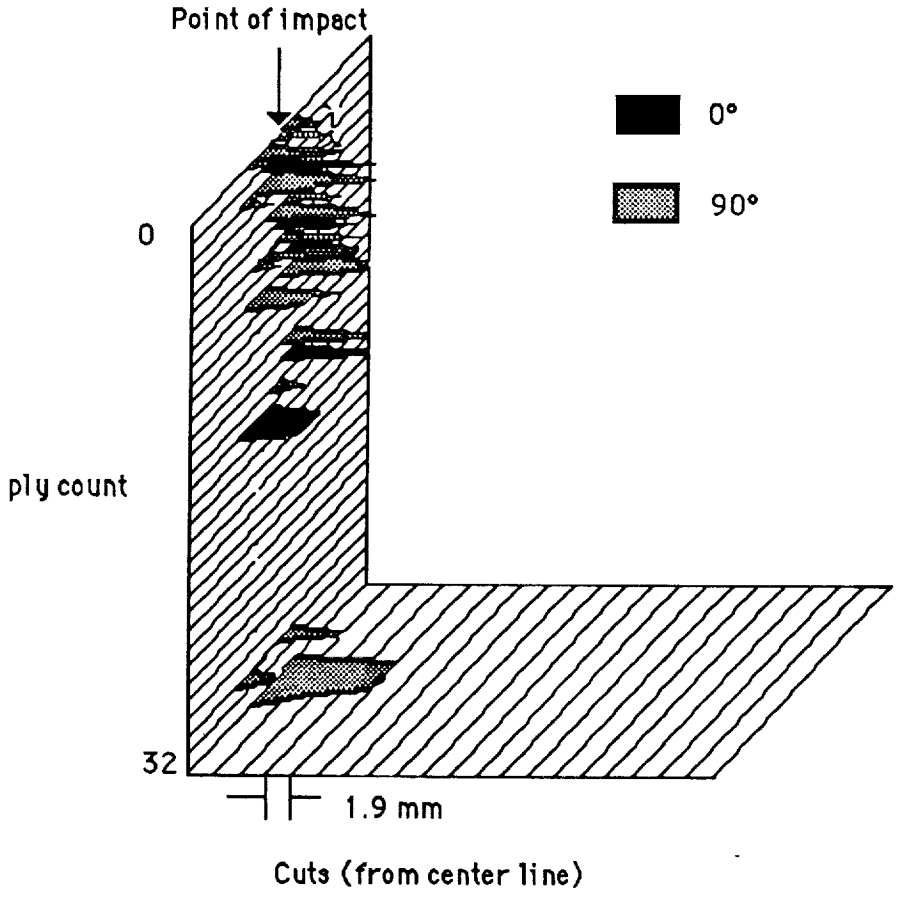

Figure 48 - Damage map of AS4/polycarbonate, $(0/90)_{16s}$ at Σ I. E. = 270J

AS4/polycarbonate(±45) laminate: Stiffness and percent transferred energy vs ΣI.E are shown in Fig.49. A C-scan and damage map for ΣI.E of 250J are presented in Figs. 50 and 51 respectively. The reduction in stiffness and the extent of damage were even less than for the (0/90) laminate.

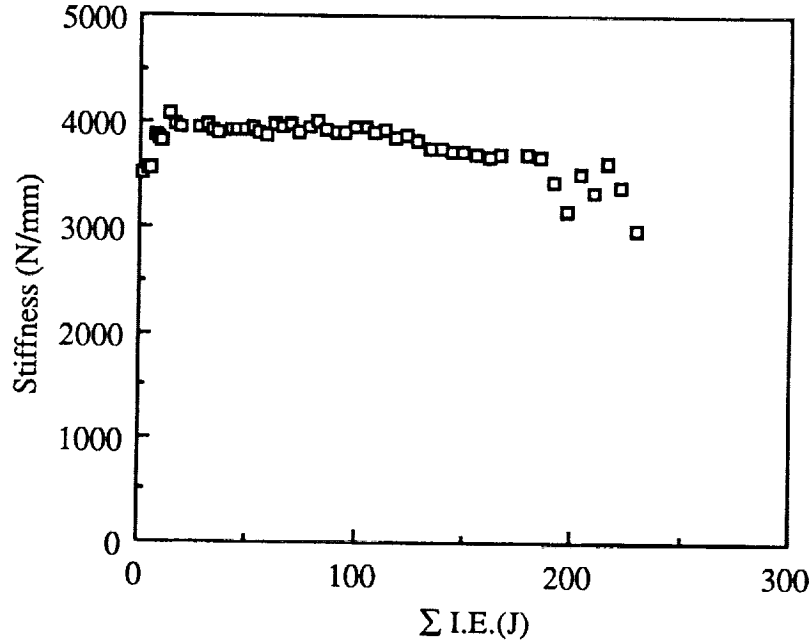

Figure 49A - Stiffness vs cumulative impact energy for AS4/polycarbonate, $(\pm 45)_{16s}$

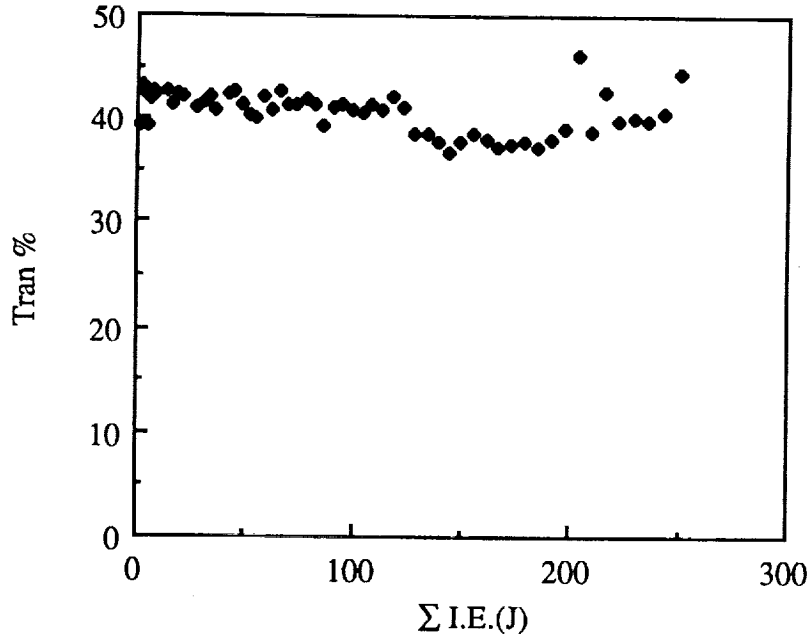

Figure 49B - Percent transfered energy vs cumulative impact energy for AS4/polycarbonate $(\pm 45)_{16s}$

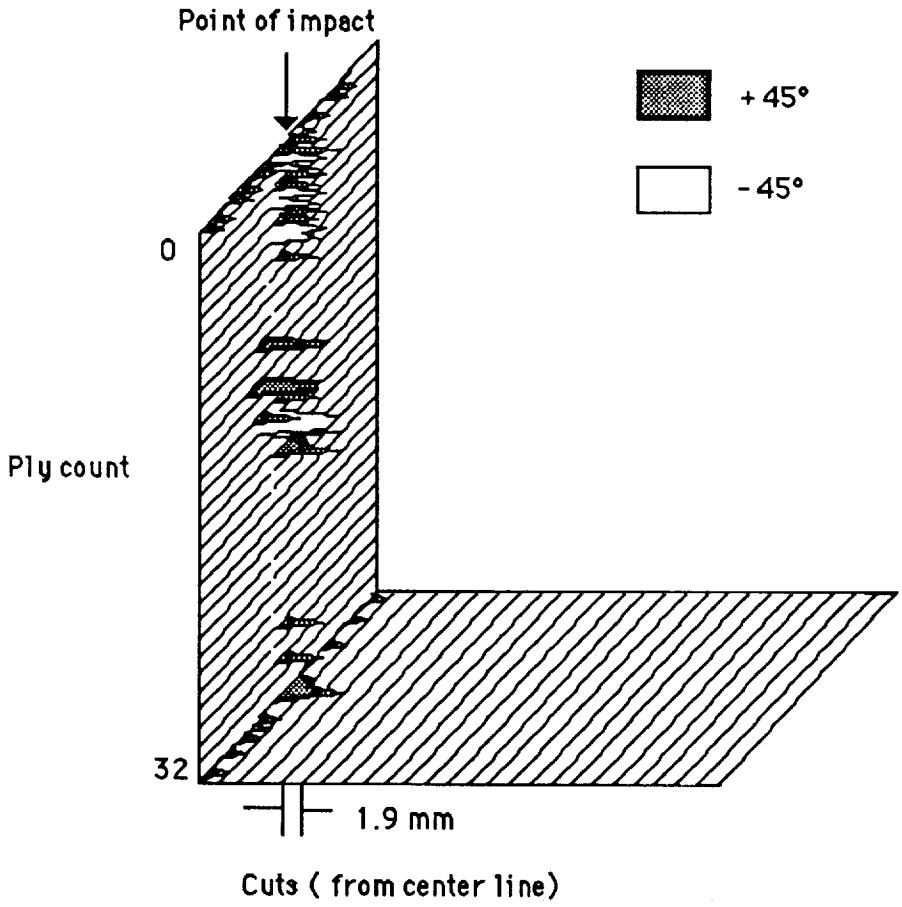

Figure 50 - Damage map for AS4/polycarbonate, (±45) at Σ I.E. = 250J

Effect of Sample Dimensions and Thickness: The size of the unsupported specimen area was increased from 5cm x 5cm to 10cm x 10cm. In separate experiments the unsupported size was maintained at 5cm x5cm but the sample thickness was decreased from 32plies to 16 plies.

The effect of increasing the sample size for AS4/3501-6 is shown in Fig 51 and for AS4/PEEK in Fig 52. As expected, the 10x10cm specimens had much lower stiffness and the changes in stiffness with cumulative impact energy were less pronounced. In the case of the AS4/3501-6 there was a transition at about the same Σ I. E. as was observed for the smaller, 5x5cm, specimen. In the case of the AS4/PEEK the 10x10cm specimen did not undergo any detectable change in stiffness. In fact, the experiment was

extended to almost 4000 J without any observable change in stiffness.

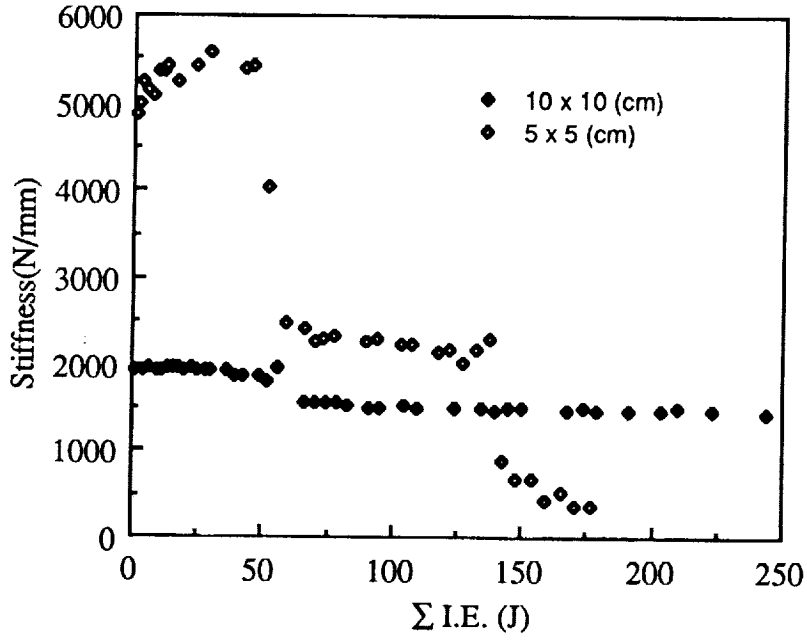

Figure 51 - Comparison of stiffness vs Σ I. E. for plates of AS4/3401-6, $(0/90)_{16s}$ with unsupported dimensions of 5cm x5cm and 10cm x 10cm.

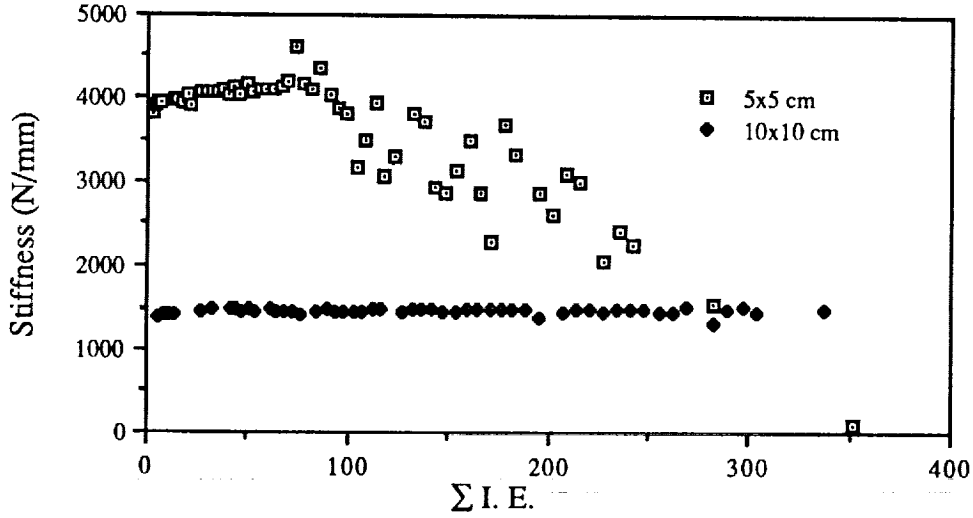

Figure 52 - Comparison of stiffness vs Σ I. E. for plates of AS4/PEEK, $(0/90)_{16s}$ with unsupported dimensions of 5cm x5cm and 10cm x 10cm.

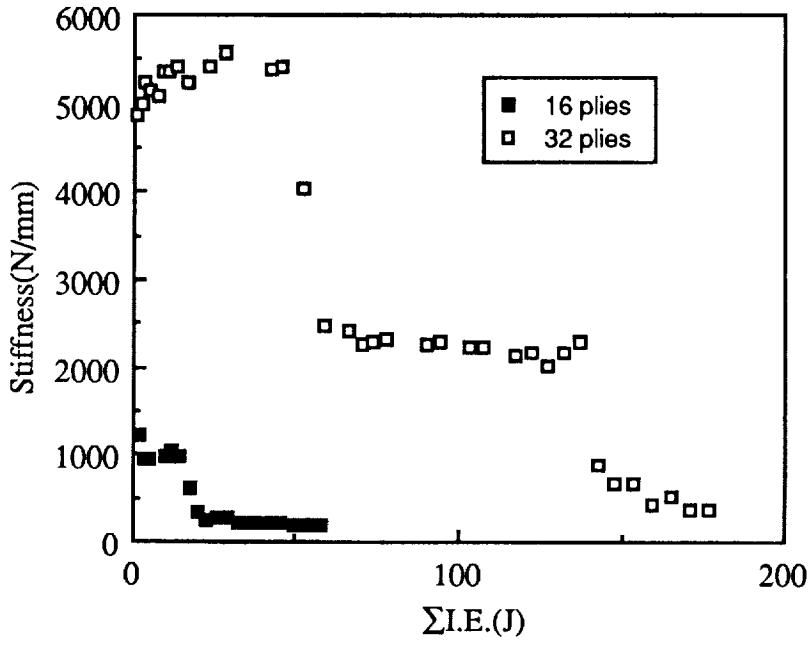

Figure 53 - Comparison of stiffness vs cumulative impact energy for AS4/3501-6 $(0/90)_S$ laminates having 16 plies and 32 plies

Decreasing the AS4/3501-6 specimen thickness from 32 plies to 16 plies caused the initial change in stiffness to occur at a Σ I. E. of about 5 J, Subsequently, there was a short plateau in stiffness (second stage) followed by a transition to a lower stiffness (third stage). Evidently, reducing the specimen thickness results in the same sequence of damage modes but over a much shorter range of cumulative impact energy than for the thicker, 32 ply specimen.

A damage map of a 16 ply specimen from the second stage (Σ I.E. = 10J) is shown in Fig. 54. The damage was through the thickness of the specimen and had a conical profile..

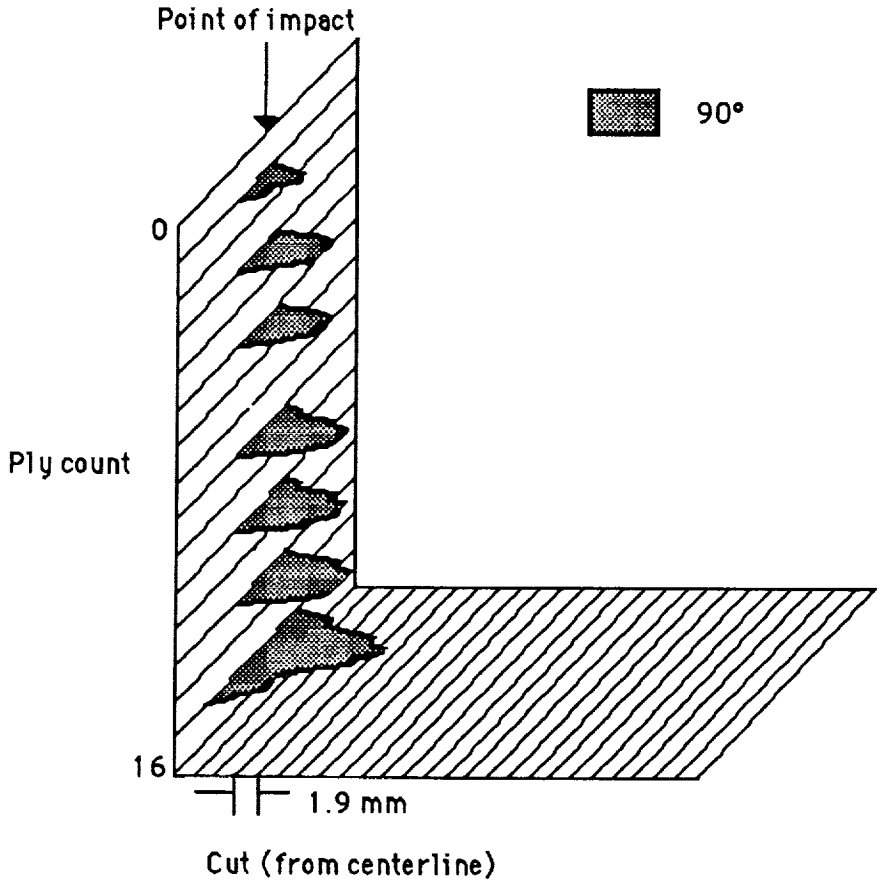

Figure 54 - Damage map for AS4/3501-6 $(0/90)_{8s}$ at Σ I. E. = 10J

Fatigue Testing vs RIIE Testing: Specimens of AS4/3501-6 were tested in a "fatigue" mode in which the specimen was impacted repetitively but at a constant impact load. The results of these tests are compared with the repetitive impact with increasing load (RIIE) in Fig 55. In the fatigue test, the stiffness dropped after the first impact to the second stage level of the RIIE test but then remained constant with further loading.

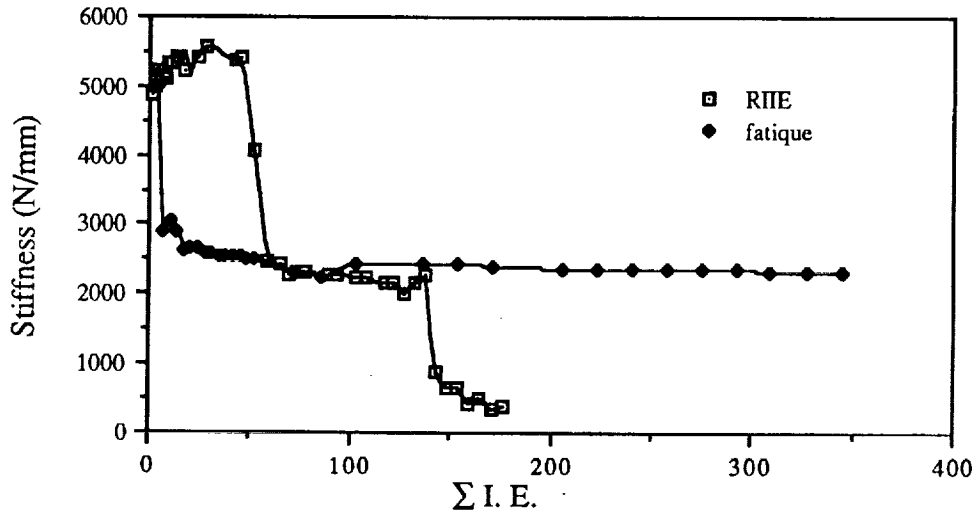

Figure 55 - Comparison of the change in stiffness vs cumulative impact energy for fatigue loading vs repetitive impact with increasing energy (RIIE) for AS4/3501-6$(0/90)_{16s}$.

These data can be viewed from a different perspective by plotting the change in stiffness with actual impact energy rather than with cumulative impact energy. The data plotted in Fig. 56 are from the RIIE testing and the data plotted in Fig. 57 are from the fatigue testing A comparison of Figs.56 and 57 show that the loss in stiffness occurs at about 3 J whether this level of energy is arrived by incrementally increasing the impact load (RIIE test) or is the initial load in the fatigue test.

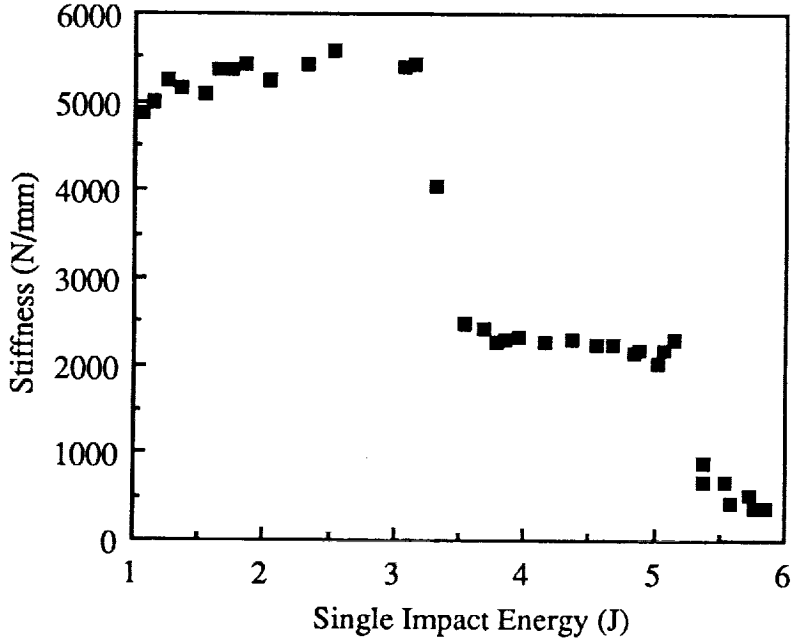

Figure 56 - Stiffness vs impact energy (noncumulative) from RIIE data for AS4/3501-6, $(0/90)_{16s}$ (Fig. 18)

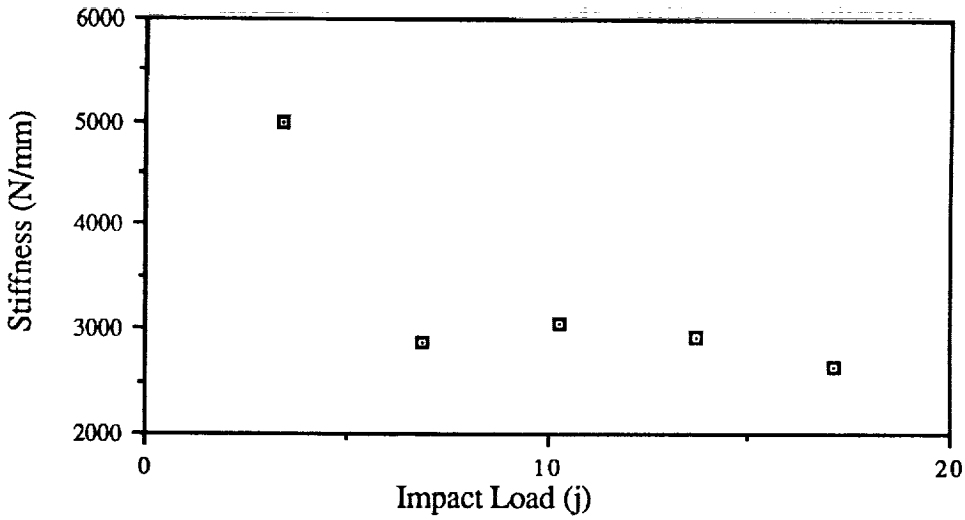

Figure 57 - Stiffness vs impact energy (noncumulative) from fatigue tests for AS4/3501-6, $(0/90)_{16s}$.

Figure 58 shows the fatigue data *vs* the RIIE data for AS4/PEEK $(90/0)_{16s}$. In the fatigue test, even after 1200(J), the stiffness did not drop significantly compared to the RIIE data. However, the initial decline in fatigue stiffness was relatively gradual compared to the AS4/3501-6 fatigue data (Fig. 55)

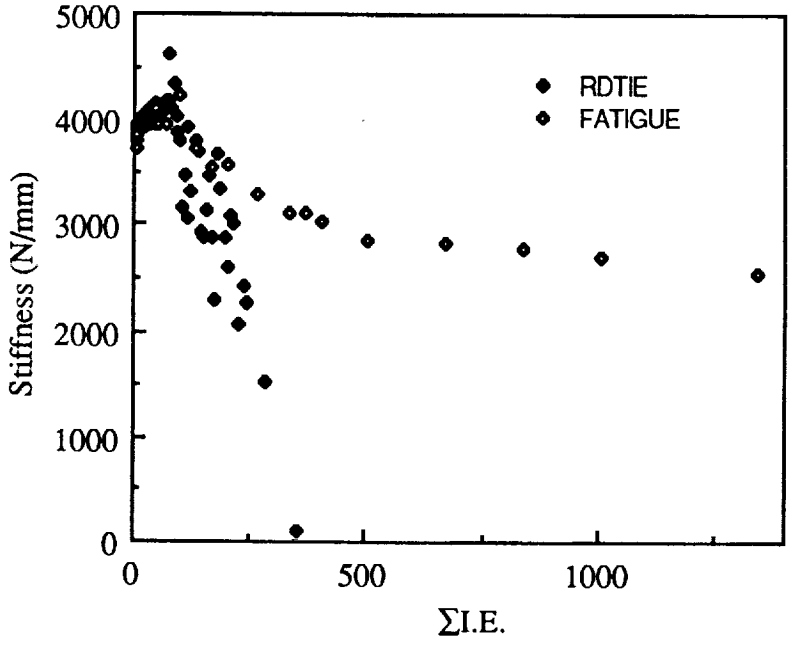

Figure 58 - Comparison of the change in stiffness vs cumulative impact energy for fatigue loading vs repetitive impact with increasing energy (RIIE) for AS4/PEEK$(0.90)_{16s}$

STATIC LOADING

A comparison was made between dynamic impact damage vs damage resulting from static three point bend loading. The strain rate of the static test was 0.005mm/sec.. The loader was hemispherical with a tip having the same radius as the impact loader (0.5cm) and the specimens were supported identically as in the dynamic tests. Load was applied to failure and from the resulting load displacement plot, specimens were loaded to key points along the initial load displacement curve and then C-scanned, potted, sectioned and the sections examined to develop damage

maps. These tests were performed on $(0/90)_{16s}$ panels of AS4/3501-6, AS4/PEEK and AS4/polycarbonate.

AS4/3501-6 Three distinct regions were observed in the static load displacement plot (Fig.59). In the first region, the stiffness was 5000 N/mm, which was similar to the stiffness (max load/max deflection) in the dynamic test (Fig 18). This stiffness abruptly decreased to 2300 N/mm, which was approximately the same as the stiffness of the second region in Fig 18. The third stage stiffness was 500 N/mm.

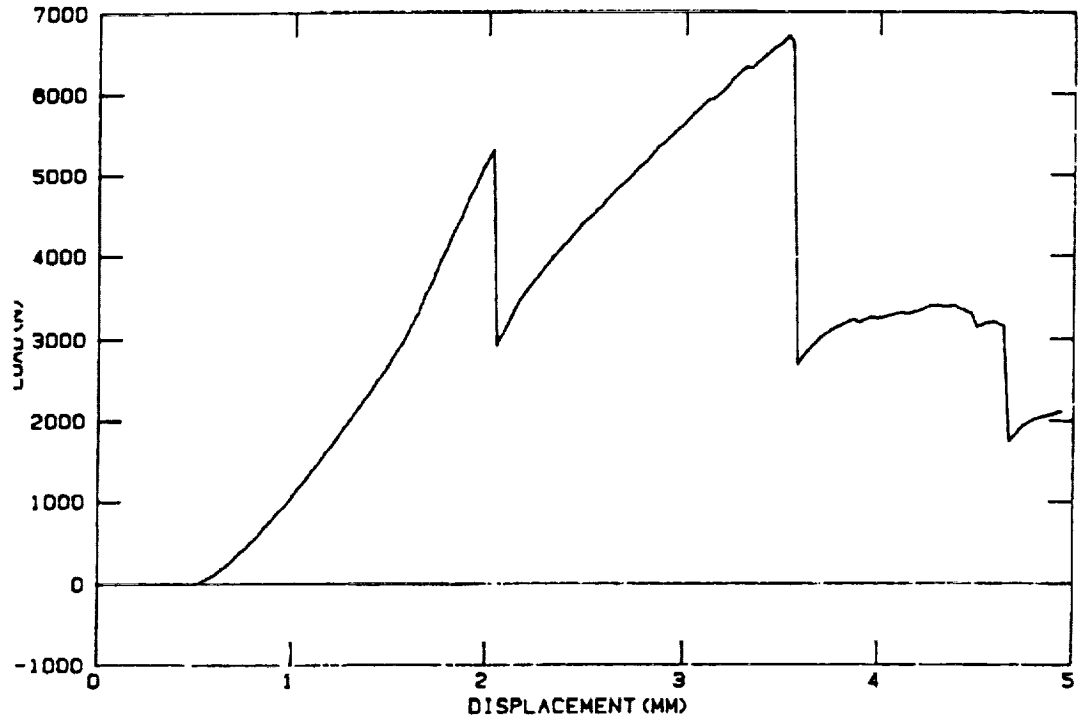

Figure 59 - Static force-displacement plot for AS4/3501-6, $(0/90)_{16s}$

The damage patterns from C-scans were similar to those of the dynamic test (compare Fig. 59 with Fig. 21). Damage maps of each of the stages from the static test are presented in Figs. 60-62. In the first damage stage of the static test, there was no contact damage on the front surface. In the second stage of this test, the pattern of damage was the same as that for dynamic loading, i.e., through the thickness and consisting of transverse cracking and delamination .

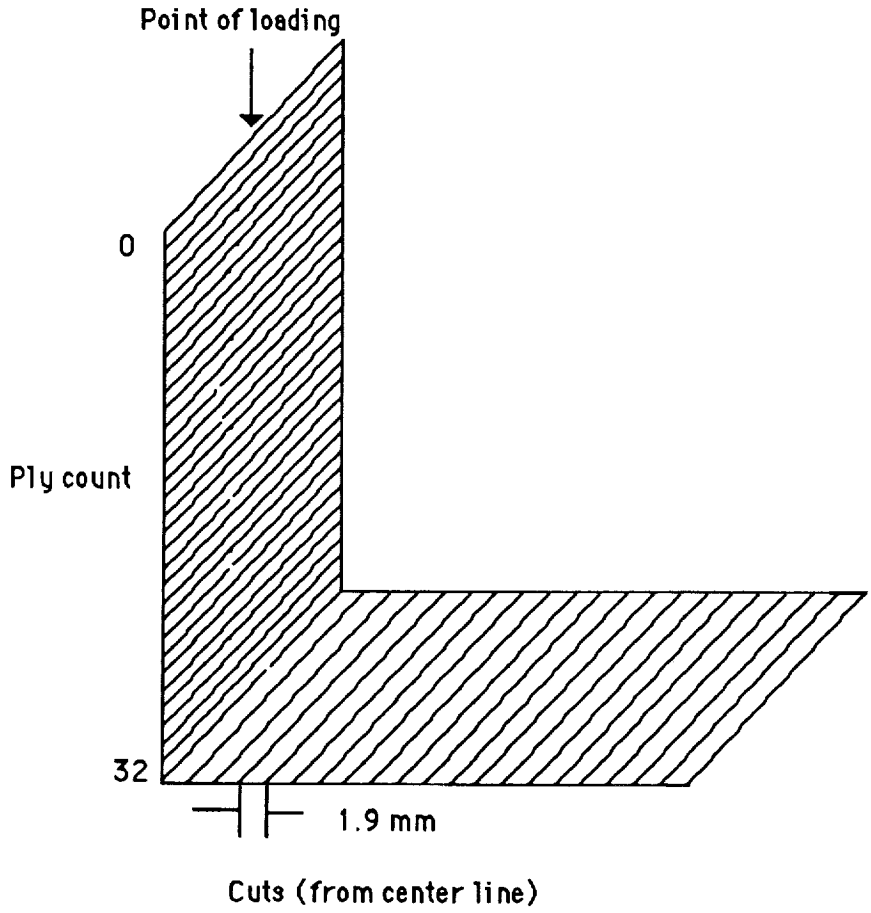

Figure 60 - Damage map of AS4/3501-6,$(90/0)_{16s}$ laminate loaded to a displacement of ~ 1.5mm

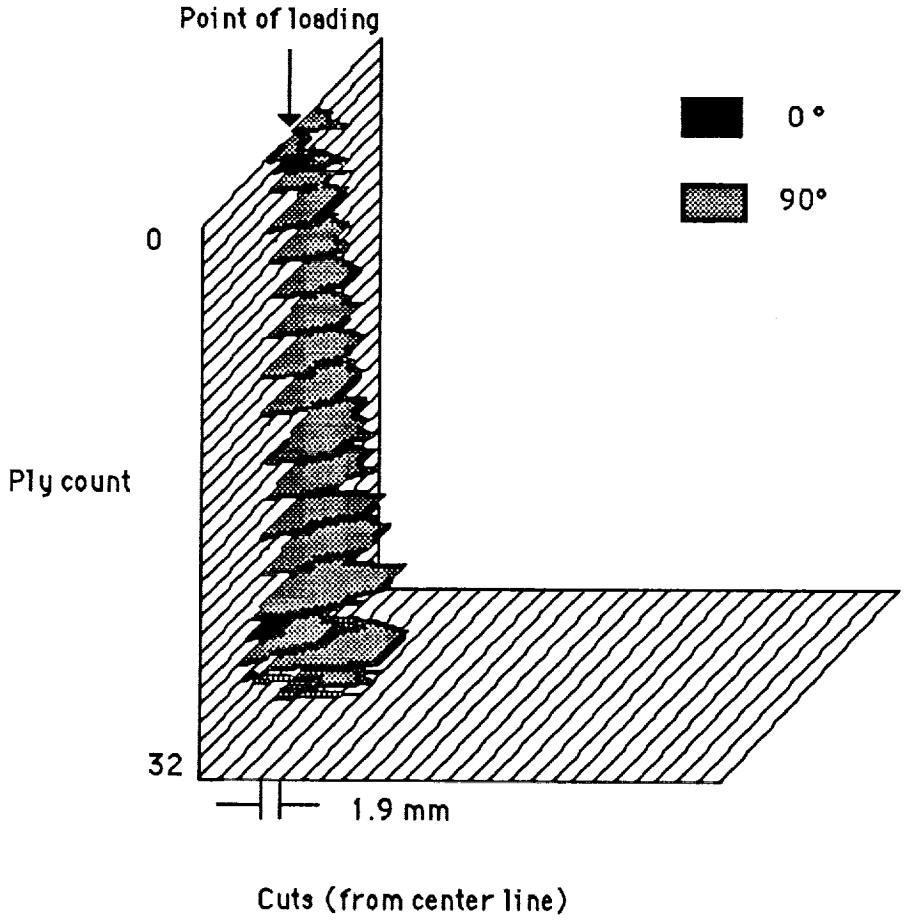

Figure 61 - Damage map of AS4/3501-6,$(90/0)_{16s}$ laminate loaded to a displacement of ~3mm

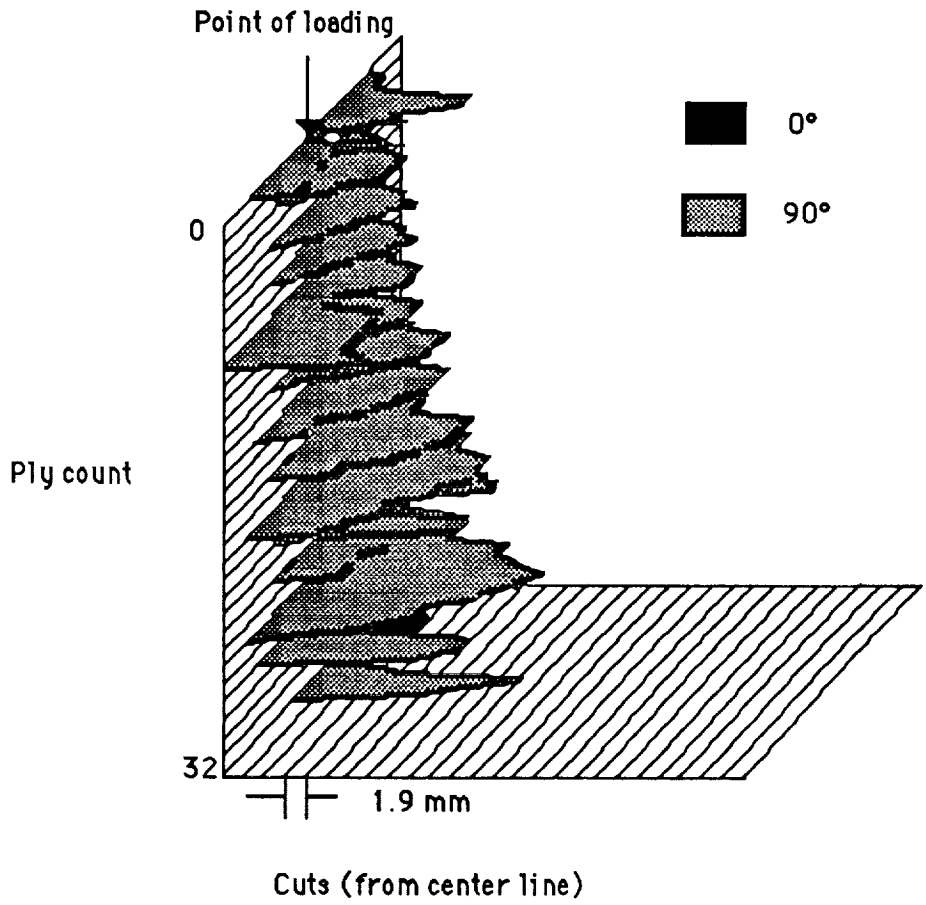

Figure 62 - Damage map of AS4/3501-6,$(90/0)_{16s}$ laminate loaded to a displacement of ~ 4mm

In the microscopy examination of the specimen loaded to 4mm displacement (Fig 62), fiber breakage was found on the back surface plys (Fig. 63) whereas fiber breakage was found in the front surface plys of the impacted specimen (Fig. 25B). Both the statically tested and impacted specimens showed the similar conical shape damage under the indenter.

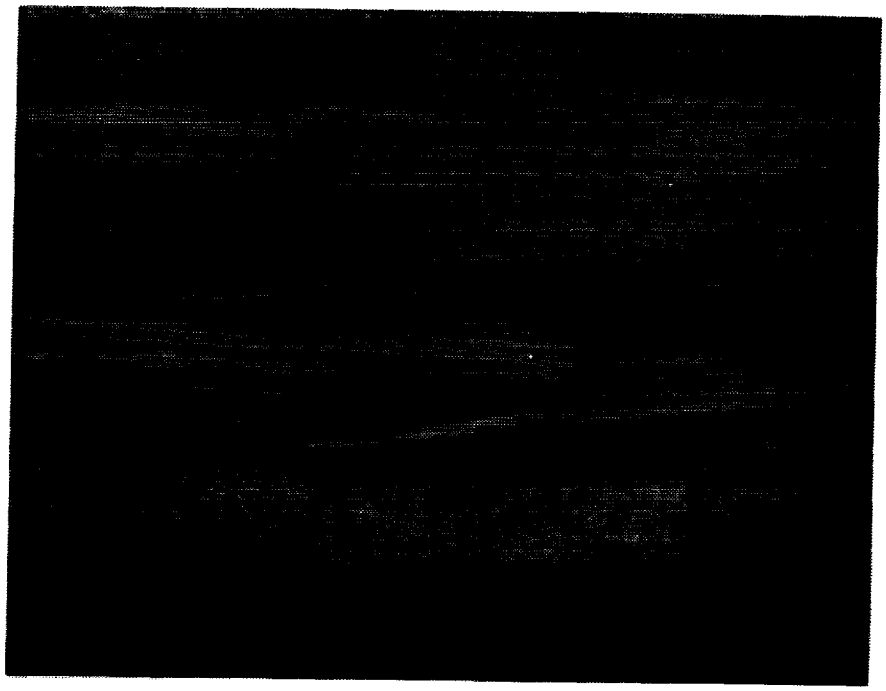

Figure 63 - Photomicrograph of backside damage of static loaded AS4/3501-6,$(90/0)_{16s}$ laminate loaded to a displacement of ~ 4 mm

Figure 64 is the static force-displacement curve for AS4/3501-6,(±45) in the static test. The stiffness of the first region was around 3300 N/mm which was the same as the stiffness of the first region in the dynamic tests. Subsequently, the stiffness was about 1700 N/mm until the displacement reached 5 mm at which point the force started to drop until 7.5 mm and C-scanning indicated that the damage had reached the specimen edges.

AS4/PEEK: Figure 65 is the load displacement plot for AS4/PEEK $(0/90)_{16s}$. There is an initial constant stiffness followed by a more or less continuous decrease in stiffness that becomes very pronounced after 4.5 mm. The shape of the plot in Fig.65 is clearly different from that for AS4/3501-6,(0/90), see Fig.59. Damage maps at three positions along this load-displacement curve were constructed (Figs. 66-68).

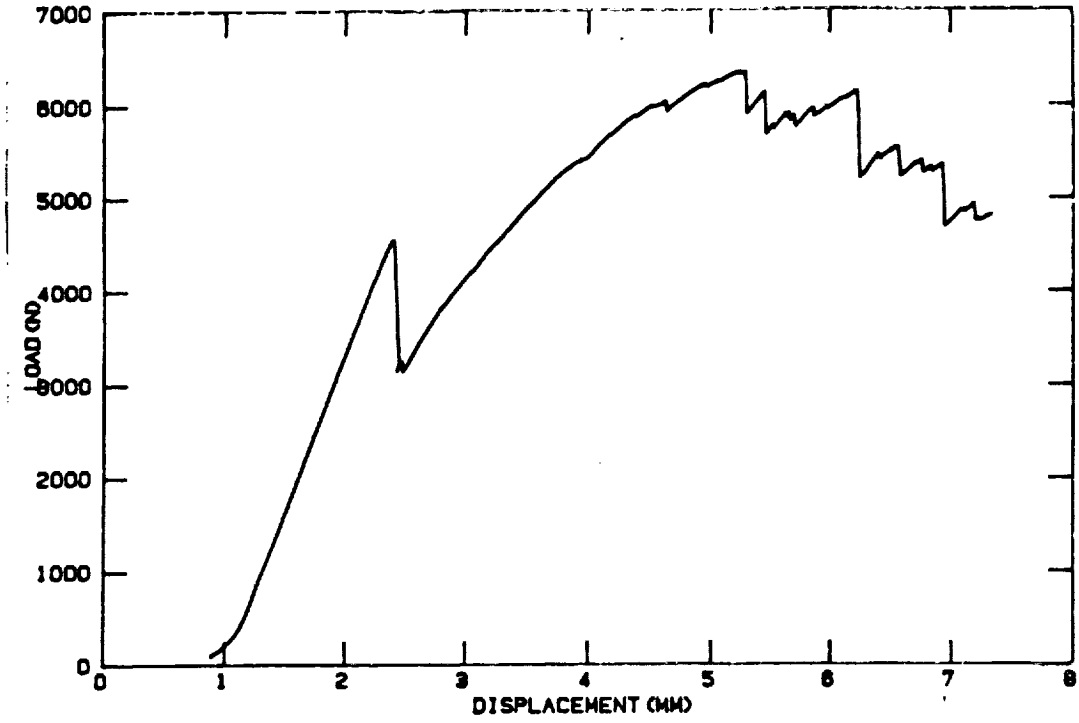

Figure 64 - Static load-displacement plot for AS4/3501-6 $(0/90)_{16s}$

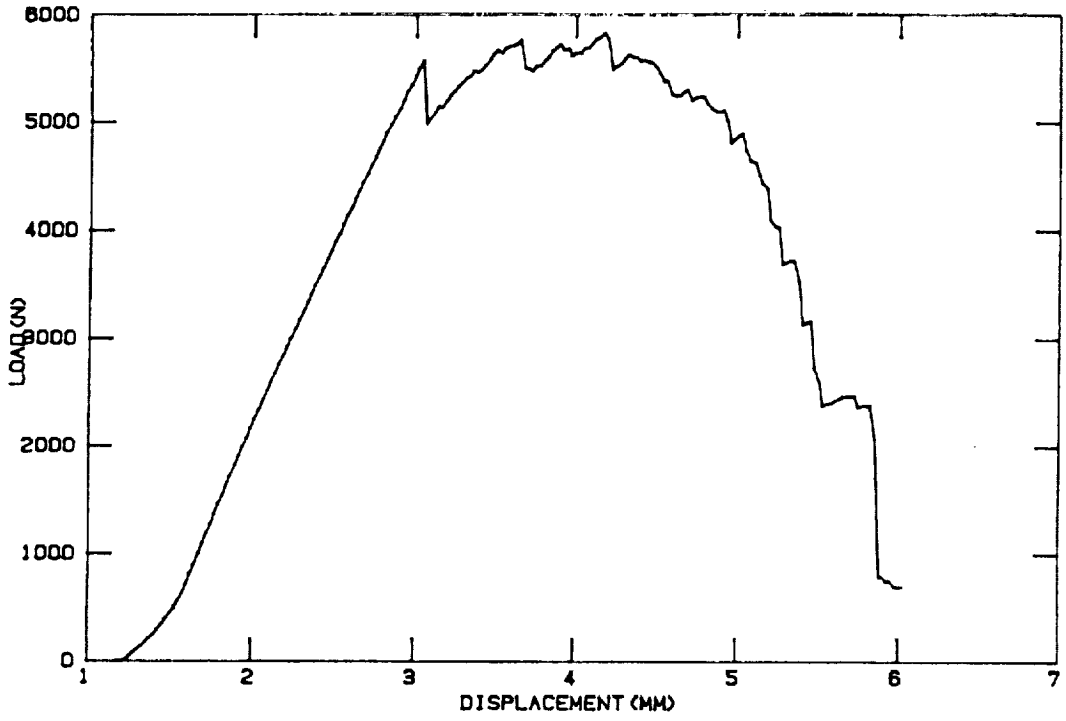

Figure 65 - Static load displacement curve for AS4/PEEK $(0/90)_{16s}$

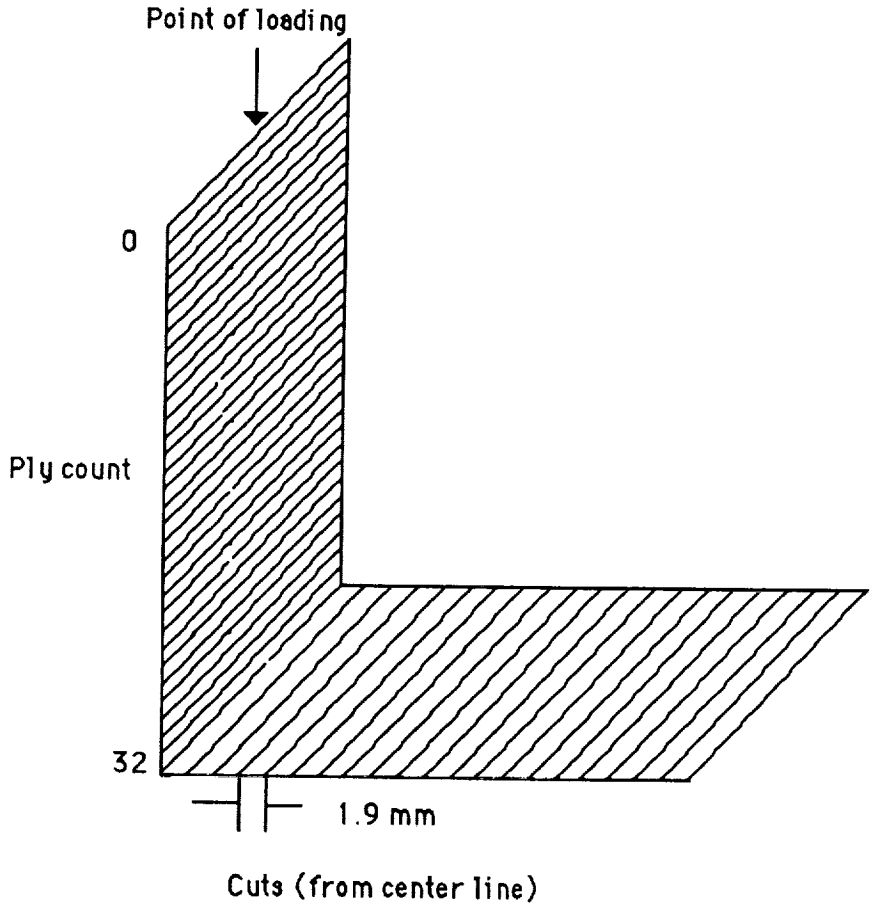

Figure 66 - Damage map for an AS4/PEEK,$(90/0)_{16s}$ laminate loaded to about 2.5mm displacement

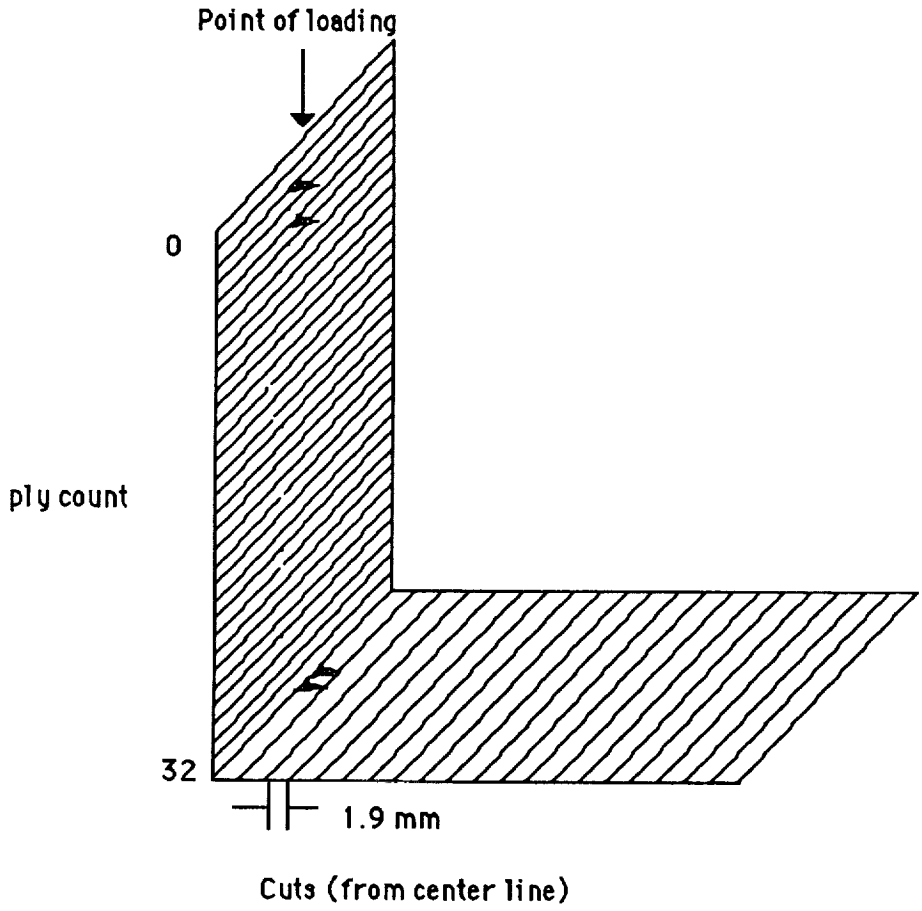

Figure 67 - Damage map for an AS4/PEEK,$(90/0)_{16s}$ laminate loaded to about 4mm displacement

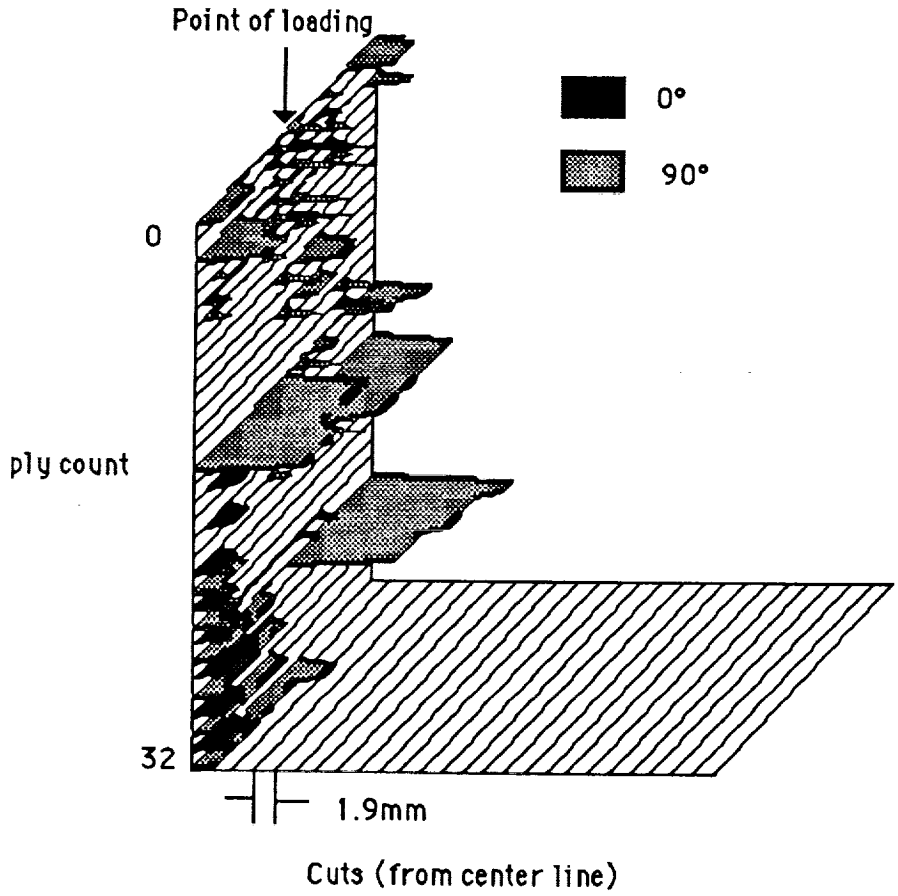

Figure 68 - Damage map for an AS4/PEEK,$(90/0)_{16s}$ laminate loaded to about 5.5mm displacement

No damage was found in the first linear region of the static test (Fig. 66). The second damage map (Fig.67) was drawn after the initial drop in force and showed transverse cracking near the front and back surfaces. In addition there was a noticeable bulge in the back surface of the specimen. This type of deformation had not been observed for any of the 3501-6 laminates.

The stiffness (~3500 N/mm) in the initial region in the static load displacement plot was less than that of the impact test (~4300, Fig 34A). In the static test at 5.5mm displacement both fiber-breakage and also fiber displacement were observed (Fig.69).

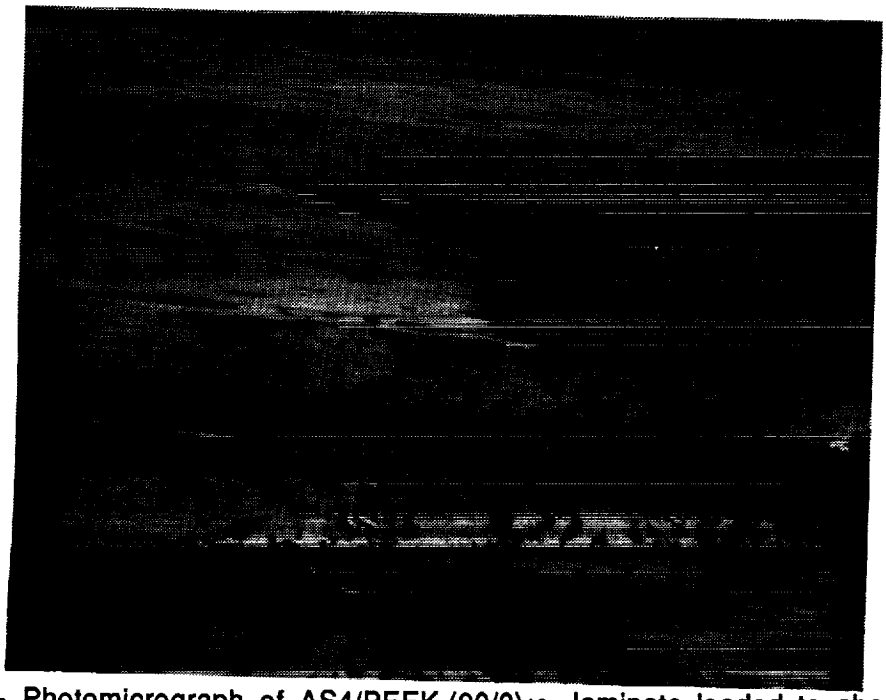

Figure 69 - Photomicrograph of AS4/PEEK,$(90/0)_{16s}$ laminate loaded to about 5.5mm displacement showing displacement of fiber plys

Figure 70 is the static load - displacement plot for AS4/PEEK, $(\pm 45)_{16s}$. The stiffness of the first linear region was ~2200 N/mm which was less than the stiffness observed in the dynamic test (~3000 N/mm, Fig 43A). After the initial drop in load, the force decreased continuously. The damage was still inside the sample even at 7mm displacement (Fig.71).

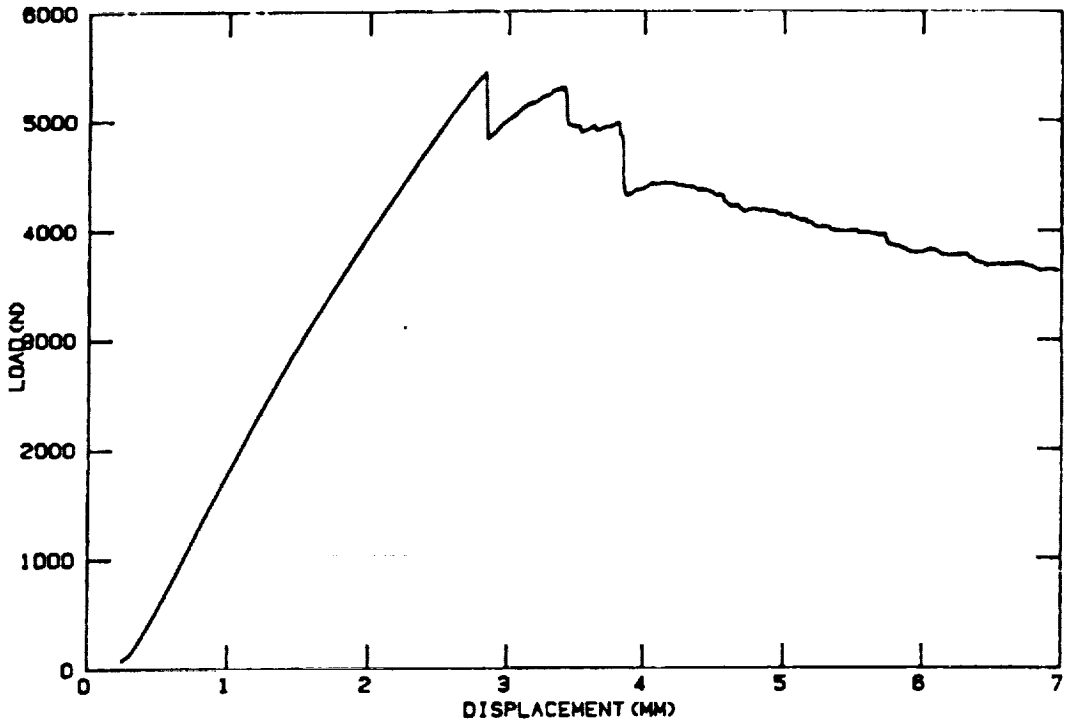

Figure 70 - Static load-displacement plot for AS4/PEEK $(\pm 45)_{16s}$

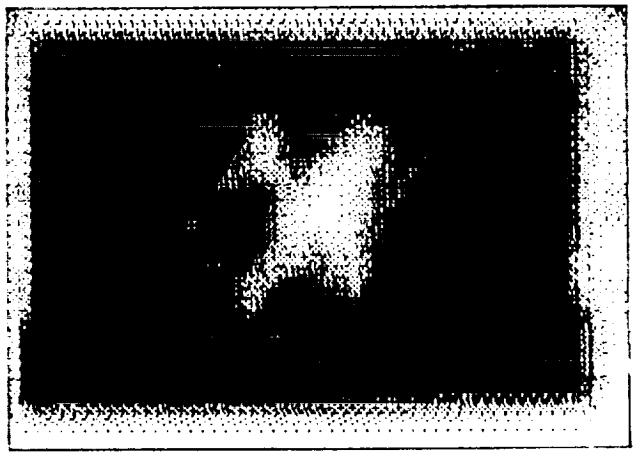

Figure 71- C-scan of AS4/PEEK $(\pm 45)_{16s}$ laminate at 6.5mm displacement.

Figure 72 is the static load-displacement plot for the AS4/polycarbonate$(0/90)_{16s}$ laminate. At first the slope is linear up to 2.3 mm and then decreased at 3.8 mm displacement and again at 4mm. The constant slope in the linear region indicated a stiffness of ~3700 N/mm, which was less than the ~5300 N/mm observed in the impact tests (Fig. 46A). From C-scans, the sudden drop in force at 4 mm corresponds to the damage reaching one edge of the sample (Figs 73 and 74).

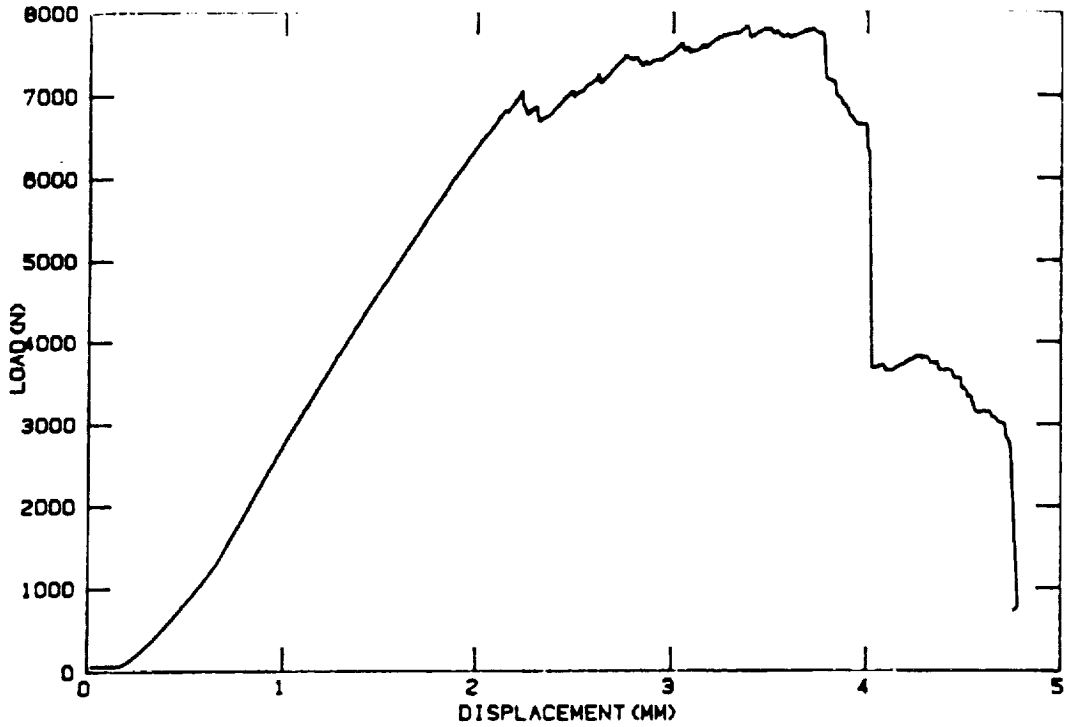

Figure 72 - Static load-displacement plot for AS4/polycarbonate$(0/90)_{16s}$

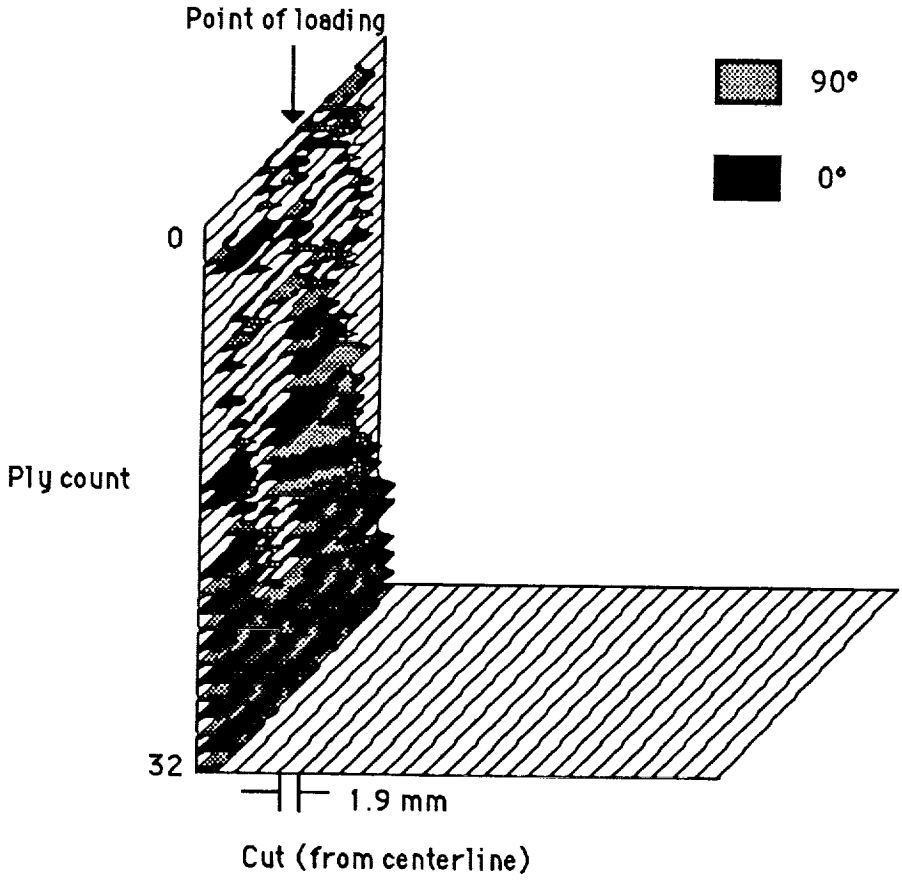

Figure 73 - Damage map of AS4/polycarbonate$(0/90)_{16s}$ after 4.5mm displacement

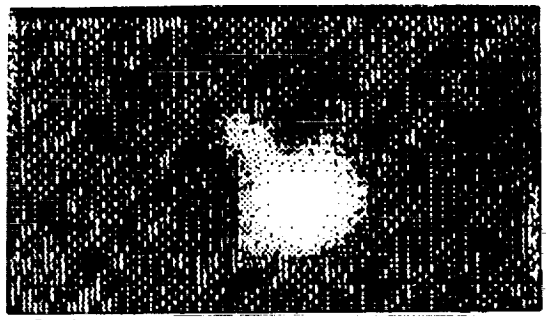

Figure 74 - C-scan of the damage of AS4/polycarbonate$(0/90)_{16s}$ after 4.8mm displacement.

Post-Impact Tensile Modulus

Three impacted samples were selected from the AS4/3501-6, IM6/3501-6 and the AS4/PEEK dynamic RIIE studies and tested for residual tensile modulus (Fig. 75). All specimens were $(0/90)_{16s}$ orientation. The test specimens were selected from the high,

intermediate and low damage "stages".

For the brittle 3501-6 matrix laminates, the tensile moduli decreased continuously with increasing Σ I. E.. For the tough PEEK matrix, the modulus did not decrease significantly below a cumulative energy of about 100J. At the lower Σ I. E. the IM6/3501-6 had a higher modulus than the AS4/3501-6 due to the higher modulus of the IM6 fiber. At Σ I. E. greater than 200J, the the moduli of the two 3501-6 laminates were essentially the same suggesting that the damage was so sever that it was essentially determined by the matrix, i.e., the fibers were severely broken and unable to carry load. On the other hand, the AS4/PEEK still had a high modulus even at Σ I. E. of 275J due presumably to the relatively small area of damage even though there had been considerable fiber fracture.

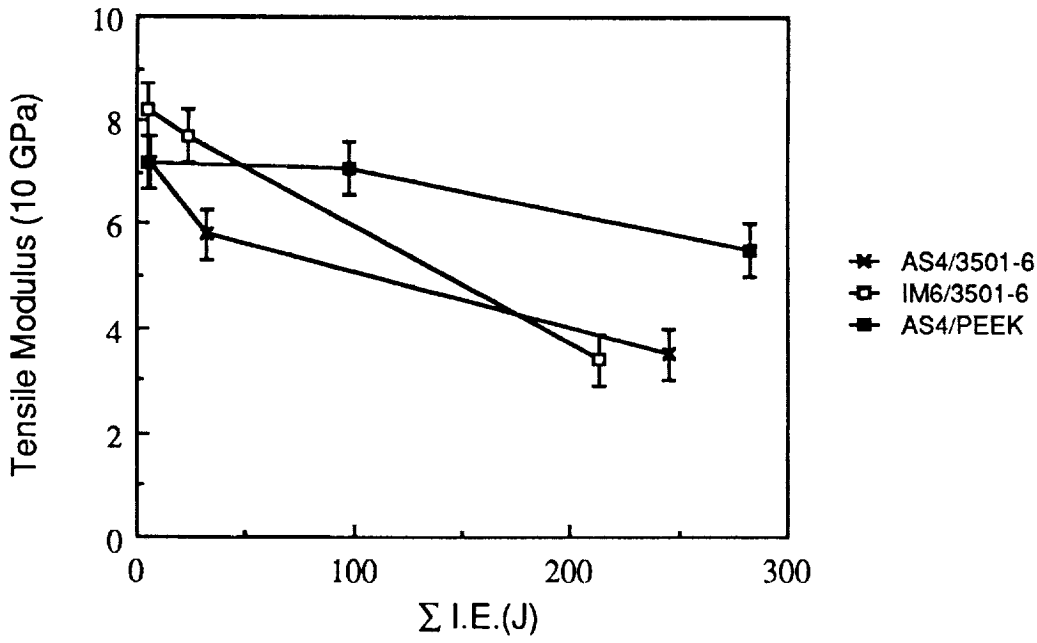

Figure 75 -Residual tensile modulus *vs* cumulative impact energy

DISCUSSION

From the stiffness *vs* cumulative impact energy and the percent of transferred energy *vs* cumulative impact energy, two and sometimes three distinct stages of behavior were observed for the AS4 /3501-6 and IM6/3501-6 laminates. During the first stage, the stiffness was essentially constant as was the percent of transferred energy. The damage observed in this stage was primarily transverse cracking in the top layers.

After an abrupt decline in stiffness, a second stage of relatively constant stiffness was observed. The onset of this stage was always accompanied by a peak in the transferred energy. The type of damage observed was a network of delamination and transverse cracking which extended through the thickness of the specimen.

This second state was sometimes followed by another abrupt drop in stiffness followed by a third plateau of relatively constant stiffness. The transferred energy was greater and even more erratic than for either the first or second stages. C-scan and damage mapping indicated that the damage progressed to the specimen edges during this third stage. In addition, some fiber breakage was observed. The only difference noted between the AS4 and the IM6 reinforced laminates was that the stiffness of the IM6/32501-6 plates were greater due to the higher modulus of the IM6 fiber.

The stiffness plots and the percent of transferred energy for the thermoplastic matrix laminates were distinctly different from the 3501-6 laminates. In the case of the thermoplastics, there was a progressive decrease in stiffness with cumulative impact energy. In addition, the level of transferred energy was consistently higher and variable from one impact to the next. C-scans and mapping indicated that essentially the same type of damage was occurring as for the 3501-6 matrix: initially a few delaminations and transverse cracks at the top and bottom sides of the plate which had little effect on the stiffness, (in fact, some of the data suggest a small increase in stiffness). Subsequently, damage was through the thickness and then extended to the plate edges. However, these were more progressive events than in the case of the thermosetting materials.

These differences in the behavior of the thermoplastic matrix and the thermosetting matrix laminates are probably due to the higher resistance of the thermoplastics to the extension of delamination. Once the stiffness begins to decline, the damage in the thermoplastic materials is confined to a relatively narrow cylindrical region under the point of impact. With continued impacting, this region undergoes even further damage along with some extension toward the specimen edges.

In the case of the thermosetting matrix laminates, the development of through the thickness damage is followed by extensive delamination from the center toward the specimen edges.

In a comparison of the RIIE test with the simple fatigue test, the impact energy is increased incrementally in the RIIE test whereas in the fatigue test, the energy is constant for each successive impact. The fatigue study was done using an impact energy of 3.2J and after the first impact the laminate stiffness was reduced from about 5000N/mm to about 2000N/mm. In the RIIE test the cumulative energy reached 100J before the stiffness dropped from 5000 to 2000N/mm (Fig.18). However, data from Figure 18 are replotted in Fig.76 but showing the actual energy at each impact. As in the fatigue test, the drop in stiffness occurred at an impact energy of about 3J. It would appear that some specific damage condition occurs at this impact energy level.

Continuing the fatigue test at 3J for each impact resulted in no further change in stiffness. On the other hand, in the continuation of the RIIE test, a second change in stiffness occurred at about 5J (Figure 76). The fact that through the second stage the stiffness is relatively constant suggests that whatever damage is occurring, it is not sufficient to alter the plate stiffness. None of less, damage is occurring as evidenced by the increase in transferred energy. The fact that the transferred energy varies considerably from one impact to the next, suggests that the amount of microdamage that occurs for a given impact varies considerably. One impact may result in only a minor amount of cracking but creates a condition that precipitates more extensive damage during the next impact event.

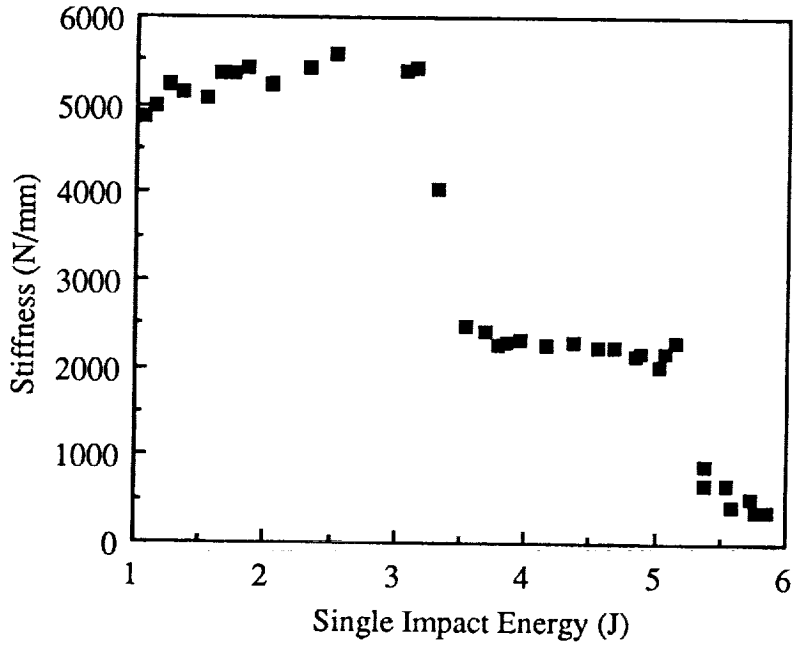

Figure 76 - Stiffness *vs* single impact energy for AS4/3501-6

The effect of the two stacking orientations , (0/90) and (±45), were similar for all of the laminate materials studied here. As expected, the initial stiffnesses for the (±45) orientations were always lower than that of the (0/90) orientations. As the stiffness began to decrease, the (±45) stacking sequence showed more resistance to damage propagation than the (90/0) stacking sequence both in the dynamic and static tests. Evidently the ±45 stacking sequence can absorb larger amounts of impact energy than 90/0 stacking sequence by elastic shear deformation; an elastic, "scissoring" deformation.

For the 3501-6 matrix laminates, the static tests gave very similar results to those of the dynamic tests. Three distinct stiffness regions were found in the three point bending tests and the stiffness values from the static tests and dynamic tests were nearly identical. In addition, the extent of damage and the type of damage, transverse and longitudinal cracking and fiber breakage, at each stage were similar for the static and dynamic tests.

However, the stiffnesses of the PEEK and polycarbonate matrix

laminates in the static tests were lower than from the impact testing and the damage modes were also different. This observation can be interpreted in two ways. One is membrane deformation and the other is viscoelastic behavior. In ductile materials, deflection in the static test occurs not only by contact and bending deformation but also by membrane deformation, especially in a plate supported at two edges.

The fact that membrane deformation was involved in the PEEK composite is evident from the C-scan results. In the impact test, damage was confined to the contact region between impactor and sample (Fig.36c). In the static test, large amounts of damage can be found in the edge region of the sample (Fig.68) which are very likely the result of membrane deformation.

The other explanation for the differences in stiffness is the viscoelastic characteristic of the thermoplastics. The low strain rate of the static test (0.005mm/sec) results in a lower stiffness than at the high strain rate impact loading.

Also the microfracture patterns from static test and impact tests are different for thermoplastic matrix. In the static testing of the thermoplastic materials, not only was there fiber breakage but also significant displacement of the plies (Fig.69). In the case of the polycarbonate laminate, the static damage was more restricted than for the PEEK laminate. In general, the polycarbonate laminates were more damage tolerant than the PEEK. Part of the reason for this is that the thickness of the polycarbonate sample (5.12 mm) was greater than that of the PEEK sample (4.16 mm). However, there may be more than thickness involved.

The thermoplastic laminates sustained considerable "plastic" damage, e.g. the development of a bulge on the back surface without any associated delamination or fiber breakage. This type of damage did not occur in the case of the 3501-6 matrix laminates presumably because of the lower shear yield strength of polycarbonate and PEEK compared to 3501-6.

The post-impact tensile modulus results (Fig. 75) are at first glance somewhat surprising. One would have thought that delamination and transverse cracking, that dominate the 3501-6 laminates would be less severe on tensile stiffness than the fiber breakage sustained by the PEEK laminate. In fact, the PEEK laminate

suffered less reduction in modulus than the AS4/3501-6 and the IM6/3501-6 laminates. It would appear that the extent of damage rather than the type of damage is more important in this post-impact test.

The specimen geometry effects, sample size and thickness, on damage tolerance were as expected. Increasing the unsupported area from 25 cm^2 (5cmx5cm) to 100cm^2 (10cm x 1-cm) simply allows for more energy to be dissipated by elastic flexture. Decreasing the laminate thickness from 32 plies to 16 plies (at the same unsupported area, 25cm^2) simply reduces the amount of material available to resist impact loads by elastic deformation.

It is clear that repeated impact with increasing impact energy does not distinguish different types of impact damage as claimed (18). Instead. the changes in stiffness (or in adsorbed energy as reported in reference 18) with cumulative impact energy correspond to changes in the extent of damage. Moreover, the adsorbed energy includes instrument related effects such as the friction between the impactor and the tube (14).

A comparison of the RIIE testing results with those from single impact drop tests is shown in Fig.77 taken from reference 18. Both methods display similar information but the RIIE results are compressed along the impact energy axes. This result is reasonable in that in the RIIE test the damage accumulates in the sample, i.e. less impact energy is required to see the next damage stage than for the single impact test. Therefore, the RIIE technique reduces the experimental time and materials required to investigate impact resistance.

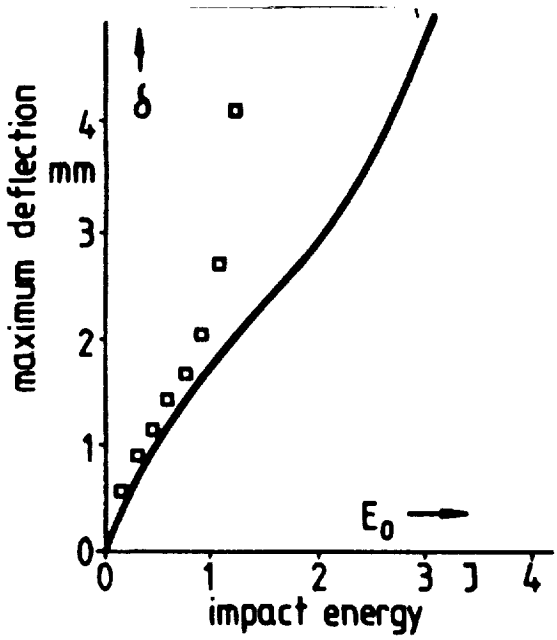

Figure 78 - Comparison of repetitive impact with increasing energy vs single drop testing (reference 18)

However, the RIIE technique has a problem in terms of data interpretation. For every impact the impact conditions are changed. For example, the area being impacted is already damaged so that the conditions of load input are different than if a fresh sample is used each time.

CONCLUSIONS

The microdamage that occurs for Mode I and Mode II delamination was examined by potting delaminated specimens in a clear epoxy, sectioning through the damage, polishing the cut sections and examining using light microscopy.

In the case of Mode I delamination of unidirectional CFRP composites, the major observation was fiber bridging including large ligaments or fiber bundles which have a significant effect on the interlaminar fracture energy and on the apparent crack opening displacement. The study of Mode II delamination of unidirectional laminates revealed a very narrow crack opening with only occasional fiber bridging.

The Mode II crack propagation in a (0,90) laminate was predominantly within the 0° plies but near the ply/matrix boundary

Impact testing by repetitive impacts with increasing energy was studied and it was found that this technique does not discern changes in the type of damage with increasing cumulative impact energy. Instead, the changes in the impact response, notably stiffness, are the result of changes in the extent of damage.

In the case of laminates based on a brittle thermoplastic matrix, 3501-6, there were distinct changes in stiffness that corresponded to the development of through the thickness damage and then to the extension of the damage to the specimen edges. In the case of two thermoplastic matrix materials, PEEK and polycarbonate, the changes in stiffness were not as abrupt as for the thermoset but instead there was a gradual decline in stiffness. None the less, the damage progressed in the same manner; first through the thickness damage then extension of the damage to the specimen edges.

Static flexure testing of the 3501-6 matrix laminates resulted in the same changes in stiffness and extent of damage as observed in the dynamic tests. Static testing of the thermoplastic matrix laminates gave results somewhat different than the dynamic tests. These differences were attributed to the lower modulus thermoplastic laminates undergoing membrane deformation in the static tests and the greater time dependent viscoelastic nature of the thermoplastics compared to the thermoset.

Literature references suggest that the repetitive impact test gives similar results as for single impacts of fresh specimens. However, interpretation of the repetitive impact test results are difficult, especially in terms of the micromechanics of impact damage, since for each sequential impact event the condition of the specimen surface changes so that conditions of load input into the specimen are undefined.

REFERENCES

1. O'Brien, T. K., "Characterization of Delamination Onset and Growth in a Composite Laminate, " in Damage in Composite Materials, ASTM STP 775, K. L. Reifsnider, ED., American Society for Testing and Materials, Philadelphia, I982, p. 140

2. Sinclair, J. H. and Chamis, C. C., "Compression Belhavior of Unidirectional Fibrous Composites," NASA Technical Memo 82833, I982, p. 19

3. Hibbs, M. F. and Bradley, W. L., "Correlations Between Micromechanical Failure Processes and the Delamination Toughness of Graphite/Epoxy Systems," in Fractography of Modern Engineering Materials, J. E. Masters and J. J. Au, Eds., ASTM STP 948, American Society for Testing and Materials, Philadelphia, I982, p. 68

4. O'Brien, T. K., Raju, I. S. and Garber, D. P., "Residual Thermal and Moisture Influences on the Strain Energy Release Rate Analysis of Edge Delamination," J. Comp. Technology and Research, Summer 1986, American Society for Testing and Materials, Philadelphia, p. 37

5. Toughened Composites N. J. Johnston, Ed., ASTM STP 937, American Society for Testing and Materials, Philadelphia, I987

6. Bascom, W. D.; Boll, D. J.; Weidner, J. C.; and Murri, W. J.; "A Microscopy Study of Impact Damage of Epoxy-Matrix Carbon Fiber Composites," J. Mat. Sci., 21 2667(1986)

7. Guynn, E. G., Bradley, W. L., "A Detailed Investigation of the Micromechanisms of Compressive Failure in Open Hole Composite Laminates," J. Comp. Mat., 23 479, I989

8. Bascom, W. D., Bitner, J. L., Moulton, R. J., and Siebert, A. R., "The Interlaminar Fracture of Organic-matrix, Woven Reinforcement Composites," Composites 11 9 (1980)

9. Bascom, W. D., Bullman, G. W., and Hunston, D. L., Proceedings, 29th National SAMPE Symp., Reno, 1984

10. Dugdale, D. S., J. Mech. Phys. Solids, 8 100 (1960)

11. Russell, A. J. and Street, K. N., "Moisture and Temperature Effects on the Mixed-Mode Delamination Fracture of Unidirectional Graphite Epoxy, ' ASTM STP 876, I985 American Society for Testing and Materials, Philadelphia, p. 349

12. Stellbrink, K., "The Repetitive Dropweight Test with Increasing

Energy," Wissenschaftlich-technische Tagung :12, Verstarkete Paste '88, Berlin, DDR , l988 p.21

13. P.Zoller, Polymer Testing, 3,197(1983)

14. P.O.Sjoblom, J.T.Hartness, T.M. Cordell "On Low Velocity Impact Testing of Composite Materials " J. of Composite Materials 22 30 (1988)

16.. Stellbrink, K " On the Behavior of Impact Damaged CFRP Laminates" Fiber Science and Technology 18 81(1983)

17. Akoi, R and Stellbrink, K "The Influence of Defects on the Behavior of Composites" Proc. 4th Int. Conf. Composite Materials, p12.1(1980)

18. Stellbrink, K., "Effect of Hybridization on Impact Behavior of CFRP Laminates.". DFVLR Report IB 435-85/22 (1985), Stuttgart, FRG.

APPENDIX

COMPUTER PROGRAM FOR PLOTTING DAMAGE MAPS[c]

[c] Requires Apple Computer, Inc Macintosh Plus™ or higher

COMPUTER PROGRAM FOR PLOTTING DAMAGE MAPS

Written in True Basic™ using the Run Time Package™.

```
library "3dlib*"
library "Pictlib*"
call Copy_printer(1)

dim damCut(32,40),damage(32,40),pangle(32),npts(32)

open #3: NAME "PC (3s)", ACCESS input, Organization text
input #3: nplies,ncuts,dmax
for i=1 to nplies
    input #3:plyn,pangle(i),npts(i)
   for j=1 to npts(i)
       input #3:damCut(plyn,j),damage(plyn,j)
   next j
next i
close #3

let plyTick=1
let dTick=1
let angle=45
let xs=.8
let ys=1.4

do
  clear

   print "AS4/Polycarbonate (90/0)  STAGE 1 "
    call ScaleParaWindow(1,dmax,1,ncuts,1,nplies,work$)
   call SetViewPlane3(0,1,0,work$)
   call Cabinet3(angle,work$)
   Ask Window x1,x2,y1,y2
   let xm=(x1+x2)/2
    let xmin=xm-(xm-x1)/xs
   let xmax=xm+(x2-xm)/xs
   let ym=(y1+y2)/2
    let ymin=ym-(ym-y1)/ys
    let ymax=ym+(y2-ym)/ys
   Set Window xmin,xmax,ymin,ymax
```

™ Trademark of True BASIC, Inc.

```
    call MyFrame
    for i=nplies to 1 step -1
      call plyplot(i)
    next i
    get key hold
    input prompt "New Window Scale:":xs,ys
    input prompt "New Angle:":angle
loop

stop

sub plyplot(np)
    dim ptmp(40,3)
    mat redim ptmp(npts(np),3)
    for j=1 to npts(np)
        let ptmp(j,1)=damage(np,j)
        let ptmp(j,2)=damCut(np,j)
        let ptmp(j,3)=nplies-np+1
    next J
    if(pangle(np)=0) then
      set color "black"
    else
      set color "red"
    end if
    call MatArea3(ptmp,work$)
    set color "black"
    call MatLines3(ptmp,work$)
end sub

sub MyFrame
    dim atmp(11,4)
    let atmp(1,1), atmp(2,1), atmp(3,1), atmp(7,1), atmp(8,1),
atmp(10,1)=0
    let atmp(1,2), atmp(2,2), atmp(6,2), atmp(7,2)=1
    let atmp(1,3), atmp(5,3), atmp(6,3), atmp(7,3), atmp(8,3)=1
    let atmp(9,3), atmp(10,3)=1
    let atmp(1,4), atmp(2,4), atmp(3,4), atmp(4,4), atmp(5,4),
atmp(6,4)=1
    let atmp(2,3), atmp(3,3), atmp(4,3), atmp(11,3)=nplies
    let atmp(3,2), atmp(4,2), atmp(5,2), atmp(8,2), atmp(9,2),
atmp(10,2)=ncuts
    let atmp(4,1), atmp(5,1), atmp(6,1), atmp(9,1)=dmax
    let atmp(7,4), atmp(8,4), atmp(10,4)=1
```

```
    let atmp(11,1), atmp(11,4)=0
    let atmp(11,2)=ncuts
   let atmp(9,4)=0
    call MatPlot3(atmp,work$)
   for i=0 to dmax step dTick
      call LineOff3(i,1,1,i,ncuts,1,work$)
  next i
   for i=1 to nplies step plyTick
      call LineOff3(0,1,i,0,ncuts,i,work$)
  next i
end sub
call Copy_done

end
```

ACKNOWLEDGEMENTS

The author wishes to thank the following students who were involved in the work reported here; Lisa Conception, Christine Ellison, Ralph Oakson, and Jill Bohney.

A special thanks to Mr. Seong-Yun Gweon who performed all of the impact investigation and to Professor John Nairn for many helpful discussions during the course of this work.

NASA
National Aeronautics and Space Administration

Report Documentation Page

1. Report No.	2. Government Accession No.	3. Recipient's Catalog No.
NASA CR-181965		

4. Title and Subtitle	5. Report Date
Fractography of Composite Delamination	July 1990
	6. Performing Organization Code

7. Author(s)	8. Performing Organization Report No.
W. D. Bascom	
	10. Work Unit No.
	505-63-01-05

9. Performing Organization Name and Address	11. Contract or Grant No.
University of Utah Materials Science and Engineering Department Salt Lake City, Utah 84112	NAG1-705
	13. Type of Report and Period Covered
12. Sponsoring Agency Name and Address	Contractor Report
National Aeronautics and Space Administration Langley Research Center Hampton, VA 23665-5225	14. Sponsoring Agency Code

15. Supplementary Notes

Langley Technical Monitor: John H. Crews, Jr.

16. Abstract

The microdamage that occurs for Mode I and Mode II delamination was examined by potting delaminated specimens in a clear epoxy, sectioning through the damage, polishing the cut sections and examining using light microscopy. For Mode I delamination of unidirectional CFRP composites, the major observation was fiber bridging including large ligaments of fiber bundles. The Mode II delamination of unidirectional laminates revealed a very narrow crack opening with only occasional fiber bridging.

Impact testing by repetitive impacts with increasing energy was studied and it was found that this technique does not discern changes in the type of damage with increasing cumulative impact energy. Instead, the changes in the impact response, notably stiffness, are the result of changes in the extent of damage. For laminates with a brittle thermoplastic matrix, 3501-6, there were distinct changes in stiffness that corresponded to the development of through the thickness damage and then to the extension of the damage to the specimen edges. For PEEK and polycarbonate, the changes in stiffness were not as abrupt as for the thermoset. None the less, the damage progressed in the same manner.

17. Key Words (Suggested by Author(s))	18. Distribution Statement
Laminates Delamination Microdamage Repeated Impacts Stiffness	Unclassified - Unlimited Subject Category - 39

19. Security Classif. (of this report)	20. Security Classif. (of this page)	21. No. of pages	22. Price
Unclassified	Unclassified	90	A05

NASA FORM 1626 OCT 86